

THROMBUS FORMATION UNDER HIGH SHEAR
IN ARTERIAL STENOTIC FLOW

A Thesis
Presented to
The Academic Faculty

By
Conor James Flannery

In Partial Fulfillment
of the Requirements of the Degree
Master of Science in Mechanical Engineering

Georgia Institute of Technology
May 2005

THROMBUS FORMATION UNDER HIGH SHEAR
IN ARTERIAL STENOTIC FLOW

Approved by:

Dr. David N. Ku, Advisor
School of Mechanical Engineering
Georgia Institute of Technology

Dr. Larry V. McIntire
School of Biomedical Engineering
Georgia Institute of Technology

Dr. Andres J. Garcia
School of Mechanical Engineering
Georgia Institute of Technology

Date Approved: April 14, 2005

ACKNOWLEDGEMENTS

First and foremost I would like to thank Dr. Ku for allowing me the opportunity to study and address *de novo* research, for presenting me with the challenge that I hoped for, and for good advice at the right time.

I would like to thank my committee Dr. McIntire and Dr. Garcia for their time and consideration in this research and for teaching me the skills to complete it.

I would like to thank Jack Horner and the Phlebotomy Lab for technical services and Tracy Couse for histological services. I would like to thank Robert Cutwrite at the American Red Cross for donating platelet transfer bags and Don Woodyard for glass blowing services. I would also like to thank Mr. Holifield and Tommy at Holifield Farms.

I would like to warmly and earnestly thank my sister Deirdre for two years that brought us closer than ever. Our friendship has taught me some of the greatest lessons in graduate school and I really appreciate this time that we have been able to share together.

I would like to thank my Dad for always helping me to be the best I can be and for setting an example that has guided me throughout my education.

I would like to thank and send lots of love to Mom, Clare, Una, Ryan, Ann and Jean for all of their support.

A special thanks to the members of the Ku lab, Crystal, Rahul, Tarek, Guilhem, Luc, and Paul.

TABLE OF CONTENTS

	Page
Acknowledgements	iii
List of Tables	vi
List of Figures	vii
List of Equations	xi
Summary	xii
CHAPTERS	
I. Introduction	1
Clinical Relevance	1
Hemostasis and Thrombosis	5
Hemodynamics of Stenoses	9
Platelet Deposition under High Shear	11
Adhesive Strength of Platelets	16
Propagating Fibrin Tails	18
Specific Aims and Hypotheses	19
 II. Methodology	 21
Experimental Design	21
Blood Samples	23
Viscosity Determination	24
Stenotic Test Sections	25
Collagen Coating	27
Flow System	28
Cleaning and Sanitation	30
Water Flow Experiments	31
Blood Flow Experiments	31
Thrombus Formation Imaging	34
Thrombus Removal Experiments	35
Histology	38
 III. Model of Occlusive Thrombosis in Stenoses under High Shear	 41
Blood Flow Experiments	42
Effect of Increased Percent Stenosis	46
Severely Stenotic Experiments	46
Mildly Stenotic Experiments	51
Non-Stenotic Experiments	55
In Vitro Model of Occlusive Thrombosis	57
Effect of Coating Collagen	60
Determination of Height	64

Calculation of Shear Rate and Reynolds Number	66
IV. Thrombus Formation until Complete Occlusion	68
Platelet Deposition based on Flow Rate	70
Thrombus Formation Movies	78
Platelet Deposition Based on Thrombus Formation Images	83
Rate of Platelet Deposition under High Shear Rates	97
Histology and Composition Analysis	100
Fibrin Tail Propagation	115
V. Detachment Strength of Thrombus	117
Detachment Strength of Thrombus	118
Thrombus Removal Experiments	119
VI. Discussion	133
In Vitro Model of Occlusive Thrombosis	134
Formation of Completely Occlusive Thrombus	134
Rate of Platelet Deposition versus Shear Rate	136
Thrombus Removal Experiments	139
Estimation of the Adhesive Strength of Platelets	140
1. Platelet Detachment Strength based on Removal of Thrombus	141
2. Platelet Attachment Strength based on Shear Rate	145
Fibrin Tail Propagation	147
VII. Conclusions	150
Future Work	150
APPENDIX:	153
A-1: Matlab Codes for Image Analysis	153
A-2: Matlab Code for Histological Composition Code	156
REFERENCES	157

LIST OF TABLES

		Page
Table 1:	Comparison of <i>in vitro</i> model to coronary flow parameters.	41
Table 2:	Data on the seven complete occlusions in order increasing percent stenosis.	69
Table 3:	Platelet deposition (PD) rates and the parameters used in their calculation.	76
Table 4:	The rates of platelet deposition for each platelet deposition model.	99
Table 5:	Status of Histological Samples.	100
Table 6:	Appearance of Blood Species after Carstairs Staining.	101
Table 7:	Summary of all removal experiments including removal of emboli.	118
Table 8:	Adhesion force estimates based on detachment and attachment strengths.	141
Table 9:	Comparison of fibrin tail observation.	148

LIST OF FIGURES

	Page
Figure 1: Example of atherothrombosis in a coronary artery.	3
Figure 2: Three phases of platelet deposition over time.	12
Figure 3: Platelet deposition onto collagen as a function of shear rate at 5 minutes of exposure time.	14
Figure 4: Stenotic test section.	25
Figure 5: Collagen coating set up.	27
Figure 6: Flow system illustration.	28
Figure 7: Flow system picture.	30
Figure 8: Image of thrombus formation visualization set up.	34
Figure 9: Pressure transducer calibration.	37
Figure 10: Thrombus removal system.	38
Figure 11: The average flow rate and average upstream pressure for blood experiments over collagen.	43
Figure 12: Average Reynolds numbers (Re #s) for blood flow experiments over collagen.	44
Figure 13: Occurrence of complete occlusion increases with % stenosis.	45
Figure 14: Pressure and flow rate in a severely stenotic test section.	47
Figure 15: Totally occlusive thrombus images A and B.	48
Figure 16: Pressure and flow rate for an embolus experiment.	49
Figure 17: Embolus image in stenosis throat.	50
Figure 18: Histological sample of embolus.	51
Figure 19: Pressure and flow rate in a mildly stenotic test section.	52
Figure 20: Patent stenosis image with thrombus deposition.	53
Figure 21: Image demonstrating striations of thrombus in throat.	55
Figure 22: Pressure and flow rate in a non-stenotic test section.	56
Figure 23: Visible thrombosis in non-stenotic test section.	57
Figure 24: Blood and water normalized flow rates versus % stenosis.	58
Figure 25: Flow rate model for blood in stenoses $\geq 85\%$.	59
Figure 26: Pressure and flow rate in a non-collagen coated stenosis.	61
Figure 27: Thrombosis not visible in image of non-collagen coated stenosis.	61

Figure 28:	Flow rate of water for test sections with and without collagen coating versus % stenosis.	63
Figure 29:	Flow rate of blood for test sections with and without collagen coating versus % stenosis.	64
Figure 30:	Comparison of height of fluid reservoir on flow rate.	65
Figure 31:	Reynolds numbers of heigh-dependent flow versus % stenosis.	65
Figure 32:	Pressure and flow rate for a total occlusion experiment.	73
Figure 33:	Example of platelet deposition over time with flow rate model.	74
Figure 34:	Acute platelet deposition rate increased with percent stenosis.	77
Figure 35:	Acute rate of platelet deposition in an 85% stenosis.	77
Figure 36:	Thrombus formation image sequence in the 85% stenosis; 85per_sten_TO_40sec_12-15-9_2fps_C.mov (4.64 MB).	79
Figure 37:	Thrombus formation image sequence in another 85% stenosis; 85per_sten_TO_19sec_12-8-9_2fps_C.mov (2.54 MB).	80
Figure 38:	Thrombus formation image sequence in the 96% stenosis; 96per_sten_TO_39sec_12-15-33_2fps_C.mov (4.21 MB).	81
Figure 39:	Embolus image sequence in the 93% stenosis; 93per_sten_E_12sec_1-24-39_2fps.mov (1.17 MB).	82
Figure 40:	Thrombus formation image sequence in the 0% stenosis; 0per_sten_N_20sec_1-26-20_2fps_C.mov (2.19 MB).	83
Figure 41:	An example of grayscale image that exhibits thrombus.	86
Figure 42:	Histogram of grayscale image.	87
Figure 43:	A black and white image after conversion from grayscale.	87
Figure 44:	Another black and white image after conversion from grayscale.	88
Figure 45:	Various thresholds for image analysis method.	89
Figure 46:	Outline of the visible area at the time of total occlusion.	92
Figure 47:	Platelet deposition using image analysis model.	94
Figure 48:	Platelet deposition using image analysis with a logarithmic scale.	95
Figure 49:	Platelet deposition based on image analysis of a 96% stenosis.	96
Figure 50:	Platelet deposition based on image analysis of an 85% stenosis.	97
Figure 51:	Comparison of platelet deposition models.	98
Figure 52:	Histology – coagulation control with Carstairs at 4x.	102

Figure 53:	Histology – coagulation control with Carstairs at 40x.	102
Figure 54:	Histology – coagulation control with vWF at 4x.	103
Figure 55:	Histology – thrombus 12.8.1.9 with Carstairs photostitched.	104
Figure 56:	Histology – thrombus 12.8.1.9 with vWF photostitched.	104
Figure 57:	Histology – thrombus 12.8.1.9 with Carstairs at 10x.	105
Figure 58:	Histology – thrombus 12.8.1.9 with vWF at 10x.	106
Figure 59:	Histology – thrombus 11.22.4.33 with Carstairs photostitched.	106
Figure 60:	Histology – thrombus 11.22.4.33 with Carstairs magnified.	107
Figure 61:	Histology – thrombus 11.22.4.33 with Carstairs magnified at 40x.	108
Figure 62:	Histology – thrombus 11.22.4.33 with vWF photostitched.	109
Figure 63:	Histology – thrombus 12.15.2.33 with Carstairs photostitched.	110
Figure 64:	Histology – thrombus 12.15.2.33 with Carstairs – occlusive thrombus.	110
Figure 65:	Histology – thrombus 12.15.2.33 with vWF magnified.	111
Figure 66:	Histology – thrombus 12.15.2.33 with Carstairs – connection.	111
Figure 67:	Histology – thrombus 12.15.2.33 with Carstairs – RBC packet.	112
Figure 68:	Histology – thrombus 12.15.2.33 with Carstairs – tail.	113
Figure 69:	Histology – thrombus 12.15.2.33 with Carstairs – tail magnified.	114
Figure 70:	Histology – thrombus 12.15.2.33 with vWF – tail.	115
Figure 71:	Image before removal of sample 12.1.2.33 at 2x	120
Figure 72:	Image before removal of sample 12.1.2.33 at 4x.	120
Figure 73:	Image before removal of sample 12.1.2.33 at 10x.	121
Figure 74:	Pressure recording for sample 12.1.2.33.	122
Figure 75:	Image after removal of sample 12.1.2.33 at 2x.	123
Figure 76:	Image after removal of sample 12.1.2.33 at 10x.	123
Figure 77:	Image before removal of sample 12.8.1.9 at 2x.	124
Figure 78:	Pressure recording for sample 12.8.1.9.	125
Figure 79:	Image after removal of sample 12.8.1.9 at 2x.	126
Figure 80:	Image after removal of sample 12.8.1.9 at 4x.	126
Figure 81:	Image before removal of sample 12.15.2.9 at 2x.	127
Figure 82:	Image before removal of sample 12.15.2.9 at 4x.	127
Figure 83:	Image before removal of sample 12.15.2.9 at 10x.	128

Figure 84:	Pressure recording for sample 12.15.2.9.	129
Figure 85:	Image before removal for sample 12.15.2.33 at 2x.	129
Figure 86:	Pressure recording for sample 12.15.2.33.	130
Figure 87:	Image before removal for embolus sample 12.15.2.39 at 2x.	132
Figure 88:	Pressure recording for embolus sample 12.15.2.39.	132
Figure 89:	Acute rate of platelet deposition for continuous thrombosis studies.	137
Figure 90:	Rate of platelet deposition onto collagen in multiple thrombosis studies.	138
Figure 91:	Surface area of throat representation.	142
Figure 92:	Histological section of thrombus 12.1.2.33.	144

LIST OF EQUATIONS

	Page
Equation 1: Percent stenosis by diameter.	2
Equation 2: Einstein's viscosity equation.	24
Equation 3: Percent stenosis by area.	26
Equation 4: Targ's equation.	32
Equation 5: Flow reduction model.	60
Equation 6: Shear stress assuming Poiseuille pipe flow.	66
Equation 7: Shear rate.	66
Equation 8: Reynolds number.	67
Equation 9: Volume of thrombus calculation.	71
Equation 10: Number of platelets in thrombus calculation for flow model.	71
Equation 11: Platelet deposition calculation for flow rate model.	72
Equation 12: Platelet deposition calculation for image analysis model.	92
Equation 13: Number of platelets in thrombus calculation for image model.	93
Equation 14: Maximum force on thrombus calculation.	119
Equation 15: Maximum force equivalent to sum of bonds.	141
Equation 16: Approximation of surface area of throat.	143
Equation 17: Number of platelets on the throat surface estimation.	143
Equation 18: Attachment force based on shear.	145

SUMMARY

In many cases, the last event that precipitates myocardial infarction is total occlusion of a coronary artery due to acute thrombotic occlusion. High shear rates due to stenosis in the arteries are a dominant cause of the thrombotic reaction. Studies of thrombosis under arterial stenotic flow conditions have shown that the rate of platelet deposition increases under increasing shear rate and may or may not occlude the vessel. A thrombosis model that leads to complete occlusion *in vitro* reproducibly has been developed in this work with recording of video, flow, and histology. This model includes porcine whole blood anticoagulated with heparin and flowed through glass stenoses coated with collagen Type I. Visualization of thrombus formation in this model illustrates how platelets adhere to stenoses, form thrombus in concentric striations in the throat, and completely occlude at the throat of stenosis causing flow cessation.

Poiseuille flow in the stenosis region estimates that shear rates were initially between 10,000/s and 40,000/s. Platelet deposition has been quantified using optical and flow modeling throughout the experiment and both methods show reasonable concordance with similar studies. The rate of platelet deposition has been shown to increase with shear rates as high as 40,900/s. The adhesive strength of a platelet on the periphery of the thrombus has also been measured by removing a completely occlusive thrombus from the stenosis surface under elevated upstream pressure.

CHAPTER I

INTRODUCTION

Clinical Relevance

In 2002, 696,947 deaths in the United States occurred due to diseases of the heart, which is 28% of the total deaths [1]. Cardiovascular disease has consistently been the leading cause of natural death in developed nations, of which, 50% are estimated to be caused by sudden death from cardiac causes [2]. 80% of these sudden deaths are caused by acute ventricular tachyarrhythmias often triggered by *acute coronary events* [2]. The surprising feature of these occurrences is that they may occur in persons without previous cardiac symptoms. Most cases of sudden death occur in larger, lower-risk subgroups such as patients with high coronary risk as opposed to patients with previous myocardial infarction [3]. It is the unexpected nature of sudden cardiac death (SCD) that makes the predictions of acute coronary events so important.

SCD has been shown to link to acute myocardial infarction caused by coronary thrombosis or to an arrhythmia arising within a scarred left ventricle [4]. Of 168 cases of sudden ischemic death, a ratio of 2.7:1 cases showed coronary thrombosis [4]. Therefore, an important precipitating event in many cases of sudden death is mural thrombosis that occludes the lumen and restricts blood flow distally. When blood flow is reduced to the heart muscle a low oxygen state referred to as ischemia exists and without return of blood flow, will lead to irreversible infarct in the myocardium. Tissue that is ischemic does not conduct the electrical signals that produce contractions in the heart ventricles, leading to an arrhythmia which causes heart arrest and ultimately death.

One of the most clinically significant problems of thrombosis is when a thrombus forms superimposed on ruptured atherosclerotic plaque, sometimes referred to as *atherothrombosis* [5]. This term describes the combination of both the acute and chronic events in arterial disease [6]. In the heart, acute thrombosis leads to most cases of unstable angina or myocardial infarction through the embolization of thrombi or the formation of occlusive thrombus. Thrombus formation in stenotic arteries is largely dependent on platelet function and the goal of this research is to gain new understanding of the ability of platelets to aggregate under high shear conditions in regions of stenosis.

In coronary artery disease (CAD), the vessel progressively becomes narrowed by the enlargement of a plaque, called an atheroma, in the intimal layer. The atheroma consists of smooth muscle cells, lipids, collagen, elastin, and sometimes calcium deposits. The constriction caused by the atheroma is clinically referred to as a *stenosis* [7]. A stenosis is typically defined by the diameter reduction, as in Equation 1, where D_1 is the upstream diameter and D_2 is the diameter at the throat of the stenosis.

$$\%Stenosis = \frac{D_1 - D_2}{D_1} \times 100\% \quad \text{Equation 1}$$

There are very high velocities at the stenosis throat and one effect is that there is low pressure at the stenosis throat according to Bernoulli's law. This low pressure may in extreme cases be lower than the external pressure [7, 8]. As a result, local collapse in the artery leading to choked flow or in combination with pulsatile flow can cause oscillating compressive stress on the plaque cap [9]. The cyclical compressive stress can lead to fracture fatigue in the surface of the plaque [10, 11].

Thrombus formation is initiated when an atherosclerotic plaque cracks or fissures. In a study of 90 patients that died of ischemic heart disease within six hours of onset symptoms, Davies found plaque fissures in 86, and of these 31 (36%) had thrombus that occluded the artery [12]. He also found intravascular masses of platelets in 27 of the 90 which he thought represented an embolic phenomenon and potential cause of unstable angina. Therefore, atherothrombosis may block at the rupture site or dislodge and block flow in smaller vessels downstream. Figure 1 shows an example of a ruptured plaque with mural thrombus.



Figure 1. Atherothrombosis is commonly found in autopsy studies of heart disease. [13]. The lipid core has been filled with thrombus but does not occlude the lumen.

Pathologists Davies and Falk independently studied coronary lesions that produced unstable angina and myocardial infarction. Both studies concluded that platelet masses are only found downstream of plaques where thrombus has developed [12]. Therefore unstable angina has been linked to embolism from coronary atherothrombosis. Although typically more than one coronary artery has plaques present, on autopsy, it is found that most deaths occur because of the thrombotic occlusion of a single plaque [14].

Falk introduced a concept of ‘dynamic’ thrombosis where the degree of flow obstruction caused by the stenosis varies due to (1) focal vasospasm, and (2) transient platelet aggregation at the site of a severe atherosclerotic stenosis. In 14 out of 15 patients examined during autopsy, he concluded that the period of unstable angina before the final heart attack was characterized by an ongoing thrombotic process where recurrent mural thrombus formation was followed by thrombus fragmentation [15]. Therefore stenosis severity may increase with increased plaque deposits or through repeated mural deposits of thrombus.

Coronary plaque rupture is dependent on the composition and vulnerability of the atheroma. Thrombosis due to plaque disruption is usually seen in plaques with lower degrees of initial stenosis which may not be visible by angiography [16]. Vulnerable plaques are typically soft and have a large core of extracellular lipid, densely accumulated macrophages, and reduced numbers of smooth muscle cells which is covered by a thin cap [17]. Angiographic studies early on demonstrated that nearly two-thirds of all myocardial infarction (MI) originate at atherosclerotic lesions that lack hemodynamic significance [14]. The hemodynamic significance of a lesion is determined by the reduction in cross-sectional area of the stenosis which contributes to the pressure loss [18]. Therefore vulnerable plaques may have initially low percent stenosis yet lead to clinical symptoms.

So how long does thrombotic occlusion take *in vivo*? In a study of 100 subjects who died of ischemic heart disease in less than six hours, Davies categorized the time between onset of symptoms and death with the presence of a thrombus in the coronary artery. He found that 20 died within the first 15 minutes, 65% of which had a thrombus,

and 39 died between 15 and 60 minutes, 77% of which had a coronary thrombus [19]. 20 of the subjects were found dead and the time span was unknown, and 85% of those had coronary thrombus. Sudden death is typically defined as within the first hour, although it is clear that thrombotic occlusion may occur rapidly within 15 minutes.

Whereas SCD may occur within the general population to persons without diagnosed cardiac disease, survival is dependent on immediate attention. The American Heart Association has introduced a ‘chain of survival’ to rescue people suffering from cardiac arrest. The four step process includes early access to medical care, early CPR, early defibrillation, and early advanced care [20]. Defibrillation has been shown to help the electrical heart arrest, but requires either an implantable device or early response with external defibrillation. The matter of the preceding heart attack may still have preventative measures based on inhibiting vulnerable plaques or thrombotic occlusion.

To summarize, the events preceding cessation of flow include plaque cap fatigue, plaque rupture and occlusive thrombosis. Mural thrombus formation may lead to unstable angina or may become occlusive and lead to myocardial infarction. In instances where thrombus formation leads to complete occlusion in a short time span, the patient has less opportunity to be rescued by the ‘chain of survival.’ Therefore understanding thrombus formation to complete occlusion and tailoring therapies to prevent it are valuable solutions to this persistent problem.

Hemostasis and Thrombosis

Thrombosis is a pathological consequence of the normal hemostatic process which leads to formation of a thrombus in diseased vessels that obstructs flow. In the

chain reaction of hemostasis, bleeding is arrested to prevent the loss of blood through the walls of damaged vessels. Hemostasis can be looked at in three phases. First, the vascular phase is triggered by a cut in the blood vessel wall and leads to smooth muscle contraction which reduces the diameter of the vessel at the site of injury. Next, the platelet phase begins when platelets attach to the site of injury and become activated due to the release of chemical factors and local hormones by endothelial cells such as adenosine diphosphate (ADP) and tissue factor. The third phase of hemostasis is the coagulation phase which begins 30 seconds or more after the vessel wall is damaged and the first two phases are initiated. Coagulation leads to a blood clot reinforced with a fibrin mesh which seals off the damaged vessel wall. This phase is promoted by thirteen procoagulant factors and their proenzymes but is also inhibited by anticoagulants such as antithrombin-III, heparin, thrombomodulin, prostacyclin and other plasma proteins [21]. Both the second and third phases of hemostasis are regulated by agonists and inhibitors using a positive feedback loop.

The key player of hemostasis in arteries is the platelet. Platelets are flattened discs that are about 4 μm in diameter and 1 μm thick. In humans, platelets are generated from megakaryocytes in blood marrow that shed cytoplasm in small membrane-enclosed packets [21]. These anucleated packets are cell fragments rather than cells and have a lifetime of 7-10 days before they are removed by macrophages in the liver or spleen. They circulate the vascular system and discriminate between areas of vascular lesion and normal endothelium [6], which may be the only nonthrombogenic surface. Platelets respond to the lesion with three functions with some interplay: adhesion, activation, and aggregation.

Adhesion of platelets occurs on the subendothelium and the atheroma contents using platelet surface receptors, called glycoproteins. The damaged vessel wall is initially covered in a thin monolayer of platelets. Platelets in this stage bind to von Willebrand Factor (vWF) which is a multimeric glycoprotein that acts as a bridge between platelets and subendothelial collagens [22]. Under high shear rates, vWF circulating in the blood system or produced from endothelial cells is required to adsorb on collagen before the initial tethering by platelets by glycoprotein GPIb α can occur [23, 24]. After the tethering, secondary platelet glycoprotein, such as GPIa/IIa and GPIIb/IIIa mediate a more permanent binding [23, 25]. The interaction between platelet GPIb α and vWF is discussed further in the next section about the adhesive strength of glycoproteins.

In the vessel wall, there are many different types of collagen which are extremely reactive with platelets, most notably type I, III, IV, V, and VI [26]. Platelets adhere to collagen via integrin- $\alpha_2\beta_1$ (GPIa/IIa) and GPVI [6]. The surface density of GPIa/IIa has been estimated to be approximately 1000-2000 copies/cell [27, 28].

Platelets become activated by the chemical agonists such as Thromboxane A₂, thrombin, collagen, platelet activating factor (PAF), and ADP or by shear stresses in the presence of vWF, ADP and Ca²⁺ [29]. After activation, platelets change into a spherical shape with cytoplasmic processes, called pseudopods that extend towards other platelets and then platelets begin synthesizing and releasing more ADP, Thromboxane A₂, platelet factors, serotonin, and Ca²⁺ that promote platelet aggregation [21]. Another important process that is triggered by activation is a conformational change in GPIIb/IIIa that allows it to bind to plasma proteins [9]. The process of vWF binding to the GPIb-IX-V complex is also dependent on conformational changes in one or both of the proteins [30].

The GPIb-IX-V complex has four subunits including GPIb α , GPIb β , GPV, and GPIX [31]. The GPIb α subunit contains the binding site for vWF although GPIb β and GPIX are also required to interact with vWF [32].

Aggregation refers to the accumulation of platelets which is necessary for formation of a platelet plug. Under low to moderate shear rates, it may occur with platelet binding using fibrinogen as a bridge or with fibrin (after fibrinogen has been cleaved by thrombin) and GPIIb/IIIa [9]. And in high shear regimes, it has been shown that aggregation requires the binding of ligands including vWF via its RGD binding domain to GPIIb-IIIa [33].

The relative proportion of blood cells in a thrombus is dependent on hemodynamic factors. Under low shear, venous thrombosis tends to have *red clot* consisting of red blood cells, platelets, and fibrin mesh. The difference with arterial thrombosis is that the high shear conditions lead to a more densely packed platelet and fibrin mesh, called a *white thrombus*. The occasional red blood cell may be trapped in a *white thrombus*, but it is primarily composed of platelets and fibrin. The relative proportion of each species may be evaluated from histology or from cell markers used during experimentation.

Although they dominate thrombus formation, vWF and fibrinogen may not be the only necessary ligands in this process. Mice deficient in both vWF and fibrinogen were able to form completely occlusive thrombi in arterioles *in vivo* which was attributed to accumulated fibronectin in the platelet α -granules [34]. Other plasma proteins that support the adhesion of platelets such as fibronectin, thrombospondin, and vitronectin are heavily researched but do not seem to be as dominant ligands as vWF and fibrin(ogen).

The vulnerable plaque and the blood constituents are two key elements in the pathology of thrombosis. A third element, in what is called Virchow's triad, is the hemodynamics that contributes to thrombotic occlusion and cardiac diseases. This component will be studied in this work.

Hemodynamics of Stenoses

High velocities in severe stenoses give rise to very high velocity gradients at the wall because of the no-slip condition. As long as blood flow at the entrance to the stenoses is fully developed, then the velocity profiles may be assumed to be parabolic at the entrance based on Poiseuille flow. The velocity profiles at the throat of the stenosis will be top hat shaped with a blunt distribution of velocities in the central jet and a high velocity gradient at the walls. A strong shear layer develops as a result of the high velocity gradient.

The location of maximum wall shear for steady flow is upstream of the throat of the stenosis in the converging region [35]. The exact location of the maximum wall shear is a function of the degree of stenosis and is independent of the Reynolds number [36]. Although the magnitude of the maximum wall shear rate can be shown to vary by the square root of the Reynolds number [36]. In estimating turbulence, the critical upstream Reynolds number is ~ 300 [37]. Flow separation occurs in the diverging region of stenoses because of the abrupt expansion. In axisymmetric models, this phenomena occurs for Reynolds numbers greater than 10 for severely stenotic vessels ($\sim 89\%$ by area) and greater than 200 for mildly stenotic vessels ($\sim 56\%$ by area) [37].

Strony et. al. determined that peak shear rates *in vivo* may be approximately 90,000/s and that the platelet-rich thrombi that occluded the vessel was attached at the point where shear rate was highest [38]. Platelet adhesion to thrombogenic substrates is shear dependent and accumulation of platelets increases with high shear rates. The time scale of adhesion has been estimated to be on the order of milliseconds [9]. Therefore the adhesion strength of platelets to the substrate must be great enough to offset the high shear rates in the throat.

The formation of thrombus to complete occlusion illustrates the adhesion of platelets under extremely high shear well because as the thrombus progressively narrows the lumen, the shear rates theoretically approach infinity. Folts developed an *in vivo* animal model to study the formation of thrombi and it has been used in a number of relevant studies [39]. Merino et. al. demonstrated that angiographic filling defects or total occlusion occurred in 6 out of 8 severe stenoses (>70% by diameter) which applied approximately 5,000/s shear rate in contrast to 1 out of 14 arteries that occurred in mild stenoses (<70%) [40]. They also concluded that greater depth of arterial injury enhanced platelet deposition and under critical shear conditions may progress to total occlusion. Total occlusion in the Folts model is atypical. More commonly, coronary blood flow reductions (CFRs), that occurred when thrombus formed until flow cessation and then embolized in a cyclical manner, were used to interpret thrombosis [38, 39].

The location of total occlusion is most commonly at the throat of the stenosis. Davies histological evidence that shows thrombi are often found at the apex of the stenosis [19].

In assessing the change in platelet accumulation under shear stress it is necessary to mimic a physiologically relevant substrate along with hemodynamics. Collagen is contained in the basement membrane of the tunica intima and has been shown to cause irreversible aggregation in comparison to damaged subendothelium that has platelet deposition two orders of magnitude lower [41].

Thrombosis is more likely to occur in regions of high shear and in high grade stenoses that have a smaller volume required for thrombus to occlude the lumen. But if these were the only two criteria, then capillaries would be at a high risk of thrombotic occlusion.

Platelet Deposition under High Shear

One way of looking at platelet deposition is in three phases that have been the trend for many experiments with continuous measurement of platelet deposition over time [41, 42]. Figure 2 below describes platelet deposition over time and three phases that tend to occur. A more in depth analysis of these phases may be found in Dr. Wootton's dissertation [43].

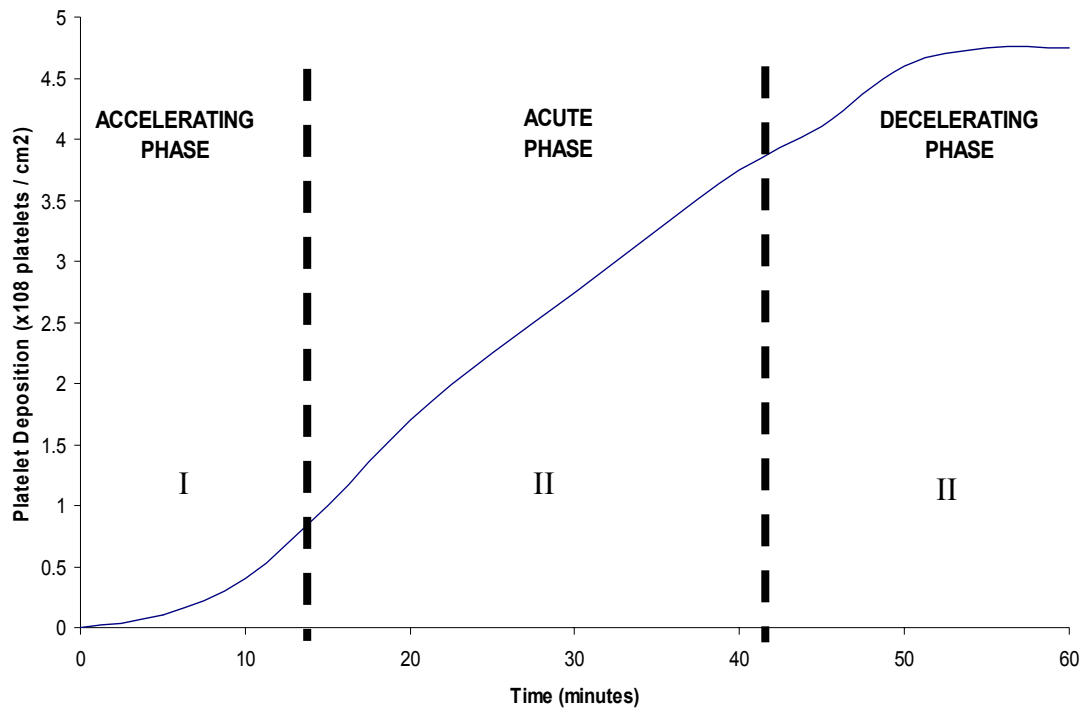


Figure 2. Three phases of platelet deposition over time. Curve interpreted from Markou et al. 50% by area axisymmetric stenosis. Shear rate 900/s. [42]

After an initial delay in the accelerating phase, platelets accumulate at an acute rate until total occlusion or until the amount of platelet deposition reaches a plateau. The decelerating or slow phase may be a result of a state of balance where the rate of platelet accumulation equals the rate of embolization. The acute phase has a linear trend and an acute phase constant can be interpreted from the slope of the curve in this phase. Markou et. al. showed that higher shear in 75% and 90% by area stenoses had greater slope to the acute phase [42]. A number of thrombosis models have quantified platelet deposition onto collagen under high shear regimes. A comparison of these studies is elucidated below with special attention to any complete occlusions observed.

Markou et al. determined that vessel occlusion stemmed from platelet deposition at the apex of the stenosis which corresponded to the highest shear region, as opposed to

the upstream or downstream sides, that had recirculation and low shear [42]. Their experiments included an *ex vivo* baboon shunt with non-anticoagulated blood for two hour observation periods. They measured platelet deposition using ^{111}In -platelet imaging with a gamma camera in collagen coated straight tubes (4mm, 3mm, and 2mm ID) and axisymmetric sinusoidally-shaped stenoses (4mm upstream ID with 50%, 75%, and 90% stenosis by area). Platelet deposition typically led to full occlusion for shear rates greater than 2120 s^{-1} in 25 minutes or less. Shear rates were spatially averaged and reached 7,500/s in the 90% stenosis.

Barstad et al. also noted some areas of thrombotic occlusion in the cross-sectional area of his flow channel, although the average thrombus occlusion only filled half of the area [44]. Non-anticoagulated human blood was perfused *ex vivo* over collagen type III in a eccentrically stenotic flow chamber for 5 minutes. They observed increased platelet deposition between shear rates of 2600 s^{-1} and $10,500 \text{ s}^{-1}$ by morphological analysis, but observed a *drop* in thrombus volume at $32,000 \text{ s}^{-1}$. They concluded that the reduced thrombus growth at the most occlusive stenosis, 89% by area, was due to the high shear stresses that either reduced platelet deposition rate or caused the tear off of thrombus fragments.

Sakariassen et al. in an equivalent flow chamber and thrombosis model showed that thrombus volume increased due to the effect of shear rate up to 2600 s^{-1} [45]. Thrombus volume decreased as a result of anticoagulation with citrate, although platelet adhesion, measured as surface coverage, did increase with citrated blood in comparison to non-anticoagulated. In this study, he used a conversion of 90 billion platelets/mL which was validated in previous work [46].

Badimon et al. found that platelets accumulated on collagen Type I according to a power type curve over exposure time [41]. Interestingly, they concluded that platelets did not reach a saturation level even after long perfusion times of 30 minutes and high wall shear rates of up to 3380 s^{-1} . Their *ex vivo* swine model used heparinized blood with radioactively labeled platelets perfused over deendothelialized pig aorta or collagen strips. In comparison to the damaged subendothelium, they found greater platelet deposition to the collagen surface by two orders of magnitude and an irreversible adhesion of platelets. In the collagen strip experiments, they found occasionally that thrombi ‘completely spanned the lumen of the chamber, without being removed,’ although they did not comment on its repeatability or its dependence on other factors.

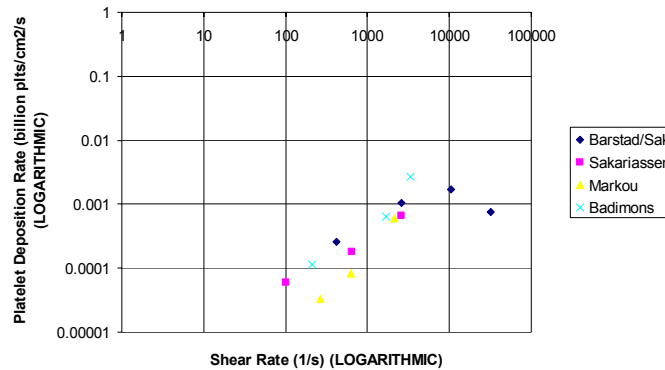


Figure 3. A compilation of platelet deposition onto collagen as a function of shear rate at 5 minutes of exposure time by several investigators. Platelet deposition rate at 5 minutes was calculated from platelet deposition data using a straight line method or differentiation from regression curves. [41, 42, 44, 45]

To summarize, it is known that platelet deposition increases for shear rates ranging from 100 s^{-1} to $10,500 \text{ s}^{-1}$ for perfusion times of 5 minutes. A similar analysis of these studies was done by Dr. Wootton [9]. The one thrombosis model that estimates the

effect of shear rates as high as $32,000 \text{ s}^{-1}$ on platelet deposition is that by Barstad. The reduced thrombus growth in his most occlusive stenosis (89% by area) led him to conclude that the high shear rates may have reduced the rate of platelet incorporation and/or caused the embolization of thrombus [44]. If high shear rates caused reduced rate of platelet deposition then platelets may have saturated their potential to attach in this environment. And if the reason for reduced thrombus volume was due to embolization and this occurred *in vivo*, then the adhesive strength of platelets may be at its threshold. The phenomenon of platelet attachment under high shear stresses does occur *in vivo* therefore understanding the nature of platelets in this scenario is critical.

The rate of platelet deposition from the second phase of Figure 2 may be a useful rate to compare among thrombosis studies because the linear growth of thrombus is dependent on shear. Caution should be taken in order to compare platelet deposition across studies because thrombosis models vary in blood source, anticoagulation and exposure time which clearly have an effect on thrombus formation. Therefore taking the rate of platelet deposition at a fixed time may not capture the maximum rate of deposition under respective conditions. In some of the cases in Figure 3, the maximum platelet deposition rates for a certain time are compared against the minimum for another model. The Barstad and Sakariassen studies only had three data points over time because they measured platelet deposition based on light microscopic morphometry. In the Markou and Badimon studies, radioactively labeled platelets provided a direct measurement of platelet deposition. In these studies, platelet deposition follows an s-shaped curve like Figure 2. Another important comparable amongst these studies and one of the most

clinically relevant endpoints is the eventual total occlusion, which may even be reached at lower shear rates given a long enough time span.

Sukaveneshar and Solen concluded that in the downstream region of stenosis, high shear stress decreased thrombus accumulation and increased embolization because thrombosis was 60% less in stenotic versus non-stenotic flow [47]. In their tubular stenotic flow loop they assessed thrombosis downstream of the stenosis using a substrate that was a stent deployed in PVC tubing and thrombosis was evaluated from the weight of thrombus attached to the stent. Their conclusion may be true for flow in the downstream region but it is not pertinent to clinically relevant thrombus accumulation which occurs at the stenosis throat. The interesting result of their research was that flow disturbances associated with stenoses enhanced embolization from the stents [48]. They measured embolism with a light scattering microembolic detector (LSMD). Embolism can be difficult to quantify and is dependent on the substrate used.

Glass tubes are a versatile way of studying thrombogenesis in stenotic flow because development of thrombus can be visualized by increased translucence as in this work or by fluorescence. Fluorescent labeled antibodies directed against species of interest such as platelets, tissue factor, and fibrinogen can be imaged with fluorescence microscopy. Studies that use intravital microscopy in mice visualize thrombus formation in arterioles which are on the order of 100 μm [34, 49].

Adhesive Strength of Platelets

In recent thrombosis research, one goal has been to measure the strength of the adhesion between platelet receptors and surface ligands at the receptor level. One goal of

this research has been to identify the most important domains on adhesive proteins so that they may be blocked in order to weaken the adhesion strength and reduce thrombosis.

Another outcome however, may be to link the maximum platelet strength with the ability of platelets to adhere under the high shear conditions before total occlusion as described earlier.

The platelet adhesive process is regulated by multiple ligand-receptor interactions. The initial adhesion of platelets is characterized by the spreading of platelets and is mediated by the binding of vWF to integrin $\alpha\text{IIb}\beta 3$ [50]. Research by Yoshioka et. al. demonstrated that platelets with diameter greater than 2.5 μm which represented spread platelets had greater strength and more irreversible adhesion to collagen than non-spread platelets which had a lesser diameter [51]. The time-dependent accumulation of fibrinogen increases the thrombus strength and height resulting in 3-dimensional thrombus development [50].

The adhesion strength of platelets increases under greater initial shear rate. Wu and Sixma perfused platelets onto fibronectin, laminin, fibrinogen, vWF, endothelial cell matrix (ECM), and collagen type III surfaces under different shear rates and then attempted to detach the platelets under various shear rates [52]. They found that at a shear rate of 300/s the firmest platelet attachment was to ECM and collagen III, and then vWF and fibrinogen, and then fibronectin and laminin. Diverse cellular responses are modulated by the surface chemistry of the substrate and may influence the adhesion [53].

Platelet deposition on collagen depends on the concerted involvement of GPIb α , GPIa/IIa, and GPVI [54]. The complete eradication of thrombus formation was achieved in human blood flow over collagen by the coinhibition of GPVI with either GPIb α or

GPIa/IIa [54]. GPVI has been associated with the ‘second wave’ aggregation response under flow, whereas GPIb α and GPIa/IIa mediate the primary adhesion.

The detachment of platelets is approximately linear with shear stress. This was evident in Siljander’s experiments and in experiments by Kumar and Arya who measured the strength of the GPIb α -vWF bond using shear stress under flow and optical tweezers, respectively. Kumar found that ~50% of platelets detached when increasing shear stress from 0.5 to 32 dynes/cm² [55]. Doggett also measured GPIb α -vWF tether bond strengths between 36 and 217 pN with a similar technique of flow dependent adhesion and utilized the Bell model to calculate adhesion force [56]. The Bell model determines the detachment strength by the rupture force between cells. Arya measured the force required to break the vWF-GPIb-IX bond with optical tweezers and determined that it was on the order of 11 pN [57, 58].

Platelet adhesion has been studied at the level of the protein but clinical manifestation is at the macroscopic level. Therefore a study that measures the adhesive strength of platelets under physiological conditions is useful in determining the strength of glycoproteins and the saturation point of a platelet.

Propagating Fibrin tails

In some cases of thrombosis in arterial stenotic flow, a propagating tail of thrombus has been observed distal to the adhered thrombus. Brown et. al. observed propagating thrombus *in vivo* when they administered streptokinase to patients during acute myocardial infarction. When viewed at high magnification, they saw the proximal part of the thrombus adhere to the site of atherosclerotic arterial narrowing in 29 of 32

cases and in 55% of these cases the thrombus extended downstream in a large ‘tail’ of thrombus [59].

In non-anticoagulated ex vivo studies with detailed flow conditions, fibrin tails have also been observed but under different conditions. In Markou’s study, fibrin tails were observed at lower shear 265/s and 630/s (in the 4mm and 3mm straight tubes) and not in higher shear experiments or stenotic experiments [42]. In contrast, the Barstad study observed fibrin tail downstream to the collagen-attached platelet thrombus that was regularly observed for high-shear stenoses (10,500/s and 32,000/s) [44].

Propagating tails may present a hazardous condition because of two possibilities. First, they may lead to blockage of flow near the site of attachment by lengthening the thrombogenic surface by the formation of a windsock or sheet. And second, they may embolize and block flow downstream. Various factors of stenotic flow influence the propagation of thrombus including shear rate and flow separation with a recirculization zone that may increase the residence time of species.

Specific Aims and Hypotheses

(1) Develop an *in vitro* model of occlusive thrombosis in stenoses under high shear.

It is hypothesized that occlusive thrombosis occurs and may lead to complete occlusion under high shear. Porcine blood is harvested, anticoagulated with heparin and perfused through glass tubes with hour-glass-shaped stenoses coated with collagen Type I. Each glass tube has a preexisting stenosis and its severity varies so that higher percent stenoses produce higher shear rates on the blood. Pressure and flow rate measurements as well as

direct visualization are made to determine the occurrence of occlusions which led to flow cessation.

(2) Determine the effect of high shear rate on the rate of platelet deposition until flow cessation. It is hypothesized that the rate of platelet deposition increases with increased shear rate beyond 32,000/s. Platelet deposition is quantified in two ways using a model based on the flow rate measurement and another model based on images of the stenoses region taken during the experiment. Results from these experiments in addition to results from similar studies found in literature are used to address the effect of shear rates of this order on the rate of platelet deposition.

(3) Determine the force required for thrombus detachment. It is hypothesized that thrombus that completely occludes the stenosis is removed at a maximum upstream pressure. The adhesion strength of thrombus attached to the surface is estimated based on a force balance given the maximum pressure recorded, the geometry of the stenosis throat, and the dimensions of the thrombus.

CHAPTER II

METHODOLOGY

Experimental Design

The purpose of this work was to create completely occlusive thrombus under high shear and to measure the force required to detach the thrombus. A flow system with arterial stenotic flow conditions was designed and a model of blood flow rate as a function of percent stenosis was produced and validated for this system. Next, platelet deposition was assessed using the flow rate model and images taken during thrombus formation. This thesis consists of three sets of experiments with some common protocol.

1 – In Vitro Model of Occlusive Thrombosis

This model of occlusive thrombosis in stenoses under high shear was developed to study thrombus formation in the stenosis region. Using this model, a curve of flow rate as a function of percent stenosis was generated by perfusion of water or freshly harvested blood through collagen-coated glass test sections of varying percent stenosis. Therefore given a measurement of flow rate, the model may be used to interpret the area of the lumen after thrombus formation. The flow system was designed to be laminar for water and blood and for flow to be fully developed upon entering the stenotic region. Next, test sections were validated and used with water and blood in order to determine the pressure and flow for various percent stenoses. The effects of collagen coating on the test sections were measured. All test sections that were perfused with blood had color images taken after experimentation in order to identify gross thrombus formation. The

markers for occlusive thrombosis include flow reduction, increased upstream pressure, and microscopic inspection of the appearance of thrombi.

2 - Thrombus Formation until Complete Occlusion at High Shear Rates

The consistent formation of completely occlusive thrombus *in vitro* is uncommon and the purposes of these experiments are (1) to define the factors present and (2) to determine the effect of high shear rates on the rate of platelet deposition. These experiments are an isolated set in which a completely occlusive thrombus formed. Additional steps were made to study the deposition of thrombus over time and the composition of the thrombus. In some experiments grayscale imaging with a CCD camera was used to observe thrombosis in the stenotic region of interest. This data as well as the flow rate model established in the first set of experiments were used to describe platelet deposition over time. Completely occlusive thrombosis was defined by flow cessation and thrombus formation across the lumen assessed by visual inspection.

3 – Detachment Strength of Thrombus

The purpose of these experiments is to remove completely occlusive thrombus and to estimate the detachment strength. Thrombus was detached from the wall by increasing pressure upstream with a syringe pump and recording the pressure with a data acquisition system. The adhesive strength between the thrombus and the surface was estimated based on the maximum pressure recorded at the time of thrombus removal, the dimensions of the thrombus, and the geometry of the stenosis throat.

The following sections specify the common protocol for these experiments. And then specific experimental protocol will be described.

Blood Samples

Whole blood samples were harvested at an abattoir from pigs through a jugular/carotid incision following electro-stunning. The blood was quickly anticoagulated with 1000 USP units/mL porcine heparin (Elkins-Sinn Inc. Cherry Hill, NJ, via Priority Healthcare) at $0.40\% \pm 0.02\%$ v/v. This is equivalent to 4.0 ± 0.2 U/mL of blood, a standard form for comparing heparin anticoagulation. In comparison to other studies this is a low but effective dosage chosen to increase the likelihood of thrombosis. In a similar porcine *ex vivo* experiment, 1.37 ± 0.036 U/mL was used and it was also concluded that the heparin levels reached did not significantly affect platelet deposition results [60]. In human donated blood experiments with an *in vitro* model of platelet deposition on collagen, heparin anticoagulation was 10 U/mL [61, 62]. And in another platelet deposition experiment under stasis conditions, 20 U/mL Low Molecular Weight Heparin (LMWH) was used [28].

The time of harvesting and the exact volume of blood obtained were recorded. From each pig, a blood sample of approximately 1000 mL was collected and typically four samples were taken in order to improve the likelihood that one or more of the samples would not be coagulated or have small aggregates by the time experimentation began. Each sample was numbered 1 through 4 and kept in a thermos during transport to Georgia Tech.

Blood samples were assessed upon arrival at Georgia Tech with regards to the presence of coagulation, floating aggregates and bubbles and the condition was recorded. If a sample was clear of visible fragments, then any bubbles were cleared along the surface of the container using a paper towel. The selected sample was mixed with a nutating mixer (Shelton Scientific) at 42 rpm for 15 minutes prior to experimentation. Blood aliquots were taken before and after experimentation for measurement of hematocrit, platelet count, and mean platelet volume in a Coulter Counter. Experiments were conducted at room temperature and were completed within four hours of harvesting.

Viscosity Determination

Viscosity was calculated based on the hematocrit of each sample. Hematocrit is the relative volume of erythrocytes, commonly called red blood cells, reported as a percentage of the whole blood volume. Hematocrit measurements for each blood sample from a Coulter Counter were used to compute dynamic viscosity based on Einstein's method of combining plasma viscosity and hematocrit (*HCT*) [63]. Einstein's equation is expressed in Equation 2.

$$\mu_{blood} = \mu_{plasma} (1 + 2.5 \times HCT) \quad \text{Equation 2}$$

where μ_{plasma} is 1.7 cP based on the dynamic viscosity of porcine plasma measured at 900/s in a cone-plate type viscometer [64]. This method is an underestimation of viscosity for Hematocrit values in the range of 0.2 to 0.6. The range of porcine Hematocrit values was 0.35 to 0.59. At high shear rates greater than 700/s, whole blood

with hematocrit values between 0.3 and 0.6 has a constant viscosity, making it Newtonian [65]. Therefore at the high shear rates applied in these experiments the viscosity may be assumed to be constant.

Stenotic Test Sections

Glass tubes were used because the material is translucent and the stenosis could be formed with very narrow throat diameters. Pyrex boro-silicate tubes of 1.5-1.6 mm inner diameter (ID) and 65 mm length were drawn by glass blowing at half the length to form varying percent stenosis of approximately 6 mm length. Figure 4 below illustrates the glass test sections.

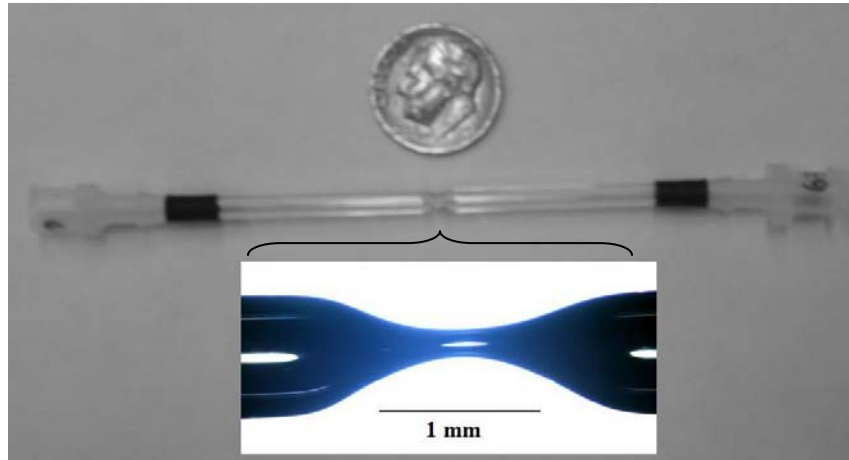


Figure 4. Stenotic test section. Scale of stenosis in comparison to a dime.

The stenosis was axisymmetric and the ends of the tubes were fire-polished in order to smooth out any cracks. The smallest diameter at the throat of the stenosis was measured by analysis of microscopic images with software to calculate distance. Images were taken by a Nikon E600 and the 2x, 4x, and 10x images corresponded to 188

pixels/mm, 376 pixels/mm, and 471 pixels/mm, respectively. Grafula software was used in combination with known outer diameter measurements with calipers to confirm the sensitivity of the inner diameter measurement. Percent stenosis was calculated by *area* as in Equation 3.

$$\%Stenosis = \frac{D_1^2 - D_2^2}{D_1^2} \times 100\% \quad \text{Equation 3}$$

where D_1 is the inner diameter of the glass tube and D_2 is the inner diameter at the throat of the stenosis. The approximate error for percent stenosis by area is 4%, calculated from the resolution of measurements and repeated measurements. For the remainder of this thesis, percent stenosis will refer to percent stenosis by *area*.

Stenoses that had a non-circular cross sectional area in the stenosis were omitted if they did not fit within the standard error of the flow rate as a function of percent stenosis curve in Figure 28 in Chapter III or if they were elliptical by visual inspection. Stenoses that did not fit on the flow rate versus percent stenosis curve were postulated to have elliptical cross sectional area because of the wet parameter.

Test sections were attached to plastic connectors using heat shrink tubing. On the plastic connector, all test sections were labeled with a number for identification purposes. And on one end of the test section, a 'C' was written to indicate that collagen was to be coated from this end making it the downstream side.

Collagen Coating

A collagen stock solution was prepared to be 1000 $\mu\text{g}/\text{mL}$ by diluting 3.1 $\text{mg}/\mu\text{L}$ Type I purified collagen by Vitrogen 100 (Cohesion, Palo Alto, CA) with deionized water. The stock solution was refrigerated at all times. Collagen type I was chosen because it is the predominant type in atherosclerotic vessels [66]. Collagen was coated from the stenosis or midline to the downstream end by injecting 75 μL of stock solution into the downstream side of the test section and leaving it in a humid environment for 15 minutes. Non-stenotic tubes were marked with a black line at half the length which corresponded roughly to the border of collagen coating. Figure 5 below shows the set up for collagen coating.



Figure 5. Collagen was coated in test sections by filling the sections and then letting them dry in a humid environment created by rolled paper towels soaked in hot water in a closed Petri dish.

The collagen concentration was determined to be 1000 $\mu\text{g}/\text{mL}$ in order to saturate the surface of the lumen. In comparison to similar collagen coating techniques for platelet adhesion studies, Ross [62] and Folie [61] used 980 $\mu\text{g}/\text{mL}$ and 850 $\mu\text{g}/\text{mL}$,

respectively. No attempt was made to determine the surface density of collagen fibrils. After collagen coating, the test sections were perfused with 1-4 mL of PBS and laid flat until used in experimentation.

Flow System

For each experiment, 240 mL of the working fluid was transferred into a 500 mL platelet transfer bag (Baxter-Fenwal, Deerfield, IL). For the first experiment of each new bag, typically a non-stenotic control, an additional 10 mL of fluid was added to fill the additional tubing. If fluid remained in the reservoir after one experiment then the required amount was added to return it to 240 mL. The platelet transfer bag was attached to 85 cm of 3 mm inner diameter (ID) vinyl tubing which connected to a three way valve with the test section and the pressure transducer. Figure 6 below shows a schematic of the flow system.

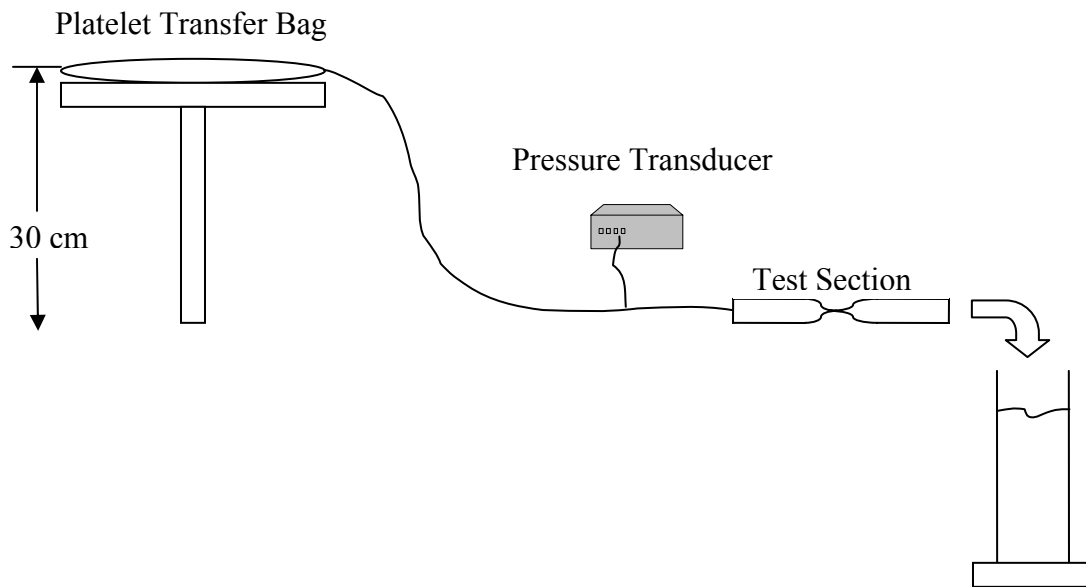


Figure 6. Flow System Illustration.

Pressure upstream of the stenosis was recorded with a pressure transducer (Harvard Apparatus, South Natick, Massachusetts) and flow rate was calculated from measurements with graduated cylinders and a stopwatch, each at intervals of 15 seconds until flow cessation or the contents of the fluid reservoir were emptied. The pressure transducer was calibrated with a water column and the pressure (mmHg) was equal to $0.91 \times (\text{pressure reading}) - 0.56$. Direct observation of the amount of thrombus formation was identified by removing the test sections after experiments and imaging them under a Nikon E600 microscope. In cases where emboli or thrombus completely occluded the throat, images were taken without removal of the blood. In cases where complete occlusion did not occur, test sections were perfused with 1-4 mL of formalin by dripping the solution through the sections.

The platelet transfer bags used as a fluid reservoir were donated by the American Red Cross of Atlanta and were used because of PL 146 plastic surface, zero contact between blood and air, and disposability. The fluid reservoir laid flat and was elevated 30 cm above the plane of the pressure transducer and stenosis because both water and blood had laminar flow in high grade stenoses at this height. If the reservoir was reduced by 220 mL, the height of the fluid reservoir changed by 1.5 cm during the experiment. This corresponds to 1 mmHg pressure change and since this is within the error of the pressure measurements, the pressure change may be considered insignificant until the reservoir is empty.

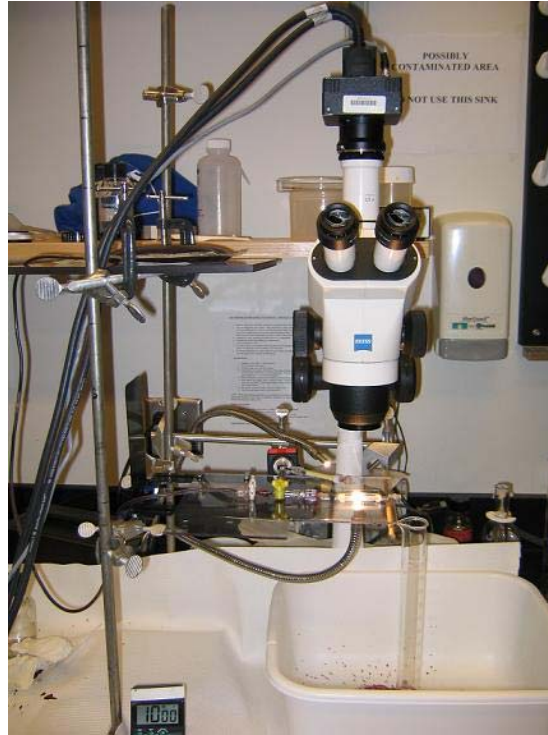


Figure 7. Experimental set up shows two platforms separated by 30 cm, with a graduated cylinder and a stopwatch below. On the middle platform, the test section is illuminated by a light source arranged below and a microscope with an attached CCD camera is positioned above it. Experiment photographed December 15, 2004.

Cleaning and Sanitization

Platelet transfer bags, tubing, and 60 mL syringes were disposed of after completion of experiments with each blood sample. Pressure transducer parts and test sections were cleaned with bleach and hot water until November 30, 2004. After this time, test sections and any additional equipment were sanitized in a Branson Sonicator 1210 (Branson Ultrasonic Cleaner, Danbury, CT) with Cidex solution (Advanced Sterilization Products, Irvine, CA). Cidex solution was diluted with water to a 1:4 ratio and disposed of after each use. The Cidex stock solution was disposed of after 14 days as recommended by the manufacturer. Often the plastic connectors and heat shrink tubing

would disconnect from the glass tube during sonication therefore test sections were sonicated one a time to prevent confusion in identification.

Water Flow Experiments

Water was perfused through each test section in order to (1) determine the height of the fluid reservoir and (2) generate a flow rate curve dependent on the percent stenosis of each test section. For each test section manufactured, excluding those that were visibly eccentric, two experiments lasting 2 minutes measured the flow rate and upstream pressure at 15 second intervals. 2 minutes was sufficient because it was the time elapsed before non-stenotic tubes had emptied 200 mL and had an approximately constant upstream pressure in this period. The average flow rate and standard deviation were calculated for each experiment and then the average of the two experiments was used to generate a curve of flow rate as a function of percent stenosis. The flow rate curve was used to verify that the measurement of percent stenosis corresponded with the flow rate measured. Test sections that had flow rate measurements that did not fit the general trend of the flow rate curve were measured a second time for percent stenosis and inspected to determine if the throat of the stenosis had a non-circular cross sectional area.

Blood Flow Experiments

Whole blood was perfused through the flow system until the fluid reservoir was emptied or flow cessation occurred. The fluid reservoir was refilled with the volume perfused after each experiment using a 60 mL syringe. Blood that had been perfused was disposed of according to Georgia Tech Biohazardous Waste Protocol and was never

recirculated. If experiments lasted longer than approximately 8 minutes then the platelet transfer bag was gently massaged every few minutes to keep the blood from separating. For each blood sample, a non-stenotic tube was used first until bag drainage as a control before perfusion of stenotic tubes. Experiments that had a non-stenotic experiment which had a change of upstream pressure equal to 2-3 mmHg before 200 mL of blood was perfused were omitted. All experiments were performed at room temperature and were completed within approximately four hours of harvesting.

Experiments were identified by a sequence of four numbers separated by periods or dashes. The first two indicate the month and day of the experiment. The third number identifies the pig sample, 1 through 4, and the fourth corresponds to the number of the test section.

Once a test section was perfused once, it was not reused on that day so that it could be cleaned sufficiently. When emboli caused a blockage in the stenotic test section, the experiment was completed and no attempt was made to continue testing. After two experiments had emboli, it was concluded that the sample was deficient and another blood sample was used.

In order to be fully developed by the time blood reaches the stenosis, the inlet length of the glass tube must match the inlet length required by Targ's equation [67], presented in Equation 4.

$$\frac{L}{R} = 0.16 \text{ Re} \quad \text{Equation 4}$$

where R is the tube radius, Re is the Reynolds number, and L is the inlet length required for fully developed flow. This is roughly 10 times the diameter.

The Fahreus effect may be excluded in this analysis because under the designated flow conditions the relative hematocrit in the tube is constant for all reservoir hematocrits [65]. Whereas the hematocrit is constant, it follows that the apparent viscosity should also be constant. In tubes, the apparent viscosity decreases with decreasing blood vessel diameter due to the Fahreus effect of lower tube relative hematocrit especially with hematocrits less than 0.3 and tube diameters less than 100 μm [65]. In these experiments, the hematocrit of blood samples was between 0.35 and 0.59 and the smallest initial diameter at the throat of the stenosis was 310 μm .

Average flow rates and average upstream pressures were calculated based on the time period when the change in pressure was < 1 mmHg for test sections with a stenosis and based on the time period when the volume perfused was less than 200 mL for non-stenotic test sections. Therefore the time period would last from the beginning of flow measurement until the change in pressure was ≥ 1 mmHg for more than one measurement. During this time period, the flow could be considered to be conserved.

During experiments that lasted longer than 10 minutes, the blood bag required mixing by gently massaging every 8-10 minutes. The time of each mixing was noted in the lab notebook. In a few experiments, when the bag was not mixed and the blood separated so that plasma was flowing through the tube, the upstream pressure decreased and the flow rate increased.

Thrombus Formation Imaging

Grayscale images of the region of stenosis or of the midline marking in non-stenotic test sections were taken on the same 15 second interval as pressure and flow data were recorded. Images were acquired with a Basler 504k CCD camera mounted to a Carl Zeiss Stemi 2000-C microscope with a 2.5x extension. XCAP for Windows was used to snap pictures until 2-4 minutes after flow cessation. Test sections were placed in an oil immersion chamber filled with glycerin (Refractive Index = 1.47, matching Pyrex glass) in order to obtain two dimensional views of thrombus formation in the stenoses. For data up to and including December 20, 2004, the microscope was set to 1x magnification corresponding to 260 pixels/mm. For experiments after that, it was set to 1.6x magnification corresponding to 420 pixels/mm.



Figure 8. Image of thrombus formation visualization set up. A CCD camera on the microscope is attached to a computer with imaging software. Equipment photographed December 15, 2004.

For these experiments, after blood flow was initiated by opening the valve from the reservoir, the equipment was adjusted so that the stenosis was centered with the camera and the light source. In some cases, this took up to thirty seconds. Once adjusted, the stop watch was started and measurements of pressure and flow began. The light source was a twin head lamp by Reichert:Jung (Cambridge Instruments Inc., Buffalo, NY) which has two flexible heads that may be bent into position. The head of one of the lights was positioned under the platform that held the test section and was pointed straight up towards the camera. The circular head was positioned so that the center coincided with the center of the stenosis or midline for non-stenotic tubes. Light intensity was determined by increasing the intensity until the walls of the lumen could be seen clearly using live imaging.

In all cases, these images were made into movies by importing image sequences into Apple QuickTime version 6.3. A selection of these movies can be found in Chapter IV.

Thrombus Removal Experiments

These experiments measured the upstream pressure required to remove thrombus stuck in the stenosis throat. Using a syringe pump, upstream pressure was increased slowly until flow returned in the stenosis in an effort to detach the thrombus from the wall. A Harvard Apparatus (South Natick, MA) withdrawal/infusion pump was used to raise the pressure at a constant rate and the changes were measured with a pressure transducer upstream of the stenosis. A 5cc syringe was used in the infusion syringe pump and the flow rate was determined by the gear used. In the 12-1 and 12-15 experiments,

the flow rate was 0.68 mL/min configured in 4th gear at 100% speed; and in the 12-8 experiments, the flow rate was 0.34 mL/min configured in 5th gear at 100% speed. These experiments were conducted following blood flow experiments that led to complete thrombotic occlusion. All thrombus removal experiments were completed within six and a half hours of blood harvesting and were done within three hours of the thrombotic occlusion.

The output voltage of the pressure transducer was recorded and converted into units of pressure using a data acquisition system. A LabView program called DAQ_ANAL was used to record the voltage input and convert the value to pressure in units of *mmHg*. Therefore the raw data was output as upstream pressure at a given time and recorded every 2 milliseconds for half a cycle. The data acquisition system was triggered to record half of a cardiac cycle, therefore if the cycle designated was 0.8 seconds then the data would be recorded every 2 milliseconds for 400 milliseconds and then stop recording for the next 400 ms. In order to obtain a continuous pressure curve for this steady flow experiment, data during the second half of the cycle was found by interpolating between each set of recorded data using the last and first data points available. The program was configured to have a 0.0117 Volt/mmHg input gain in order to convert to pressure.

The pressure transducer used was another by Harvard Apparatus (Harvard Apparatus, South Natick, Massachusetts) and it was calibrated to determine if it was linear even at high pressures. Using a 7 meter water column with measurements every 20 cm, the pressure transducer was determined to be linear in the range of 0-500 mmHg, as shown in Figure 9 below.

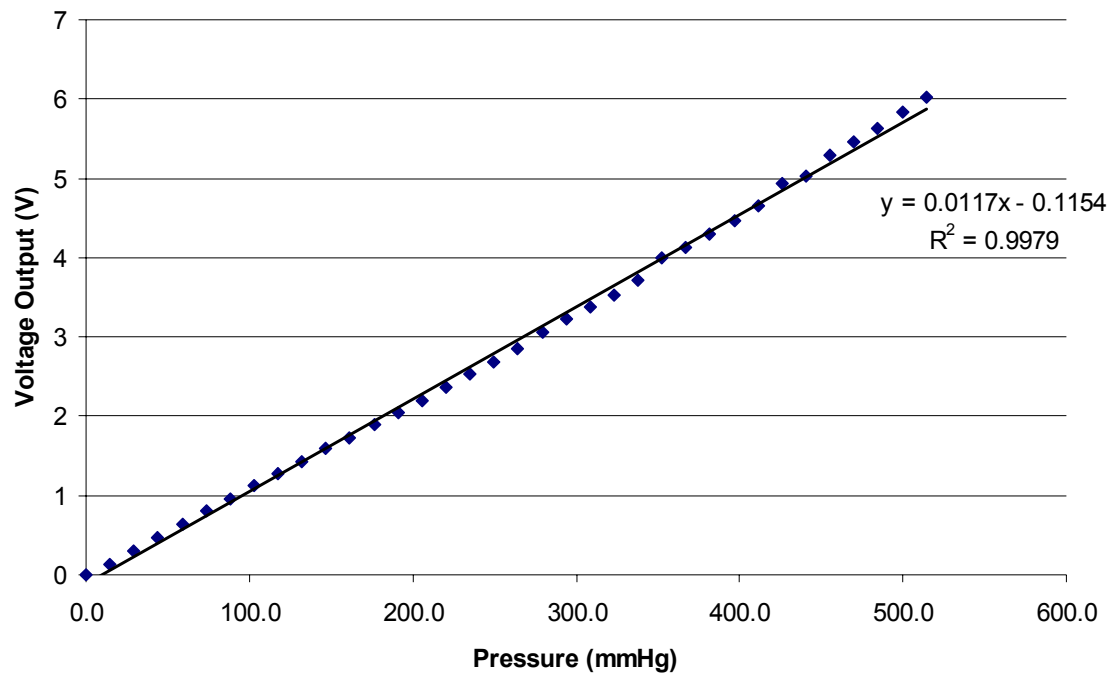


Figure 9. Pressure transducer was linear in the range of 0-500 mmHg.

The circuit board which connected the data acquisition system had a 5 Volt threshold, therefore the pressure transducer was zeroed at a negative value in order to increase the range of the pressure measurement. If the pressure transducer was zeroed at -170 mmHg then the maximum pressure threshold was around 650 mmHg.

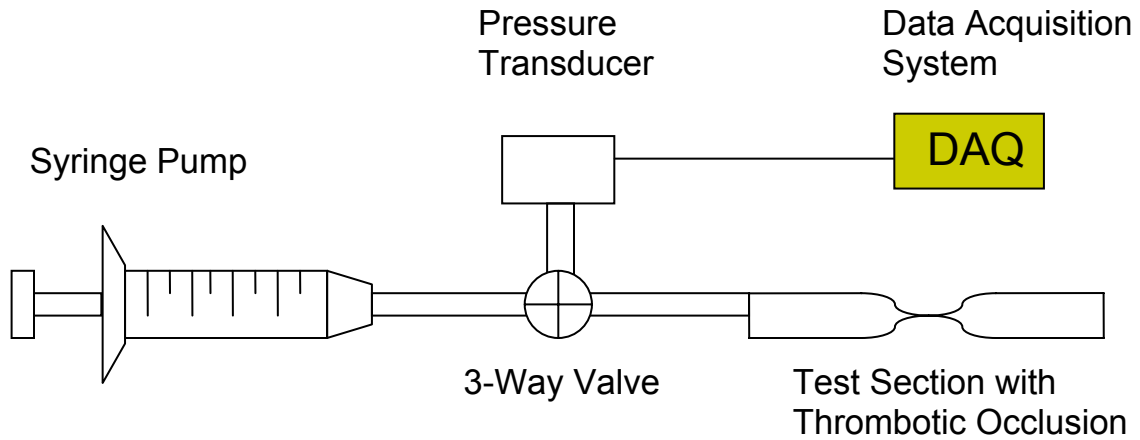


Figure 10. The thrombus removal system.

The flow system, illustrated in Figure 10, consisted of the pressure transducer connected to a three way valve which connected the stenotic test section and the syringe pump. The flow system was filled with porcine blood and before attaching the test section, pressure was relieved by opening the atmosphere end of the pressure transducer tubing and zeroing the transducer. Once the test section was firmly screwed on, the tubing on the atmospheric end of the pressure transducer was pinched and a cap was fastened. If the cap was fastened correctly, then the pressure transducer would read the same as when zeroed. If the cap was fastened incorrectly, then the transducer would no longer be zeroed because the cap applied a pressure to the closed system.

Histology

Samples of thrombus and embolus were fixed in formalin 10% (VWR International, West Chester, PA) for at least 72 hours after removal. Typically, formalin fixes at a rate of 1mm/day, therefore for large sections 72 hours was sufficient. The 10%

concentration was used because it was found to be more sensitive to cardiac tissue than glutaraldehyde. Samples were identified by the experiment number. Samples were processed and embedded in paraffin in the IBB Histology Lab. Paraffin resin is good because it does not impair the morphology like freezing. Deformation of the samples during processing may be up to 25%.

Samples were cut into 5 micron thin sections either longitudinally or by cross-section. Carstairs stain was used to identify platelets, white blood cells, red blood cells, and fibrin. In order to detect expression of von Willebrand factor, an anti-human vWF primary antibody (Sigma Product No. F 3520) was also used in an alkaline phosphatase detection system. Staining for most samples was done with a rat heart sample as a control because it had a clot with red blood cells and some platelets and fibrin. A coagulated porcine blood sample from this blood source was also prepared as a control in order to determine the composition of a clot without shear involved. Each sample has at least two slides with sections corresponding to three areas of the sample. Each slide has 10-20 sections that were each 2 μm thick. In the 12.8.1.9 sample, the downstream side was indicated and each slide was separated by 100 μm . This was the only sample with orientation information.

Information on the composition of occluding thrombi and emboli was determined from image analysis of histological sections. Images were acquired using a Nikon E600 microscope, a digital camera and Q-Capture software. In order to quantify the volumetric proportion of species in the thrombi or emboli samples, images were analyzed with ImagePro Plus. The original RGB image was segmented based on four color shades and 2-8 indices around that shade. After color pixels that represented a cell type were

segmented, they were isolated by changing them to white and the rest of the image to black. And finally, the number of white pixels was counted with the Matlab code in Appendix A-2. Whereas Carstairs stain shows a lavender color for mix of platelets and fibrin, the indices selected also overlapped. The total number of pixels counted was used to normalize the species giving a relative proportion of each species.

CHAPTER III

RESULTS: MODEL OF OCCLUSIVE THROMBOSIS

IN STENOSES UNDER HIGH SHEAR

Thrombus formed in stenotic test sections under arterial flow conditions became occlusive and in some cases led to complete occlusion at the throat of the stenosis. High grade stenoses had significantly more thrombus formation than non-stenotic control test sections and mild stenoses (defined as stenosis < 80% by area). The flow system produced fully developed blood flow at the entrance to the stenosis and in the stenosis throat the Reynolds number was approximately 130 and shear rates were in the range of 10,000 - 40,000, which is representative of stenotic flow in coronary arteries. Other blood flow parameters compared to normal coronary flow are shown in Table 1 below.

Table 1. Comparison of *in vitro* model to coronary flow parameters [9].

Vessel	Inner Diameter (mm)	Average Flow Rate (mL/min)	Upstream Pressure (mmHg)	Reynolds #	Wall Shear Rate (1/s)
Non-Stenotic Tube	1.5-1.6	31.4	13.5	120	1,500
85% Stenosis (Throat)	0.61	18.0	16.7	182	13,500
Left Main Coronary	4	174	80-120	240	460
Right Coronary	3.4	102	80-120	150	440

This *in vitro* model had Reynolds numbers and shear rates representative of arterial flow. Although the flow rates were much lower than in coronary arteries, the diameters were also lower which caused equivalent viscous forces in the region of

stenosis. Shear rates were estimated from Poiseuille profile. The non-stenotic tube in Table 1 has presented the average flow rate and upstream pressure for non-stenotic experiments ($N = 31$) and the 85% stenosis has presented the same information for a stenotic test section ($N = 7$).

Both water and blood were used in this flow system and their data overlapped when their corresponding flow rates were normalized by their dynamic viscosity. When the normalized flow rates were presented as a function of percent stenosis, then the overlapping curves showed that flow was approximately constant given percent stenosis $\leq 60\%$ and then it declined approximately linearly until zero flow when the percent stenosis was 100%. Based on this characterization, a model was proposed that used a reference measurement of flow rate, normalized by the viscosity, and solved for the percent stenosis for stenoses $> 85\%$. The effective inner diameter of the stenosis throat changed during thrombotic occlusion but was solved for based on new calculation of the percent stenosis. This technique of monitoring thrombosis dynamically demonstrated that thrombus formation became occlusive and increased resistance in this model.

Blood Flow Experiments

Porcine blood experiments had a greater standard deviation in their flow rates than water due to the variations in viscosity between blood samples. In porcine blood, the average hematocrit value was 0.468 ± 0.055 for 35 experiments. The standard deviation was as much as 12% of the hematocrit. The average dynamic viscosity was $3.3 \text{ cP} \pm 0.1 \text{ cP}$ based on calculation from Einstein's method presented in Chapter 2, Equation 2, although each respective viscosity was used for each calculation.

The data of blood flow in this analysis comes from all blood flow experiments over collagen at a 30 cm reservoir height with the exemption of experiments that had embolus blockage within the first minute and non-stenotic controls that had pressure changes greater than 3 mmHg before 200 mL was perfused, unless otherwise stated. This includes three days of experiments that had 5.0 U/mL heparin anticoagulation as opposed to the standard 4.0 U/mL in the other twenty-three days. The higher heparin dosage did not seem to have an effect on thrombus formation whereas non-stenotic controls showed thrombus consistent with other controls. In one high grade stenosis, thrombosis led to complete occlusion under the higher heparin dosage, although flow cessation occurred later than average.

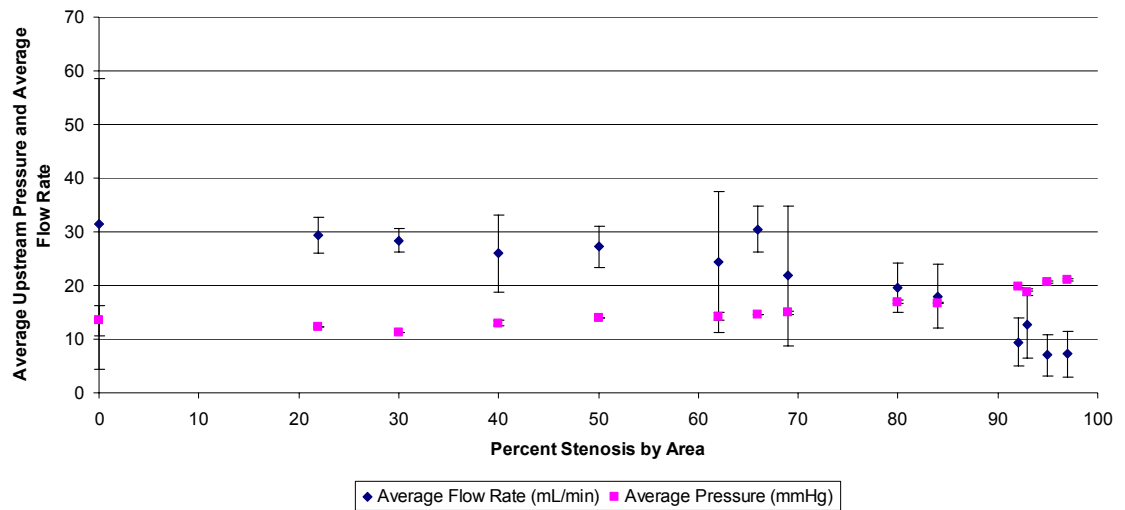


Figure 11. The average flow rate and average upstream pressure for blood experiments over collagen. Values reported as mean \pm 1 S.D. (σ).

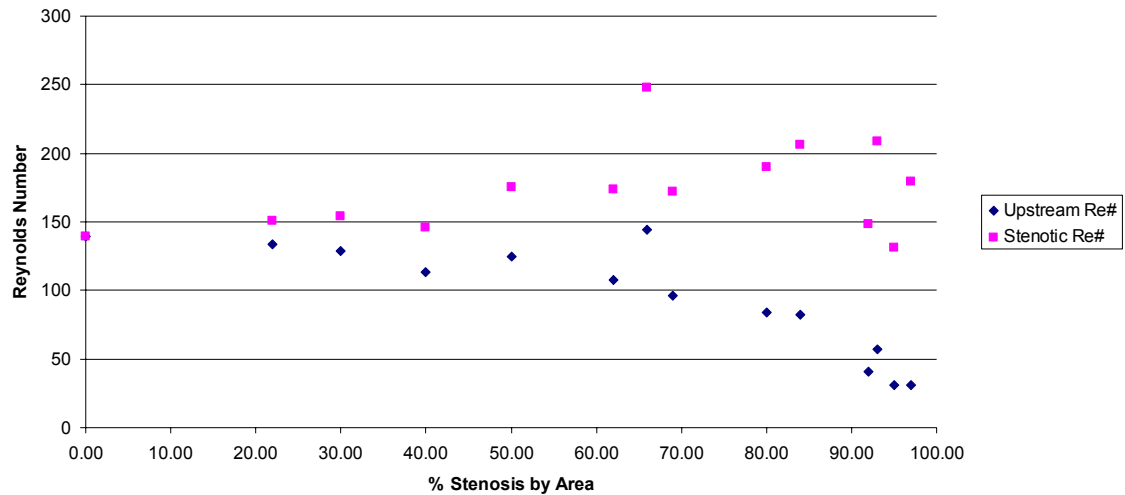


Figure 12. Average Reynolds numbers (Re #s) for blood flow experiments over collagen.

The flow was considered to be fully developed upon entering the stenotic region because the inlet length required by Targ's equation, in Chapter II Equation 4, was less than the length of the upstream side of the glass tube. From Targ's equation, the inlet length was 1.8 cm based on the upstream Reynolds number of 140. This entrance length was satisfied since the glass tubes had at least 3 cm before the stenosis.

Each experiment was classified as not occluded (N), occluded due to embolus stuck in the stenosis throat (E), or occluded as a result of thrombotic occlusion (TO). Emboli were distinguished by an abrupt increase in pressure equal to or greater than 4 mmHg or occlusion occurring within the first 5 minutes. To ensure that clotting occurred in the glass tube and not simply coagulated in the supply tubes, flow was confirmed after the stenosis was removed. Figure 13 below demonstrates that the occurrence of complete occlusions as a result of emboli or thrombosis increased with percent stenosis.

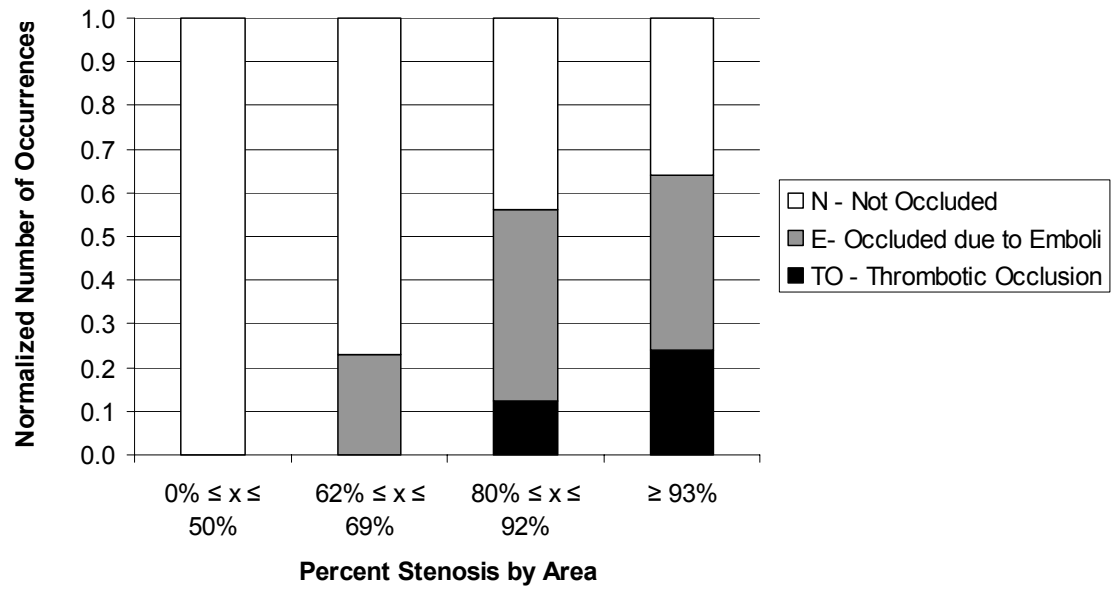


Figure 13. Occurrence of complete occlusion increased with % stenosis.

The number of occurrences of each category was normalized by the total number of experiments in each range of percent stenosis. In test sections with $\geq 93\%$ stenosis, thrombosis led to complete occlusion in 5 out of 25 experiments. And in the second range, 2 out of 7 experiments led to complete occlusion in an 85% stenosis. The number of test sections in each range used was 36, 26, 16, and 25 in order of increasing percent stenosis. This histogram was developed from data of all blood flow over collagen with the exemption of experiments that had embolus blockage within the first minute and non-stenotic controls that had pressure changes greater than 3 mmHg before 200 mL was perfused. Therefore, the total number of blood experiments was greater than the 103.

Effect of Increased Percent Stenosis

Occlusive thrombosis in stenoses under high shear was achieved using collagen-coated glass tubes and porcine blood anticoagulated with heparin. Increased percent stenosis and hence, greater shear, led to greater thrombus formation evaluated on a gross scale. Under the microscope, thrombus was visualized on the collagen coated sections of the lumen and was especially evident at the beginning of the collagen coating surface and at the throat of the stenosis, as seen in Figures 23 and 15, respectively. Often, thrombus accumulated in the converging region of the stenosis as well.

In each of the following examples, pressure and flow data were for experiments that correspond to the images provided. These microscopic images provided a sufficient means to study gross thrombus formation. These images were representative of the majority of the experiments they described and they were not been modified with the exception of some cropping in the 2x images. In 2x images, the perimeter of the light source was visible.

Severely Stenotic Experiments

Stenotic test sections $\geq 80\%$ remained patent or completely occluded due to emboli or thrombotic occlusion which occurred at the throat of the stenosis. In experiments that had thrombus formation to complete occlusion, the pressure increased over a few minutes each time in steps which corresponded with lower flow rates during these periods. The formation of a completely occlusive thrombus may be understood from these indications in measurements of the pressure and flow as in Figure 14.

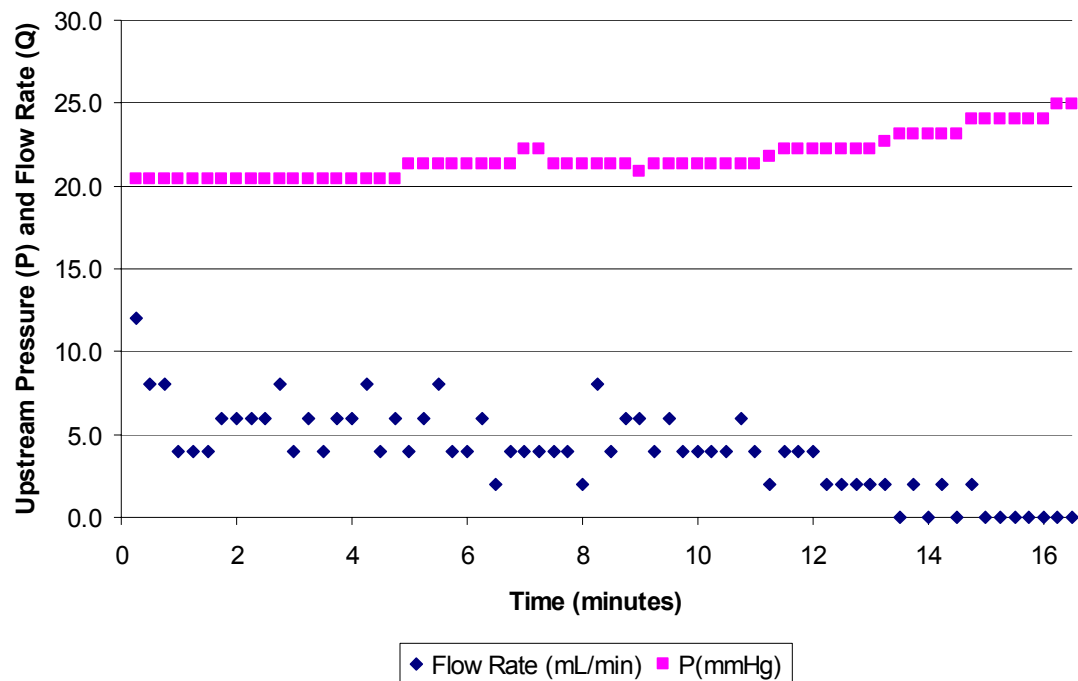


Figure 14. 95% stenosis. Flow rate decreased to zero as the upstream pressure increased due to thrombus formation in the stenosis. Average flow rate was 6.1 ± 2.1 mL/min for the first 4 minutes and 45 seconds.

Precision errors on all flow rate and pressure measurements were ± 2 mL/min and ± 1 mmHg, respectively. Observations were made during the experiment because the thrombus that formed in the throat could be seen by the naked eye. The first thrombus appeared on the diverging side of the throat and it waved in the flow, eventually spreading throughout the throat. Flow cessation occurred at about 16 minutes, although 0 mL/min flow was measured from about 15 minutes because the 0.5 mL resolution of the graduated cylinder was not small enough to measure single drops. Figure 15 below shows the completely occlusive thrombus in the throat.



Figure 15A. 95% stenosis. 2x magnification. Throat diameter was 350 μm . Thrombosis led to complete occlusion. Thrombus volume may be visualized because it is translucent. Whole blood is opaque and it inhibited view of the whole thrombus.



Figure 15B. 95% stenosis. 4x. Thrombus completely crossed the lumen only in some areas.

The images in Figure 15 were taken within one hour of the experiment. In many imaging sessions that took place after one hour, the stagnant blood in the test section separated and more thrombus could be seen.

In many experiments, flow cessation occurred as a result of emboli that were in the blood and blocked at the throat of the stenosis. Emboli were distinguished by an abrupt increase in pressure equal to or greater than 4 mmHg or occlusion occurring within the first 5 minutes. To ensure that clotting occurred in the test section and that

flow was not simply blocked in the supply tubes, flow was confirmed after the stenosis was removed. The pressure ramp and flow cessation in Figure 16 below demonstrated a typical experiment where an embolus caused flow cessation.

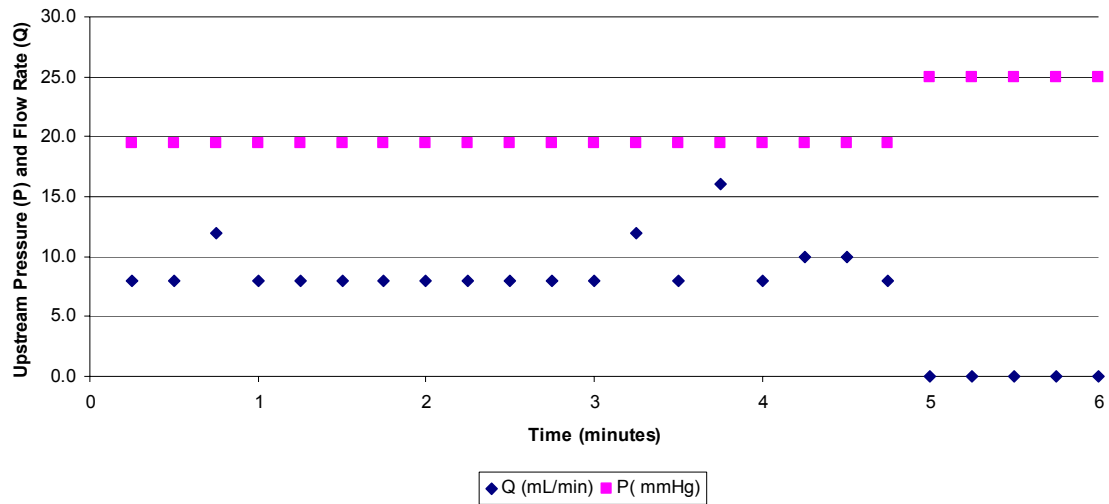


Figure 16. 92% stenosis. Pressure ramp at 5 minutes demonstrated the blockage caused by embolus that led to flow cessation. Average flow rate was 9.1 ± 2.1 mL/min for the first 5 minutes.

With the exemption of a few experiments, emboli blocked flow in the throat of the stenosis. This was the narrowest section of the flow system and emboli occurred especially in high grade stenoses. The particle could be observed in the throat, but the first indication was always the upstream pressure. Experiments that had emboli after the first minute were used for the model of flow as a function of percent stenosis described in the following section.



Figure 17. 92% stenosis. Embolus is visible in the throat. Whole blood is opaque and inhibits view on the sides.

The composition of embolus was evaluated with histology for one experiment in a 95% stenosis. The embolus was fixed in formalin, embedded in paraffin, sectioned by cross section and stained with Carstairs to identify blood species. In a color image, seen in Figure 18, white blood cells are dark purple circles, red blood cells are red, fibrin is purple, and platelets are blue. Note that in this sample embolus there are no red blood cells.

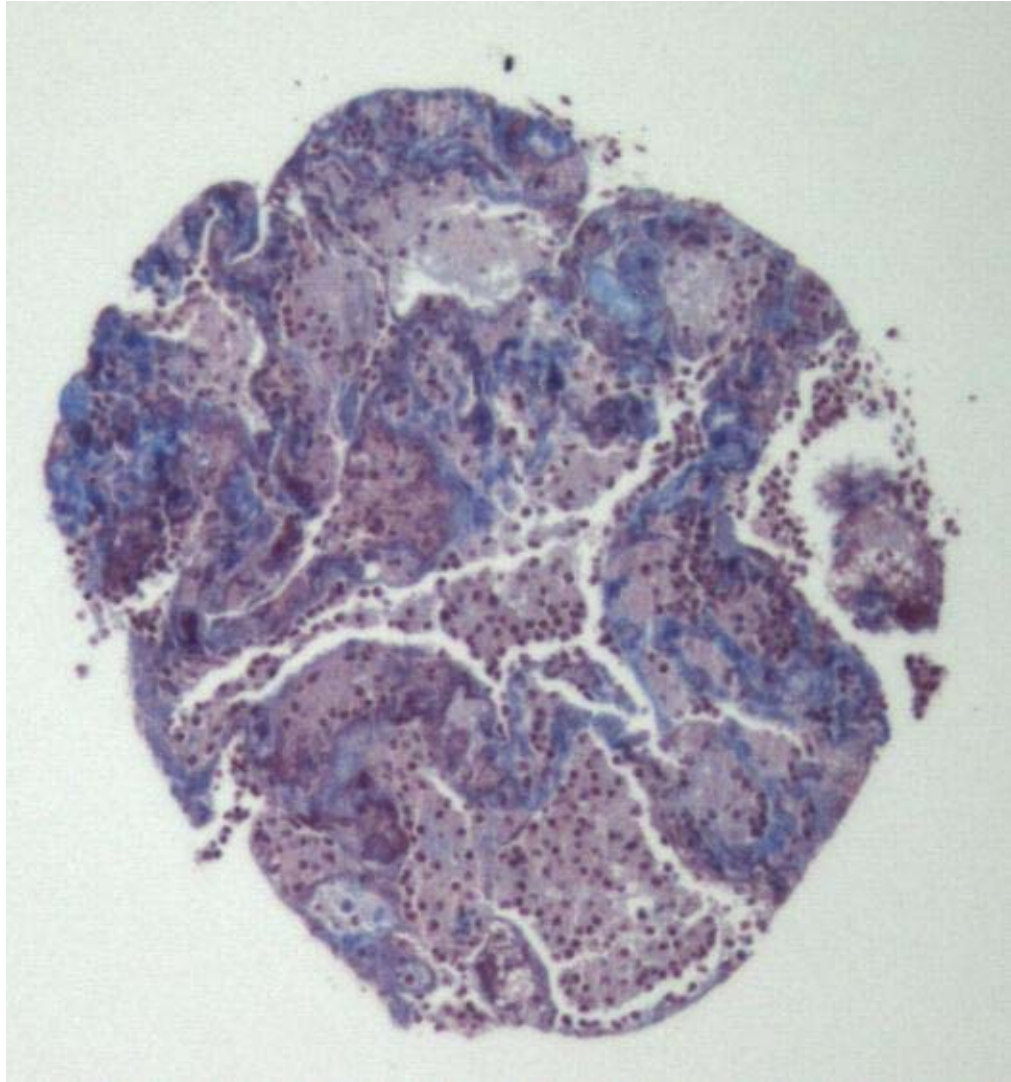


Figure 18. Sample embolus sectioned and stained with Carstairs demonstrated that the embolus was a platelet aggregate without red blood cells. Relative proportion of species: WBC 12%, fibrin 37% and platelets 51%. Sample 11.17.2.7.

Mildly Stenotic Experiments

For stenoses less than 80% stenotic by area (~55% by diameter), some thrombus was evident from microscopic inspection after experimentation. Thrombus formation was generally focal in nature. The lumen of the < 80% stenoses remained patent, however, or blocked as a result of emboli. For these experiments, the upstream pressure was only slightly greater than the non-stenotic tubes but the flow rate had much less

fluctuation. The increased resistance of the stenosis seemed to damp flow rate. Flow in these experiments dripped from the outlet of the test section.

Figure 19 below shows how the upstream pressure and flow were affected by thrombosis. The average flow rate for this experiment was 21.7 ± 2.6 mL/min calculated over the first 5 minutes and 45 seconds, which was the time period when the upstream pressure changed less than 1 mmHg. Pressure increased by 1 mmHg at 6 minutes as a result of thrombus formation in the stenosis. In experiments with less thrombus, the upstream pressure remained constant. Images of the thrombus are in Figure 20 after the test section was perfused with formalin as a fixative.

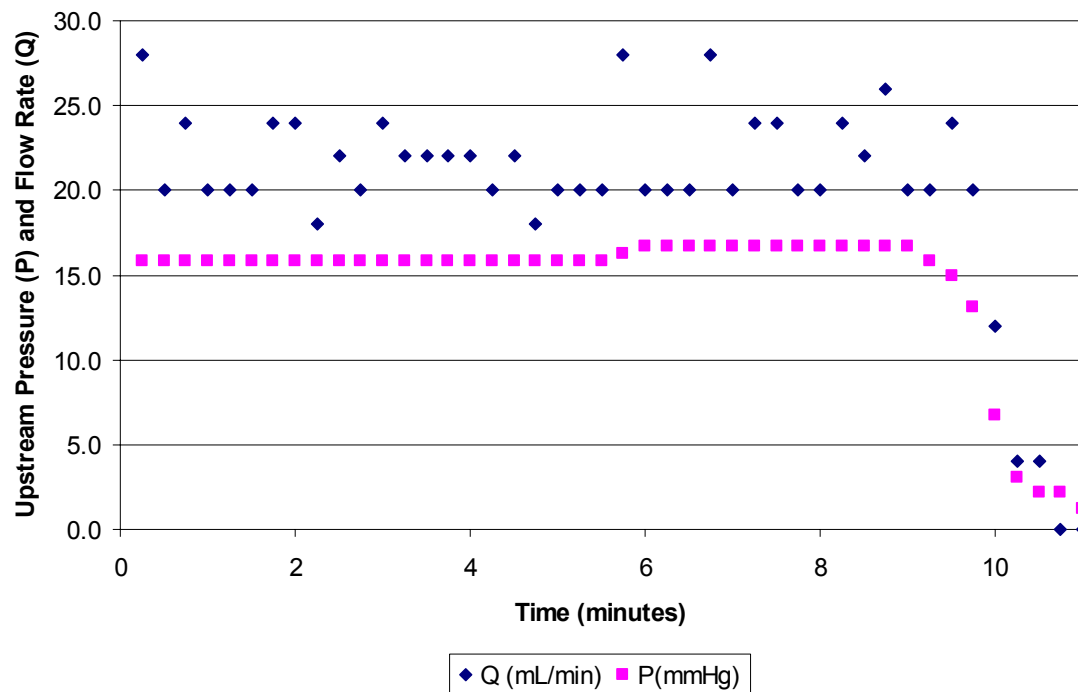


Figure 19. 69% stenosis. Pressure increased around 6 minutes due to thrombus formed in the stenosis which increased the resistance.

Inspection of the stenosis revealed that almost the entire collagen coated surface was covered with thrombus. Flow was from left to right and on the left hand side of the upstream image in Figure 20A, a large amount of thrombus is apparent. In Figure 20B, some of the surface at the throat was clear of thrombus which may have been removed during flow. Focal deposition of thrombus in the throat of the stenosis typically had circumferential striations like the two visible on the right hand side. To illustrate this feature further, Figure 21 shows the trend throughout the throat of the stenosis.

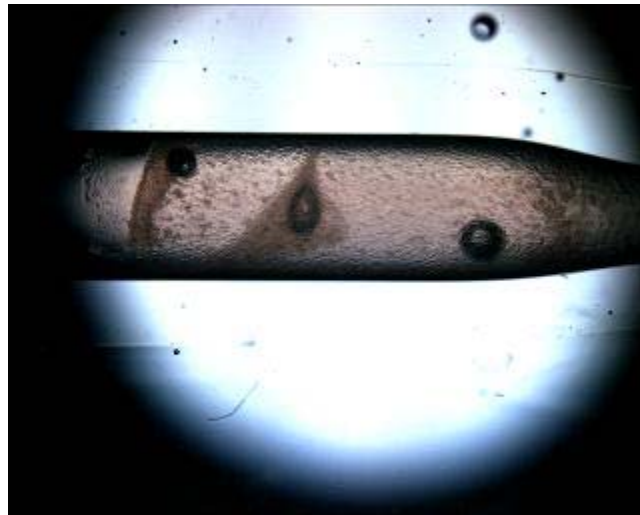


Figure 20A. 2x magnification. 69% stenosis. Upstream side of stenosis showed large amounts of thrombus at the border of collagen coating and was scattered throughout. Some bubbles in the lumen and in the oil-immersion bath were also visible.



Figure 20B. 4x magnification at the throat of the stenosis showed that some surfaces were completely clear of thrombus which may have been removed in flow.



Figure 20C. 10x magnification. Close up on the border between the cleared surface and thrombus. Image was magnified from Figure 20B at the top portion. Note the two circumferential striations of thrombus on the right hand side.

Thrombus formation was non-uniform along the length of the stenosis. The thrombus volume was great enough to occlude the pathway of blood and cause an increase in upstream pressure. Figure 21 presented another experiment where parallel bands of thrombus, called striations, formed along the circumference of the walls.

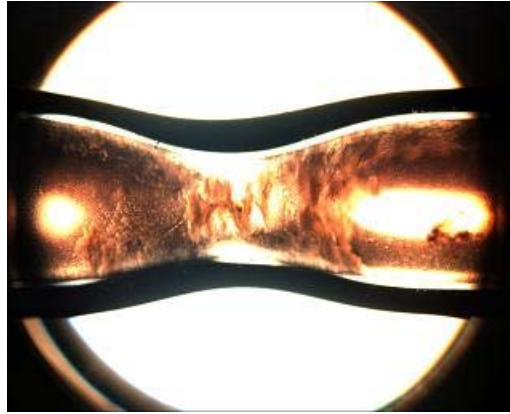


Figure 21. 62% Stenosis. 2x. Striations of thrombus were visible in the throat. This test section was photographed without the oil-immersion bath therefore the walls of the glass tube appear black.

Non-stenotic Experiments

At the beginning of each set of experiments, a non-stenotic or straight test section was tested in order to confirm that the upstream pressure was approximately constant, to compare differences of viscosity in experiments, and to compare the increased resistance of adding stenosis. Figure 22 below shows how the flow rate was approximately constant during a typical experiment until the blood reservoir, holding 240mL of blood was reduced by 200 mL, at 6 minutes for this experiment. Average flow rate and upstream pressure were calculated for this time period because they could be considered to be conserved. The average flow rate for this experiment was 33.1 ± 4.9 mL/min. Between 4 and 6 minutes the flow became more irregular and flow rate fluctuated more. The fluctuation of the non-stenotic sections was reflected in the high standard deviation.

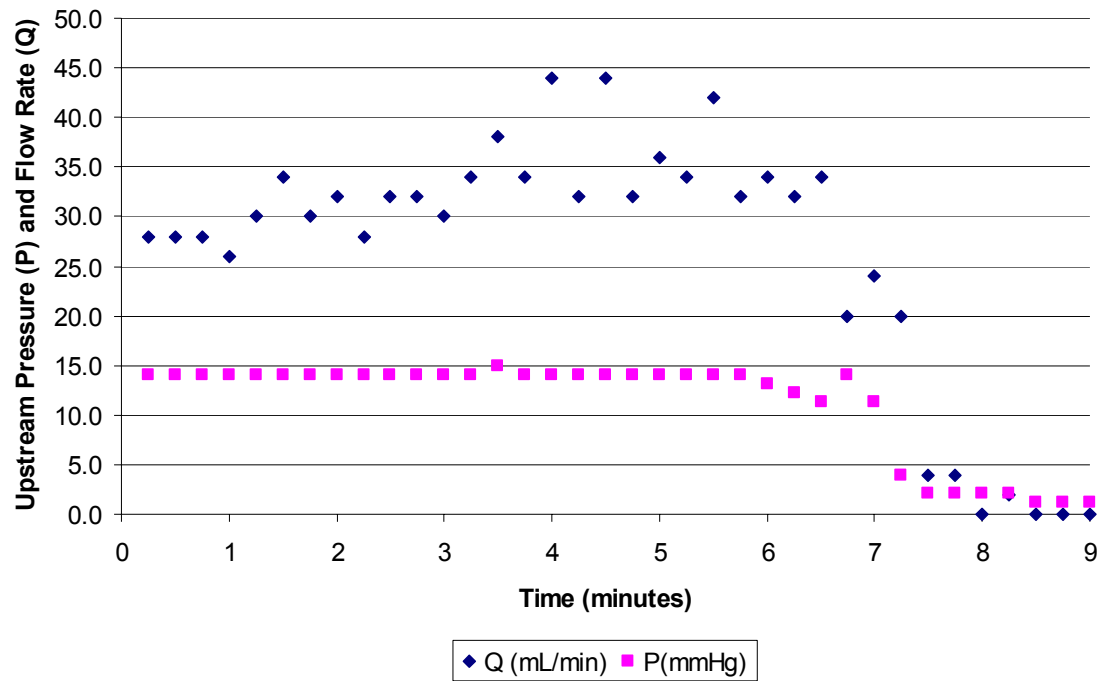


Figure 22. Non-stenotic experiment. Error bars calculated on measurement resolution. Pressure and flow rate dropped to zero once the contents of the reservoir emptied.

For non-stenotic experiments, the averages of flow rate and upstream pressure were calculated based on measurements made while the volume perfused was less than or equal to 200 mL. This typically matched the time that the pressure changed by 1 mmHg for more than 30 seconds. Reynolds number for these experiments was 139 ± 29 . Images taken for this same experiment, shown in Figure 23, indicate that thrombus formation occurred but was not significant enough to cause a change in pressure and flow.

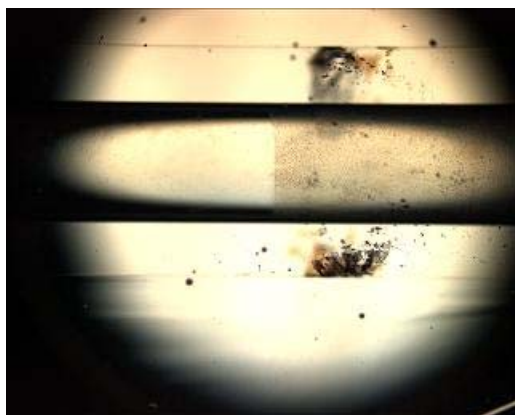


Figure 23A



Figure 23B

Figure 23. 23A was 2x; 23B was 4x magnification. Thrombus was visible on the surface of the right hand side of this non-stenotic tube that corresponds to the beginning of the collagen coated surface. The black marking on the glass indicated the midline and the border of coating. Flow was from left to right.

In Vitro Model of Occlusive Thrombosis

The blood flow experiments demonstrated that greater amounts of thrombus formed on collagen coated glass tubes when the shear rate was increased and that some experiments led to complete occlusion. Based on the data from these experiments, a model of flow rate as a function of resistance was developed and demonstrated to work for blood and water. Given the viscosity of the fluid and a measurement of the flow rate, the percent stenosis can be predicted. This model estimated the effective diameter of the stenosis throat after it has been narrowed as a result of thrombosis. Data used in the validation of this model were from measurements of flow rate in collagen-coated water experiments and all collagen coated blood flow experiments with the exemption of (1) experiments that had a non-stenotic control which had an upstream pressure that decreased more than 3 mmHg before 200 mL was perfused, and (2) experiments that had an embolus cause flow cessation before the first minute of flow. This data includes some

experiments that had 5 U/mL heparin for three dates of experiments: 8-30-04, 9-1-04, and 9-3-04.

The flow rate curves overlapped for water and blood when they were normalized by their dynamic viscosity and were plotted as a function of percent stenosis. The curves show that flow was approximately constant given percent stenosis $\leq 65\%$ and then it declined approximately linearly to zero flow when the percent stenosis was 100%.

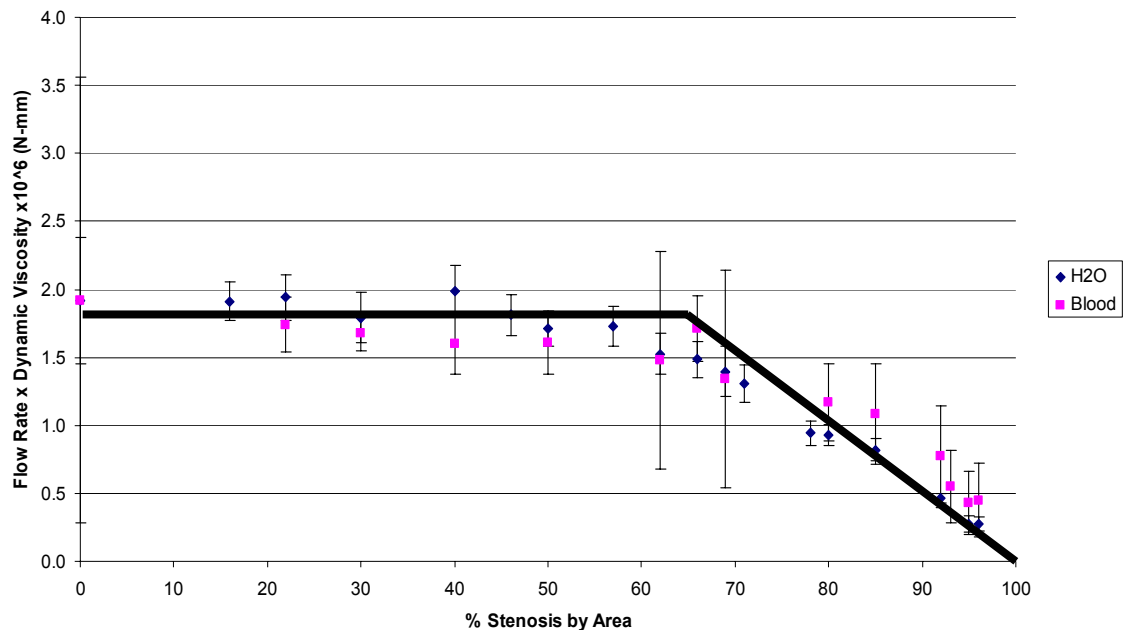


Figure 24. Blood and water normalized flow rates were approximately constant until around 65% stenosis and then they decreased linearly until 100% stenosis. The flow rate for each fluid was normalized by its viscosity and reported as mean $\pm 1\sigma$.

Many of the stenoses had normalized flow rates that matched well for blood and water. At greater percent stenosis, the normalized flow rates for blood were higher than water which may have been a result of fluctuation of blood viscosity. Using the data for

blood alone, a more exact characterization of flow rate in severe stenosis is presented in Figure 25 below.

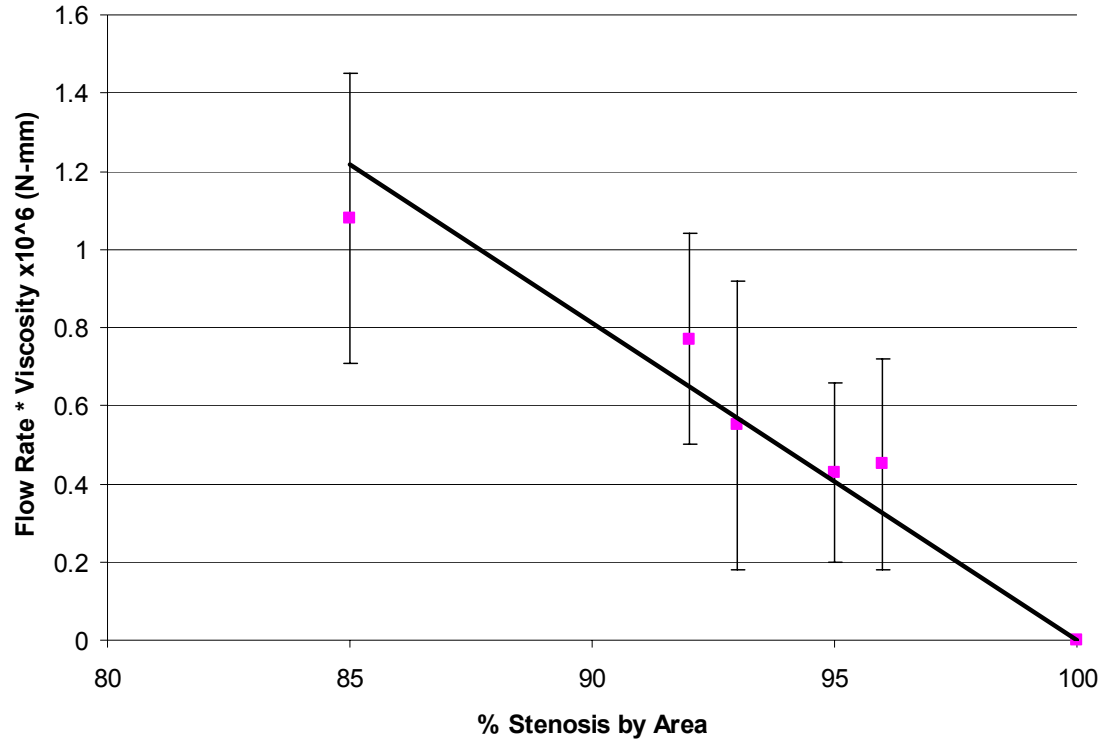


Figure 25. Flow rate model for blood in stenoses $\geq 85\%$. Linear approximation has $R^2 = 0.94$. Data presented as mean $\pm 1\sigma$.

A boundary condition was imposed on the empirical data for this linear approximation so that at 100% stenosis there was zero flow. Consequently, the x-intercept at 100 % was included because logically there was no flow once the lumen closed. This condition was imposed by reversing the coordinates, setting the y-intercept to 100, and finding the best-fit line. Since the square of the correlation coefficient was 0.94, the linear assumption in this region was a good approximation. The equation of this line is in Equation 5.

$$Q\mu = -12.314 \times (\%Stenosis) + 100 \quad \text{Equation 5}$$

where Q was the flow rate and μ was the dynamic viscosity of blood and % stenosis was calculated by area. Based on Equation 5, it was possible to solve for percent stenosis greater than 85% for a given flow rate and viscosity. For blood flow in this model, the upstream diameter was constant whereas thrombosis only occurred significantly on the collagen coated surface which began just upstream of the stenosis. Therefore since the only variables during thrombosis in this model were the flow rate and the throat diameter, it was possible to recover throat diameter for flow rates at a particular time. The assumption of this flow rate model was that reduced flow as a result of thrombus formation followed the flow rate curve which was developed by imposing increasing symmetrical area reductions. Platelet deposition was quantified based on knowledge of the throat diameter at different times during the experiment and the initial geometry of the stenosis. Platelet deposition and formation of completely occlusive thrombus will be analyzed in Chapter IV.

Effect of Coating Collagen

Non-collagen coated stenoses did not show significant signs of thrombus formation. The upstream pressure decreased over time because the height of the fluid reservoir changed by 1.5 cm by the time 210 mL of blood was perfused, corresponding to 1-2 mmHg change. In a 97% stenosis, the lumen remained patent for over 25 minutes

and thrombus could not be identified when inspected microscopically, as seen in Figure 26.

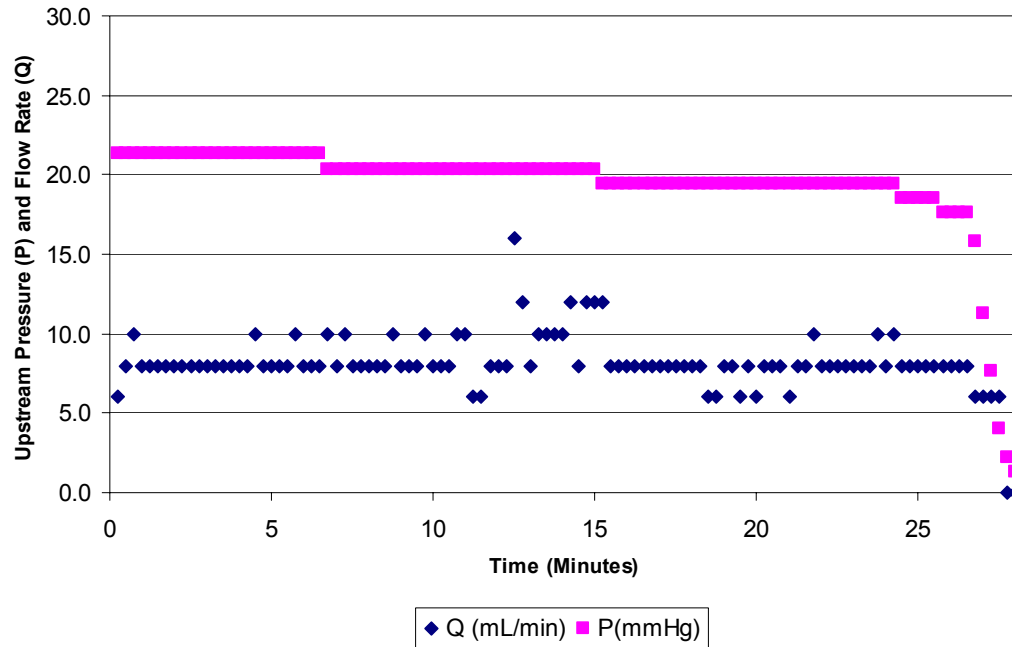


Figure 26. 97% stenosis. Flow remained approximately constant throughout the experiment.

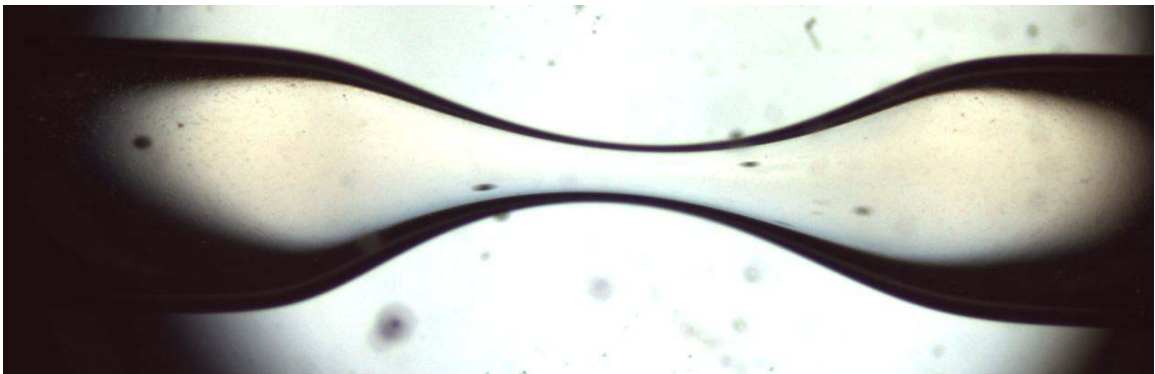


Figure 27. 97% Stenosis. Thrombus did not form on the walls of this non-collagen coated stenosis. Throat diameter was 310 μm .

The surface of the lumen in Figure 27 did not have thrombus that could be identified microscopically. In collagen-coated experiments that remained patent during

the flow until the emptying of the reservoir, thrombus formation was always apparent. At higher magnification with use of a marker for blood species, some thrombus formation may be evident. Relative to collagen-coated experiments that remained patent, however, this may be negligible.

In 3 non-stenotic and 9 stenotic experiments of blood flow through non-collagen coated test sections, thrombus formation was found in only one. In the one with thrombus, it was determined that the surface was not cleaned thoroughly from the last experiment with collagen.

In comparison to non-collagen coated test sections, the collagen coated sections had flow rates within the standard deviation for blood and water (H_2O). Figures 28 and 29 show the effect of adding collagen to test sections perfused with H_2O and blood, respectively, at 30 cm reservoir height. For H_2O , the average flow rate was calculated by taking the average of two experiments, where each experiment had a mean flow rate from 8 measurements made every 15 seconds over two minutes. Three different 0% test sections and two different 69% stenoses were tested in order to confirm the performance of stenoses with the same measured percent stenosis. The flow rates and upstream pressures measured were within one standard deviation for these. In order to use their data in Figure 8, the three non-stenotic sections were averaged together and the 69% stenoses were averaged together. For blood, the average flow rate was calculated for experiments with each stenosis using the methods described earlier for non-stenotic and stenotic test sections.

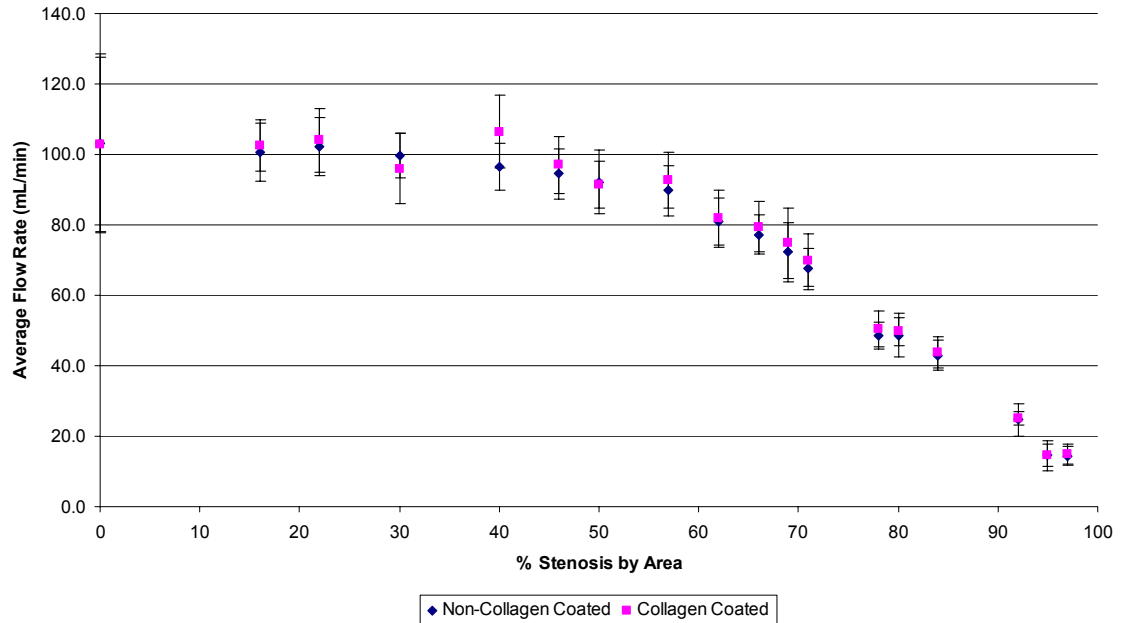


Figure 28. H₂O. Addition of collagen does not affect the average flow rate. Average flow rate is reported mean $\pm 1\sigma$.

Test sections that did not follow the curve in Figure 28 were inspected to determine if the cross sectional area at the throat of the stenosis was elliptical. Five stenoses that did not fit on the curve were omitted and not used for experimentation with blood.

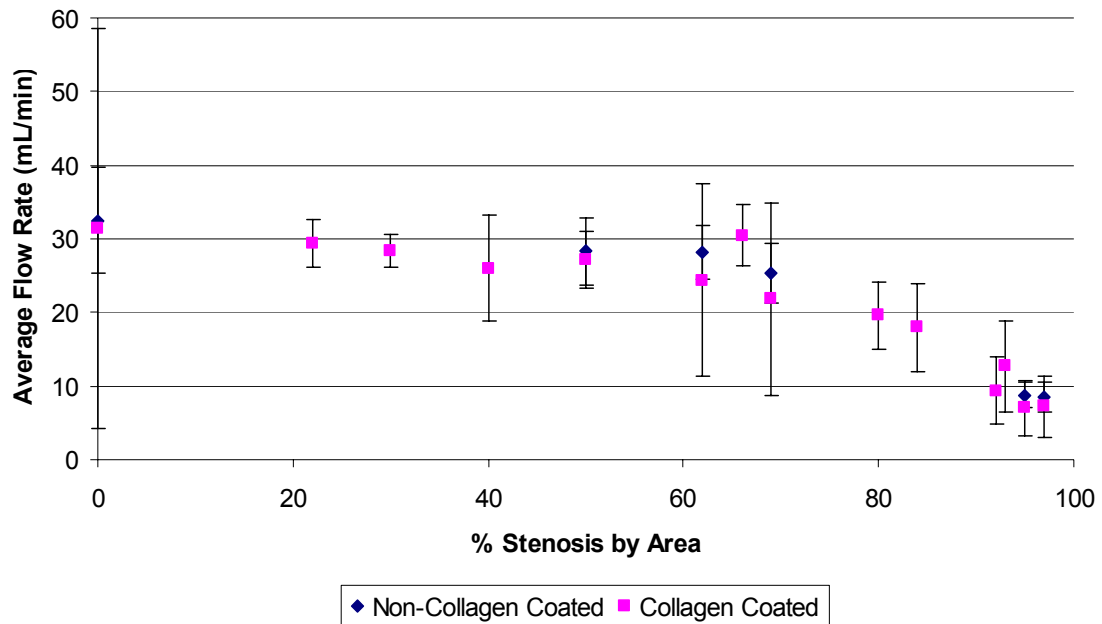


Figure 29. Blood. Addition of collagen to the test sections did not affect the flow rate of blood. Average flow rate reported as mean $\pm 1\sigma$.

Determination of Height

The height of the fluid reservoir drove the flow. Reservoir heights between 20 and 35 cm were used to measure the flow rate of water as a function of the percent stenosis. Average flow rate for these experiments was calculated from 4 measurements made every 15 seconds for one minute. After the first minute, volume in the reservoir went below 200 mL for the non-stenotic tubes in the 35 cm experiments and flow rate changed considerably. Therefore comparison of these average flow rates is only made for the first minute. Flow rates are reported as mean \pm error, where error is defined as twice the standard deviation, σ . Figure 30 shows the average flow rate at three different reservoir heights and Figure 31 shows the corresponding Reynolds number (Re) at the throat for the experiments.

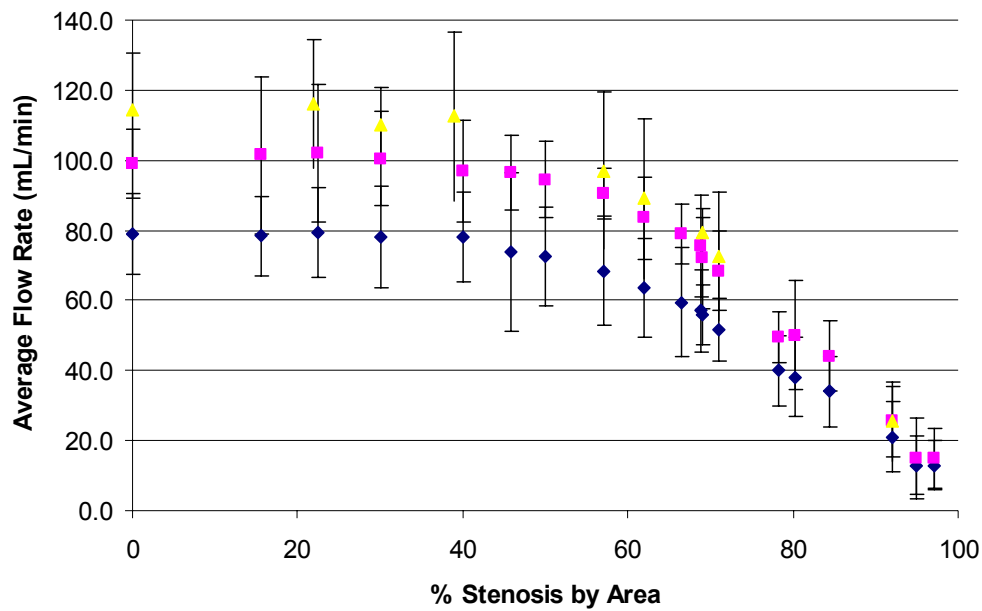


Figure 30. Greater heights of the water reservoir produced higher flow rates, especially in experiments with lower % stenosis. Error on percent stenosis was $\pm 4\%$.

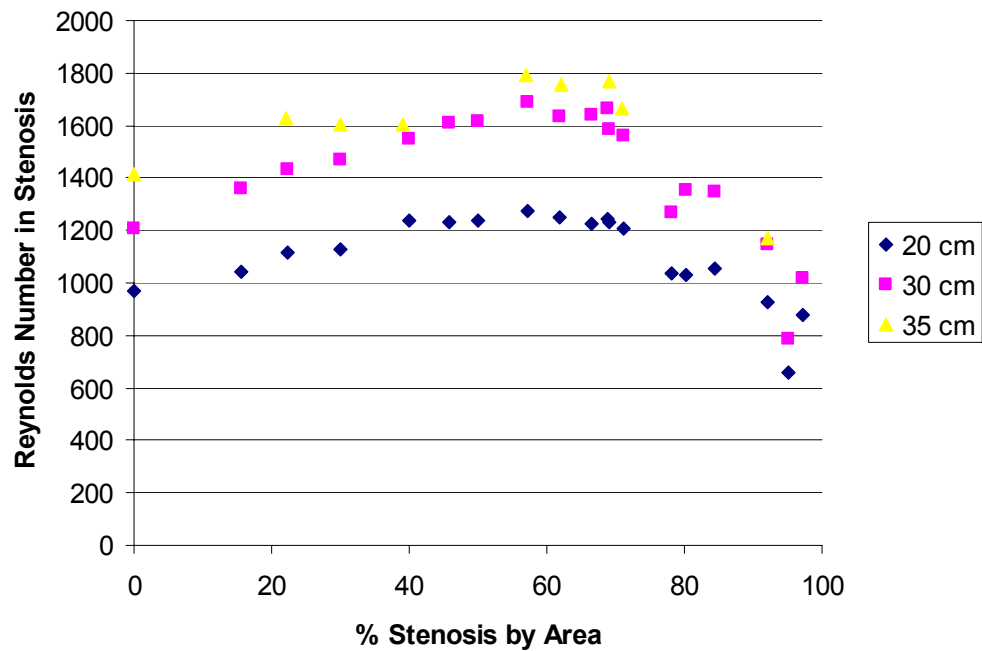


Figure 31. Reynolds number at the stenosis throat predicted transitional flow ($Re \sim 1800$) for experiments at 35 cm and laminar flow for experiments at 20 cm and 35 cm. Error on percent stenosis is $\pm 4\%$.

The 30 cm reservoir height was selected because flow remained laminar without becoming transitional when $Re \sim 1800$ and because the high flow rate produces a high shear rate on the fluid. Flow rates at this height were predicted to produce shear rates in the range of 10,000 to 60,000 for blood.

Calculation of Shear Rate and Reynolds Number

As blood moved through the flow system, shear stresses were developed due to the no-slip boundary condition at the wall. At the stenosis throat the velocity profile was blunt and the shear stress was approximated by assuming Poiseuille flow rather than measuring the shear stress which may have had an error of 20-50% [7]. Poiseuille flow predicts a lower bound of shear stress because it assumes a parabolic velocity profile that has a less severe velocity gradient at the wall. Mean wall shear stress, τ , for laminar steady flow in straight tubes or pipes has been approximated as stated in Equation 6.

$$\tau = \frac{32\mu Q}{\pi D^3} \quad \text{Equation 6}$$

where μ was the dynamic viscosity, Q was the volume flow rate, and D was the diameter of the lumen. The shear rate in this work was calculated from Equation 7 based on measurements of Q and D , without taking into account μ .

$$\dot{\gamma} = \frac{\tau}{\mu} = \frac{32Q}{\pi D^3} \quad \text{Equation 7}$$

Reynolds numbers (Re) were calculated based on flow rate using Equation 8.

$$\text{Re} = \frac{4Q}{\pi D \nu} \quad \text{Equation 8}$$

where ν is the kinematic viscosity. The kinematic viscosity was calculated for each blood sample based on the dynamic viscosity divided by the density of blood, 1035 kg/m³. The kinematic viscosity was in the range of 3.1 - 4.1 mm²/s.

CHAPTER IV

RESULTS: THROMBUS FORMATION UNTIL COMPLETE OCCLUSION

Thrombus formation led to complete occlusions in seven experiments using three different stenotic test sections. Two occurred in an 85% stenosis, one in a 95% stenosis and four in a 96% stenosis, all occurring in the throat of the stenosis. Other experiments often showed large amounts of thrombus but did not lead to total occlusion. And in many high grade stenoses the occurrence of emboli inhibited the evaluation of thrombus formation. Only blockages as a result of complete thrombotic occlusion will be reviewed in this section.

The markers for thrombotic formation to complete occlusion included increased upstream pressure in steps over time, visible white thrombus on the walls, and flow cessation. Typically, flow did not stop for another minute or longer after the measurement of flow rate was zero because a few drops could not be measured by the 0.5 mL resolution of the graduated cylinders or the presence of flow in the stenosis throat was undetectable. Upon magnification on the stenosis throat, it was found that flow did continue even after it was undetectable at the downstream exit. Table 2 below lists both the time when flow rate was undetectable and the time when flow ceased and there were no drops and flow could not be seen in the throat. The time of flow cessation was more accurately the fourth column and this time has been used for the remainder of this work.

Table 2. Data on the seven complete occlusions in order increasing percent stenosis.

% Stenosis by Area	Experiment	Time Flow is Undetectable (min)	Time of Flow Cessation (min)	Volume Perfused (mL)	Heparin v/v
85	12.8.1.9	11.5	17.5	99	0.4
85	12.15.2.9	15.75	16.5	108.5	0.36
95	10.27.4.7	16.5	16.5	65.5	0.36
96	11.3.3.33	9.25	9.5	35	0.4
96	11.22.4.33	17.25	18	94	0.36
96	12.1.2.33	11.75	13	55.5	0.37
96	12.15.2.33	12.5	13.5	84	0.36

The average time of flow cessation was 13.5, 16.5, and 17 minutes in order of decreasing percent stenosis. Less than 100 mL of perfused whole blood was necessary to completely block most of the test sections, where the highest volume required was in the 85% stenosis which had greater flow rates and a larger lumen for thrombus to fill. For the majority of experiments, 0.40% heparin volume to whole blood volume was used for anticoagulation. Many of the thrombotic occlusions in this model resulted from the slightly lower dosage of heparin. The average Reynolds number was 126 ± 15 .

Thrombus formation images were taken every 15 seconds for the three experiments in Table 2, which were completed on December 8th and 15th. These images were used to identify the time of flow cessation as well as visualize thrombus formation and measure platelet deposition during the experiment. A platelet deposition model based on these images as well as another platelet deposition model based on flow rate has been presented in the following sections.

For these experiments, upstream pressure may have been constant without the effect of thrombosis. Upstream pressure rose to 24 mmHg near the time of flow cessation which corresponds to a 31.5 cm column of blood, which is consistent with the experiment because when the blood reservoir was completely full the highest surface was approximately 31.5 cm above the plane of the pressure transducer and stenosis. After 200 mL of blood had perfused in the non-stenotic sections, a pressure change of 1-2 mmHg occurred, but since 100 mL or less was required for these experiments the upstream pressure was constant.

These experiments demonstrate that the components present in completely occlusive thrombus include platelets, collagen, fibrin, vWF, and high shear rates. Heparin did not limit the formation of thrombus to complete occlusion but the dosage of heparin may have played some role based on variation in these experiments.

Platelet Deposition Based on Flow Rate

Platelet deposition has been calculated for the seven blood flow experiments that led to complete thrombotic occlusion. The model of flow rate as a function of percent stenosis presented in Chapter III determined the effective throat diameter given a reference flow rate. Recall that the model of flow rate predicted that for severe stenoses (equal to or greater than 85%) the flow rate could be estimated by Equation 5.

In this flow rate model only the throat diameter was necessary to characterize the platelet deposition therefore the region of interest was limited to the apex of the stenosis. Platelet deposition was solved for by determining the number of platelets deposited at a time and dividing by the surface area which the thrombus covered. First, the volume of

thrombus was estimated by assuming that (1) that the thrombus was cylindrically shaped, and (2) thrombus formed uniformly and symmetrically in concentric rings on the walls of the stenosis. The volume of thrombus for a particular throat diameter was calculated by Equation 9.

$$V = \frac{\pi \times [D_2^2 - (D_2')^2] \times L}{4} \quad \text{Equation 9}$$

where V is the volume of thrombus, D_2 is the inner diameter of the stenosis throat, D_2' is the new throat diameter, and L is the length of the thrombus. The number of platelets was calculated by multiplying the volume (V) of thrombus by the proportion of platelets in the thrombus, f , and dividing by the mean platelet volume, MPV , as in Equation 10.

$$\# \text{Platelets} = f \times \frac{V}{MPV} \quad \text{Equation 10}$$

MPV was determined from measurement in a Coulter Counter for each blood sample.

The proportion of platelets in the thrombus, f , was estimated by evaluating the histological composition of occluding thrombi with image analysis as described in the last section of this chapter: *Histology and Composition Analysis*. The range of f for the thrombi analyzed was between 75% and 96%. Platelet deposition, PD , is the accumulated number of platelets per surface area in the stenosis and was calculated by dividing Equation 10 by the surface area. The surface area which the thrombus covered

was simply $\pi \times D_2 \times L$ based on the cylinder assumption. The length, L , and π cancel and yield Equation 11.

$$PD = f \times \frac{[D_2^2 - (D_2')^2]}{4 \times D_2 \times MPV} \quad \text{Equation 11}$$

The maximum platelet deposition can be estimated by setting D_2' to zero.

For this platelet deposition model, the time period selected was based on the period of each pressure step because pressure is dependent on flow rate. Although pressure and flow are directly related, the upstream pressure was more sensitive to the changes occurring in the flow loop. Figure 32 below illustrates how pressure steps increase until flow cessation and it can be seen that the flow rate is reduced until it is undetectable at 15 minutes.

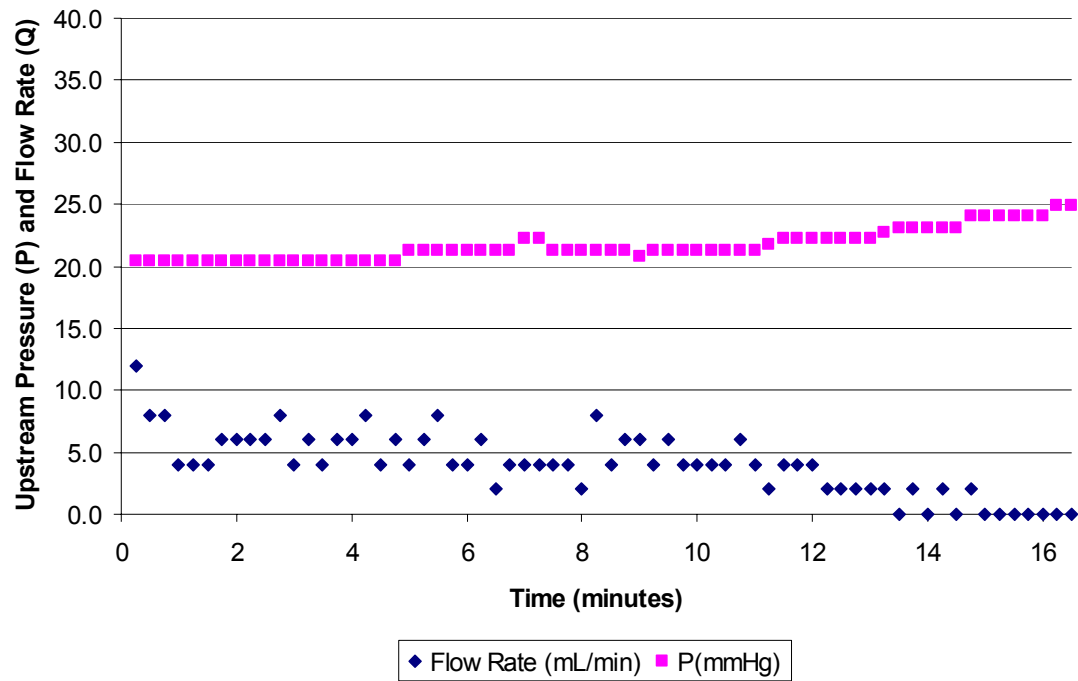


Figure 32. Flow rate and upstream pressure data for a 95% stenosis experiment that led to complete occlusion. The shear rate was 24,200/s based on the average flow rate for the first five minutes. Experiment 10-27-4-7.

Precision errors on all flow rate and pressure measurements were ± 2 mL/min and ± 1 mmHg, respectively. For each pressure step, consisting of at least 30 seconds length, an average flow rate was calculated and a throat diameter was solved for using Equation 5 and the definition of percent stenosis by area. Using Equation 11, platelet deposition was calculated for each effective diameter corresponding to that time period. The amount of platelet deposition for the experiment in Figure 32 has been shown in Figure 33 below.

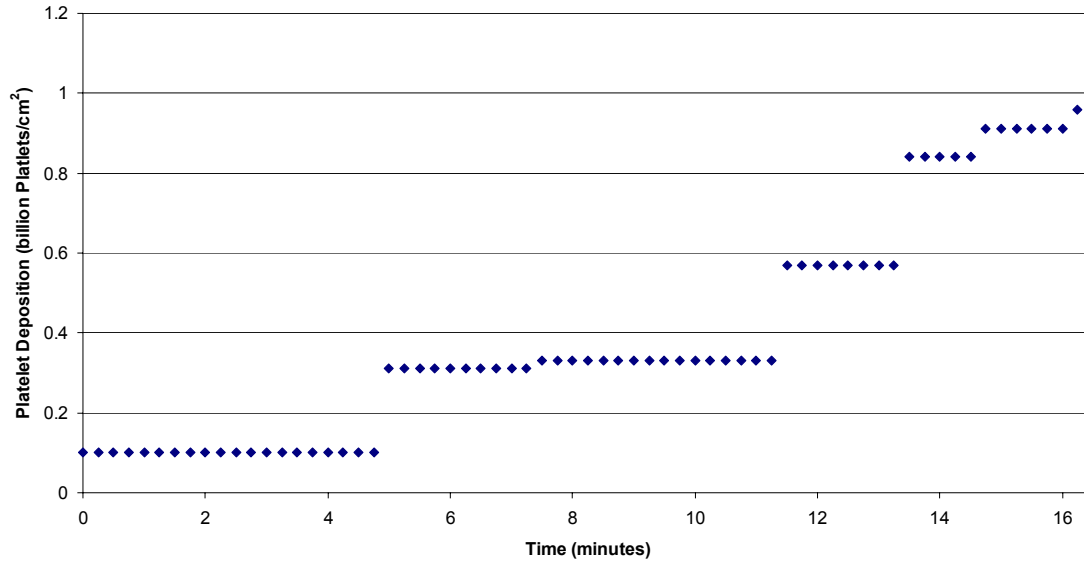


Figure 33. Platelet deposition during the experiment. The magnitude of platelet deposition corresponded to the throat diameter during that time period. Maximum platelet deposition required to block this 95% stenosis with a 350 μm lumen was 0.96 billion platelets/cm².

For the first 11.5 minutes, platelets deposited on the surface slowly indicating accelerating platelet deposition (Phase I from Figure 2) and reduced the effective diameter to 300 μm , which raised the percent stenosis to 97% by area (83% stenosis by diameter). The magnitude of platelet deposition initially was nonzero because it was based on the average flow rate for the first 4.75 minutes while at a constant pressure, therefore the average flow rate for this particular experiment may have been slightly greater or less than the flow rate used for a 95% stenosis in the model. Based on this initial difference in flow rate, the platelet deposition resulted in either positive, negative, or zero values at the beginning.

The platelet deposition doubled between approximately 11.5 and 13.5 minutes of flow. This was representative of the acute platelet deposition, Phase II, when the rate of deposition may be linear. And in the last few minutes of flow the margin between the

magnitude of platelet deposition decreased which resembled the slow phase, or Phase III. Therefore, for this experiment, the rate of platelet deposition decreased before reaching complete occlusion. This measure of platelet deposition is directly related to the changes in throat diameter, therefore the accumulation of platelets in this model is related to the change of the effective diameter of the lumen.

A useful characterization of platelet deposition is the acute rate of accumulation which was determined from the slope of a line fitted to the data between the beginning of the acute phase and the time of flow cessation. In this experiment, the acute phase was estimated to begin at 10 minutes and flow cessation occurred at 16.5 minutes. The slope of the line was 113 million platelets/cm²/minute or 1.88 million platelets/cm²/second. This model takes advantage of the reduced flow rate for each pressure step and interprets the reduction of flow as a decrease in the effective diameter, and hence a greater volume of thrombus.

Table 3 below compares the acute rate of platelet deposition to the total rate of platelet deposition which is calculated using the maximum platelet deposition and a straight line estimate over the duration of the experiment until flow cessation. The total rate does not take into account the phases of platelet deposition interpreted in Figure 2. Therefore the acute rate of platelet deposition predicts a higher rate because of the steepness of the acute phase, as seen in Figure 34.

Table 3. Platelet deposition (PD) rates and the parameters used in their calculation.

Percent Stenosis	Acute Rate of PD ($\times 10^6$ plts/cm²/s); Eqn. of PD line	Total Rate of PD ($\times 10^6$ plts/cm²/s); Eqn. of PD line	Maximum PD ($\times 10^9$ plts/cm²)	Time Flow Cessation (min)	Time of Start of Acute Phase (min)	Experiment
85	1.67 $y=1.67x+5.87$	1.88 $y=1.88x+3.24$	1.78	17.5	5.25	12.8.1.9
85	1.1 $y=1.10x+8.07$	1.25 $y=1.25x+6.05$	1.53	17.5	5.5	12.15.2.9
95	1.88 $y=1.88x-13.76$	0.91 $y=0.91x-0.87$	0.96	16.5	10	10.27.4.7
96	2.39 $y=2.39x-10.54$	1.95 $y=1.95x-7.77$	0.64	10	5.25	11.3.3.33
96	3.09 $y=3.09x-38.82$	1.56 $y=1.56x-17.12$	0.92	18	10.75	11.22.4.33
96	2.37 $y=2.37x-1.49$	2.04 $y=2.04x-12.3$	0.81	13	4.5	12.1.2.33
96	3.6 $y=3.60x-38.76$	1.39 $y=1.39x-12.4$	0.78	13.5	7.5	12.15.2.33
Average \pm S.D.	2.3 \pm 0.8	1.6 \pm 0.4	1.1 \pm 0.4	15.1 \pm 3.0		

The lowest acute rates were for the 85% stenosis and these acute rates were more similar to the total rate of platelet deposition.

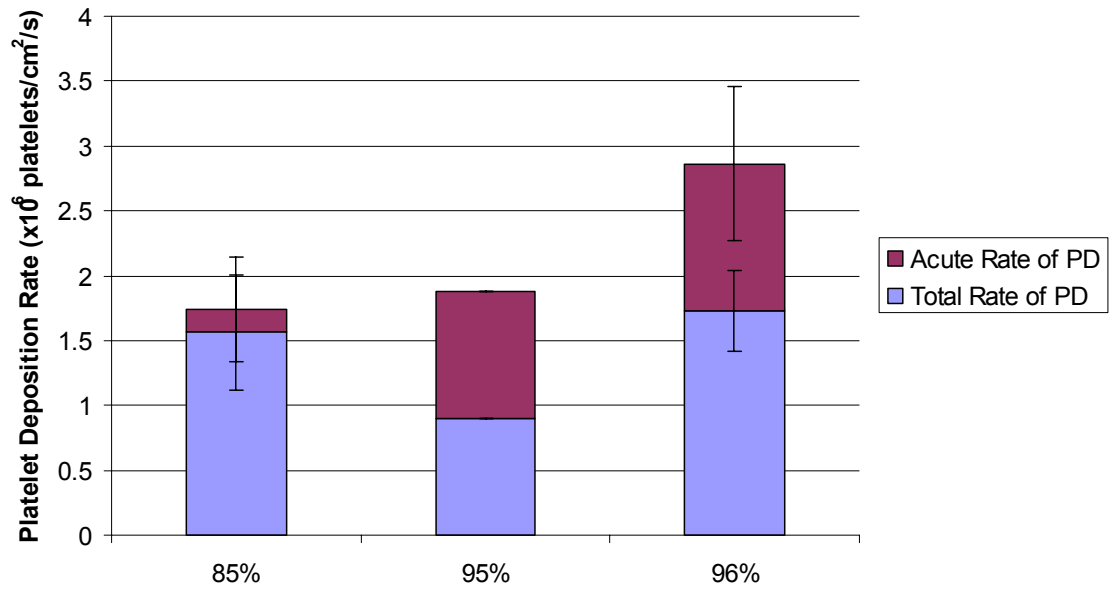


Figure 34. Acute platelet deposition rate increased with percent stenosis. Values reported as mean \pm 1 σ .

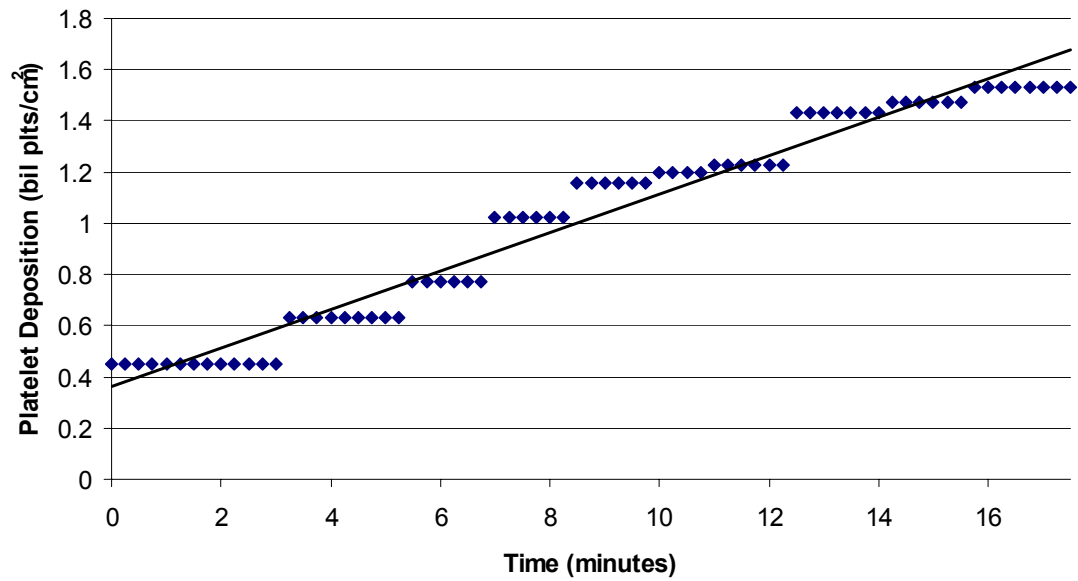


Figure 35. 85% stenosis. The initial shear rate was 10,000/s based on the first 3 minutes. Experiment 12.15.2.9.

In the 85% stenosis, presented in Figure 35, the rate of platelet deposition was more gradual and the acute rate constant was closer to the slope of platelet deposition over the whole length of the experiment. For greater percent stenosis experiments, the upstream pressure remained constant longer and then increased in short steps over a short amount of time to flow cessation.

Thrombus Formation Movies

In three of the experiments that led to complete occlusions, digital images taken every 15 seconds, corresponding to pressure and flow measurement, show the development of thrombus on the walls of the stenosis throat and ultimately, the thrombus growth across the lumen to block flow. These images demonstrate that the formation of thrombus was focal in nature and that thrombus protruded into the lumen at multiple sites. Because thrombus formation was non-uniform along the length of the stenosis the pathway of blood may have changed from being axis-symmetric.

The following image sequences are in Apple QuickTime *.mov format and may be viewed with movie players such as QuickTime or Windows Media Player. The movies were made by combining a sequence of images into a movie file. The size of the movie file is reported in parenthesis and when downloading the file from the internet this should be considered with respect to connection speed. Each of the experiments that led to complete thrombotic occlusion have been presented in Figures 36-38 and a patent non-stenotic and an embolus experiment have also been presented in Figures 39 and 40, respectively.

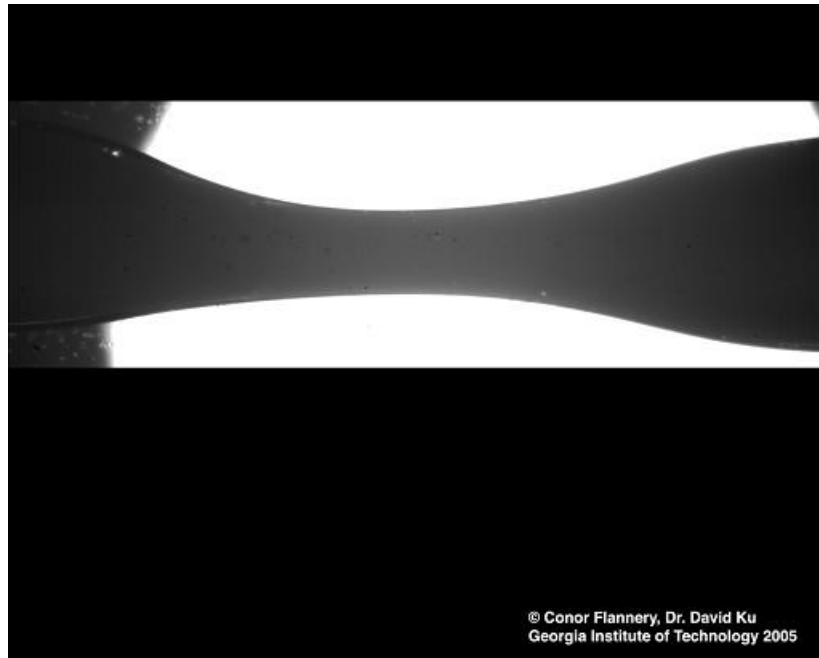



Figure 36. Thrombus formation image sequence in the 85% stenosis at time = 0. Throat diameter was approximately $610\ \mu\text{m}$. Thrombus may be visualized because it is translucent. Whole blood is opaque and inhibited view of the whole thrombus. Flow was from right to left. 1.0x magnification. Filename: 85per_sten_TO_40sec_12-15-9_2fps_C.mov (4.64 MB).

Four images were taken every minute over 20 minutes for a total of 80 images, although presented as in Figure 36 above at 2 frames per second the image sequence lasts only 40 seconds. Flow cessation in the experiment in Figure 36 was at 16.5 minutes which corresponds to approximately 33 seconds in the movie. Observation at this magnification was the best method to identify the time of flow cessation whereas flow may be undetectable at the end of the glass tube using a graduated cylinder, but may still continue in the stenosis throat. Images were snapped until 20 minutes to capture any changes and to ensure that the flow did not restart. Since flow cessation was at 16.5 minutes, the last three and a half minutes show blood separation into plasma and RBCs in addition to thrombus formation. The downstream side especially separates quickly.

Another image sequence of the 85% stenosis demonstrates technical issues with obtaining these images. Each test section was immersed in a bath of glycerin between two glass cover slips that were connected on one edge with a segment of 4 mm outer diameter Pyrex pipe. Sometimes the surface tension of the glycerin moved the test section towards this edge which disrupted imaging.



Figure 37. Thrombus formation image sequence in another 85% stenosis starting at 8.25 minutes. Throat diameter was approximately 610 μm . Thrombus may be visualized because it is translucent. Whole blood is opaque and inhibited view of the whole thrombus. Flow was from right to left. 1.0x magnification. Filename:  85per_sten_TO_19sec_12-8-9_2fps_C.mov (2.54 MB).

The image sequence in Figure 37 above started at 8.25 minutes after some technical difficulties and continued until 17.5 minutes. The stenosis was not aligned and the light source was off center. The thrombus grew in circumferential striations at the throat diameter. The time of flow cessation was identified at 17.5 minutes, although images were not taken for long enough because a small area in the lumen was still patent.

Flow rate was undetectable at 11.5 minutes therefore it would seem that the last stage of platelet deposition which completely blocked the lumen took a protracted time, greater than 6 minutes.

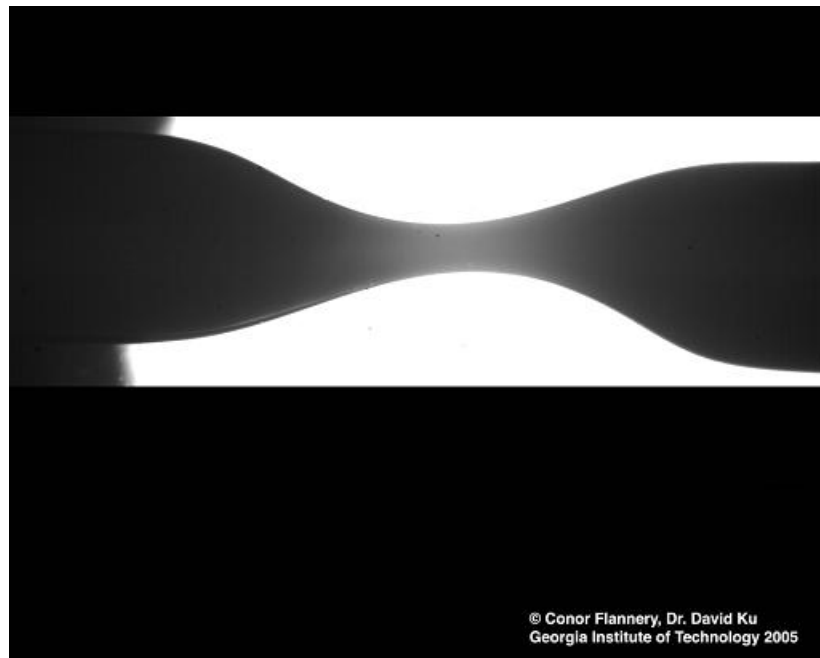



Figure 38. Thrombus formation image sequence in the 96% stenosis at time = 0.5 minutes. Throat diameter was approximately 310 μm . Thrombus may be visualized because it is translucent. Whole blood was opaque and inhibits view of the whole thrombus. Flow was from right to left. Magnified at 1.0x. Filename:  96per_sten_TO_39sec_12-15-33_2fps_C.mov (4.21 MB).

The image sequence in Figure 38 above started at 30 seconds and continued until 20 minutes. This image sequence has shown that a thrombus on the converging side of the stenosis appeared to migrate into the throat of the stenosis where it blocked flow and then thrombus formation increased rapidly. This particular thrombus was first identified at 7 minutes and over the succeeding 6 minutes the mass moved downstream until it rested in the throat at 13 minutes. Flow was not detected at 12.5 minutes, although from visual observation of the images it seemed that a very small channel remained patent until

13.5 minutes or even later. Histological examination of the thrombus removed from this experiment showed that a long propagating tail of fibrin and platelets grew from the downstream end of the occluding thrombus. Additionally, a packet of primarily red blood cells was connected between the occluding thrombus and the propagating tail. The shear rate based on average flow rate for the first 7.25 minutes was 40,900/s.

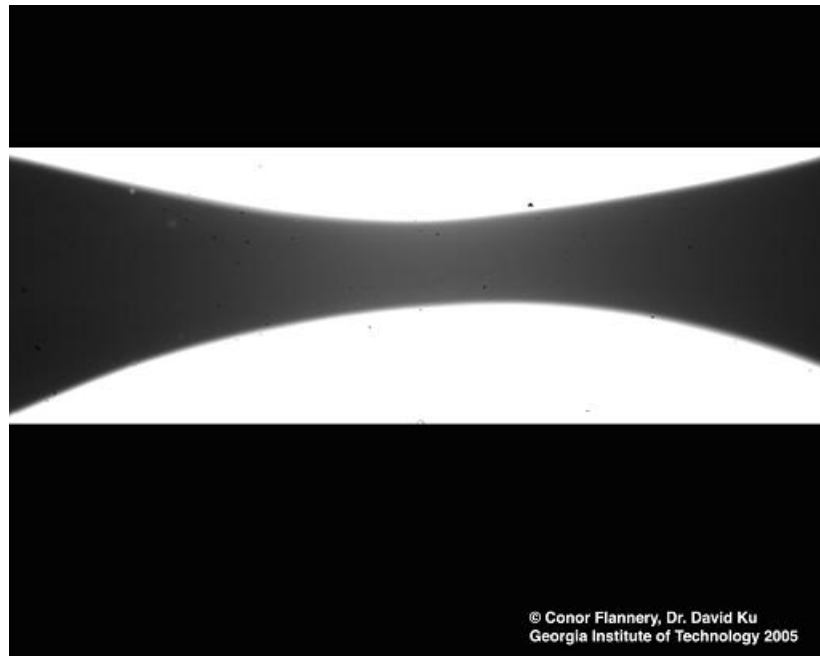



Figure 39. Thrombus formation image sequence in the 93% stenosis at time = 0. The lumen diameter was approximately 430 μm . Flow was from right to left. Magnified at 1.6x. Filename:  93per_sten_E_12sec_1-24-39_2fps.mov (1.17 MB).

The image sequence in Figure 39 above started at the beginning of flow measurement (0 seconds) and continued until 6 minutes. At 5 minutes, an embolus lodged in the throat which resulted in flow cessation. Typically, emboli occurred within the first five minutes of flow. Only rarely did an embolus or blood clot block flow upstream and the vast majority blocked at the throat of the stenosis whereas it was the least diameter by an order of magnitude or more.

These image sequences can be compared to non-stenotic experiments and experiments that remained patent throughout the blood flow.

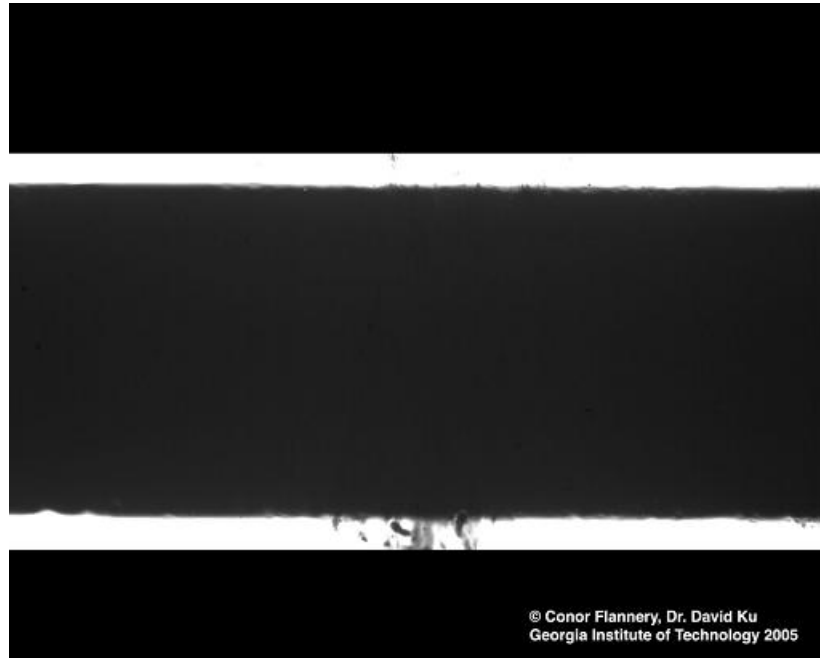


Figure 40. Thrombus formation image sequence in the 0% stenosis at time = 0. The lumen diameter was approximately 1540 μm and the black marking on the bottom indicated that the surface to the left of that line was collagen coated. Flow was from right to left. Magnified at 1.6x. Filename: 0per_sten_N_20sec_1-26-20_2fps_C.mov (2.19 MB).

The image sequence in Figure 40 above started at the beginning of flow measurement (15 seconds) and continued until 10 minutes. Although there was a slight change in shading, the thrombus deposited was not significant enough to be visualized.

Platelet Deposition Based on Thrombus Formation Images

For the three experiments that led to complete occlusion and had thrombus formation images, platelet deposition was calculated based on the composition of the thrombus, the geometry of the visible area, and a count of the number of pixels over a

certain grayscale threshold in each image. Because of the opaque nature of blood, thrombosis was only visible in a limited area of the two dimensional image. But in that visible area, thrombus could be identified by pixels that had a grayscale value greater than a specified threshold.

In order to compare the change in pixels, test sections and other equipment should not move and light intensity should not be adjusted. Typically, thrombus formation was not evident for the first few minutes and any necessary adjustments were made in that time. Platelet deposition was determined for a respective image in seven consecutive steps.

1-Designation of the Mask

The first image that had subsequent images with (a) the test section in the same position and (b) the same background light intensity was called the *mask*. The number of pixels over the threshold in this mask image was subtracted from the subsequent images in order to compare the changes in the number of threshold pixels. Therefore, the image used for a mask was the baseline in the number of pixels over the threshold. In most experiments, this was the first or second image and zero thrombus formation was assumed for the mask. Changes in light intensity and position were recorded during experimentation in the lab notebook, although in some cases slight changes in the position of the test section occurred as a result of flow in the oil-immersion bath. A single movement in the middle of the experiment was accounted for by establishing a second mask for the next applicable image and correcting for any change in the number of pixels.

2-Isolation of the Region of Interest

In order to clean up the images, a region of interest around the lumen of the test section was isolated. A black background was applied above and below the region of interest using Adobe Photoshop 6.0. To expedite the process, an action was created with the mask that made a black layer around the region of interest, and then the action was batched for all of the subsequent images.

3-Choice of a Grayscale Threshold Value

This was an important step in order to correlate the number of pixels greater than the threshold with the amount of thrombus present at the time of a particular image. For the platelet deposition calculation in this analysis, Otsu's method was used to designate the threshold for all the images processed. 8-bit TIFF grayscale images with 1280×1023 dimensions had pixel values between 0 and 255, where 255 identified a white pixel. In order to convert this image to binary black and white, a threshold grayscale value was selected so that pixels equal to or above that threshold will be converted to white pixels. For experiments that led to complete occlusion, it was clear that thrombus attached to the wall or embolus trapped in the throat was translucent and was displayed with lots of white pixels. But for experiments that remained patent and did not have gross thrombus formation this was difficult to assess. Figure 41 below has shown an example of an image that exhibited thrombus formation but needed a threshold between 0 and 255 in order to count the gray pixels and designate them as thrombus.

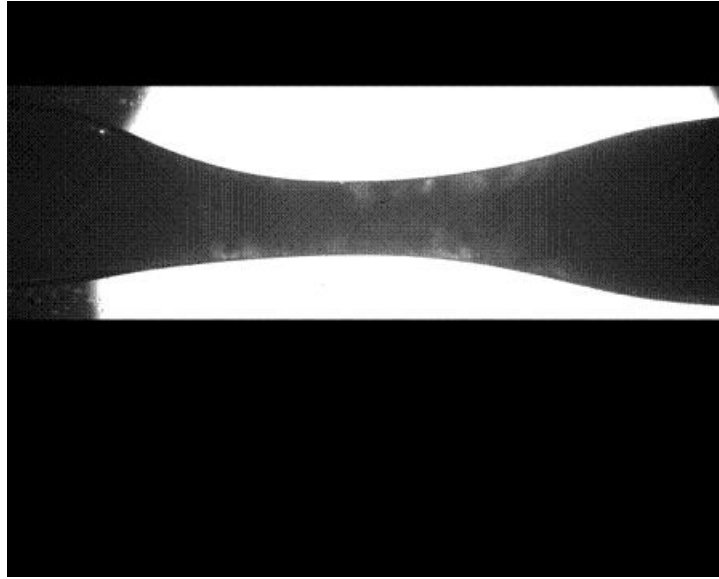


Figure 41. This is an example of grayscale image that exhibits thrombus after 10 minutes in an 85% stenosis. Some loss of quality occurred during compression for this figure.

Based on the image in Figure 41, a histogram of the grayscale pixels in Figure 42 below describes the distribution of pixels. By assigning a threshold too low, pixels in the lumen will become white very early on in the experiment, as in Figure 43.

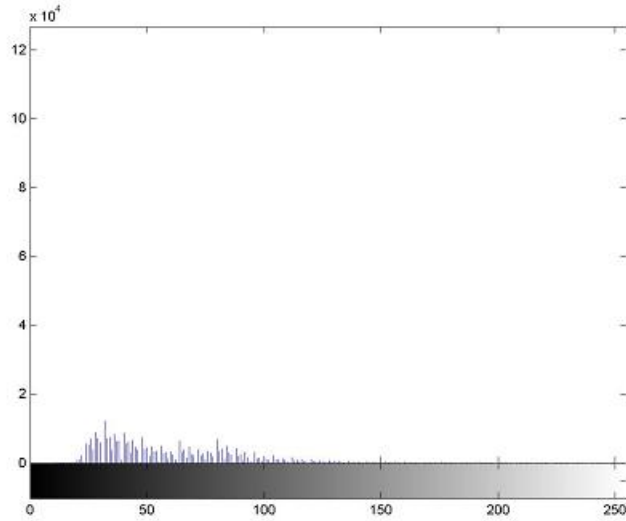


Figure 42. Distribution of grayscale pixels for corresponding image in Figure 41. Majority are either 0 (black) or 255 (white) and blend into the axis. The remainder is distributed especially between 25 and 100. Total number of pixels is 1280×1023 .

As the experiment continued, a large number of pixels, approximately 100,000 shift towards 255.

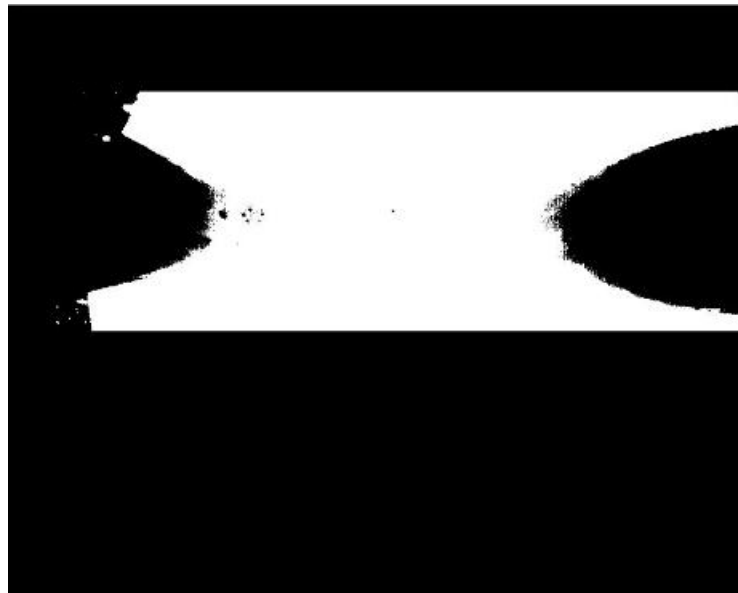


Figure 43. This is an example of a black and white image after conversion from grayscale image in Figure 10 using level as 0.25, or 64 on a grayscale.

Figure 43 does not accurately depict the formation of thrombus because at a low grayscale value, the amount of thrombus is overestimated. Conversely, designation of the threshold level as 0.75 produced a black and white image where the lumen remained black as if thrombosis had not occurred. Figure 44 below designated the threshold level as 0.5 corresponding to 128 on the grayscale. This threshold as well as Otsu's method represents the formation of thrombus well. Otsu's method chooses the threshold to minimize the interclass variance of the thresholded black and white pixels.

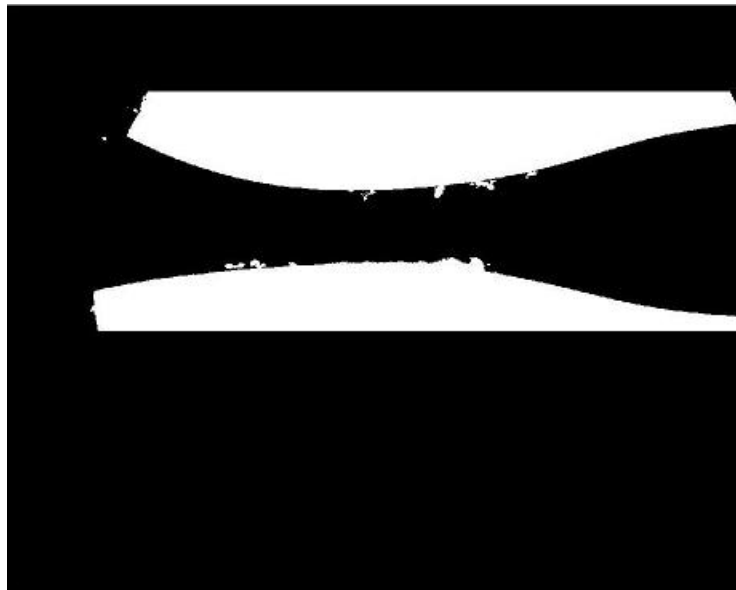


Figure 44. This is an example of a black and white image after conversion from grayscale image in Figure 41 using level as 0.5, or 128 on a grayscale. Thrombus on the walls can be identified and accounted for at this threshold.

For various thresholds, the number of pixels over the threshold illustrated much the same trend for experiments that led to complete thrombotic occlusion. Figure 45 below demonstrates that the number of grayscale pixels converted to white pixels is similar for each of the threshold methods, although the maximum number does vary.

Figure 45 uses multiple threshold levels for each image taken during the experiment described, converts them to black and white, and counts the number of white pixels over the threshold.

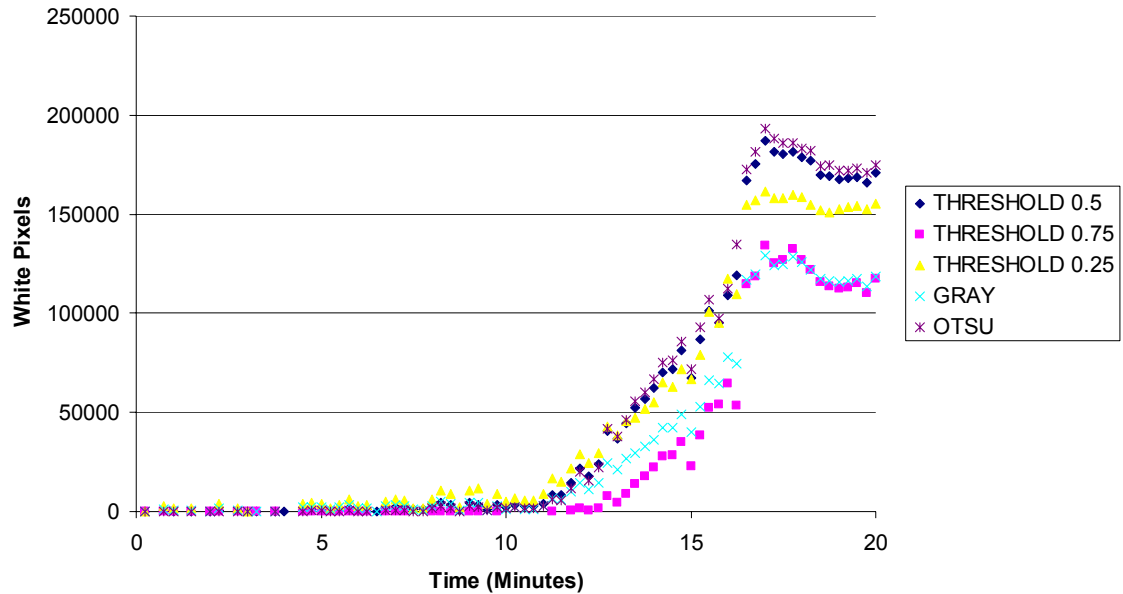


Figure 45. Various threshold levels illustrate a similar trend for an experiment that led to complete thrombotic occlusion, although Otsu’s method and a fixed 0.5 level reach the highest number. Each image was reduced by the number of white pixels in the mask at 0.

For experiments that remain patent but have some thrombus formation, a low threshold could be used to correlate the number of pixels to thrombus deposited. Whereas this method was used on experiments that led to complete occlusion, the white pixels were unmistakably thrombus and completely filled the visible area.

4-Conversion of the Image to Black and White

After the threshold was designated, images were converted to black and white images quickly in Matlab using the ‘im2BW’ function. The code for applying Steps 3, 4, and 5 is in Appendix A-1.

5-Count of the Number of Pixels over the Threshold

Two 'for' loops were used to go through the matrix of the binary data that makes up the black and white image. The count was reported for each image and represented the number of white pixels at the time the image was taken. A specific code was written for each mask and its subsequent series of images. The code and the specific parameters for each experiment are in Appendix A-1.

6-Normalize Subsequent Images by the Count of the Mask

The mask was used to reduce the number of white pixels from subsequent images that were processed in the same manner. Therefore the number of pixels representing thrombosis started at zero.

7-Scale the Count of White Pixels by a Platelet Deposition Factor

For each white pixel counted, the number of platelets was estimated. Platelet deposition was calculated based on histological analysis of the composition of an occluding thrombus, the dimensions of thrombus visible in each image, and the number of white pixels counted for each image. Each image is a two dimensional representation of a three dimensional conic section. Therefore for each pixel in the visible area of the image, a scale was used to estimate the volume of thrombus represented the single pixel. The following assumptions were made:

- The occluding thrombus is cylindrically shaped with a diameter of the least throat diameter and a length defined by the visible length at the time of flow cessation

- At the time of flow cessation, thrombus completely fills the geometry of the visible area
- The growth of thrombus volume from zero volume at time zero until full size thrombus at the time of flow cessation is linear
- The growth of thrombus volume has the same slope as the increase over time of the number of pixels greater than the threshold

The length and width of the visible area was determined from image analysis. The width was always approximated by the inner diameter at the throat and the length was calculated by measuring the distance between the borders of the visible area which is outlined in Figure 46 below.

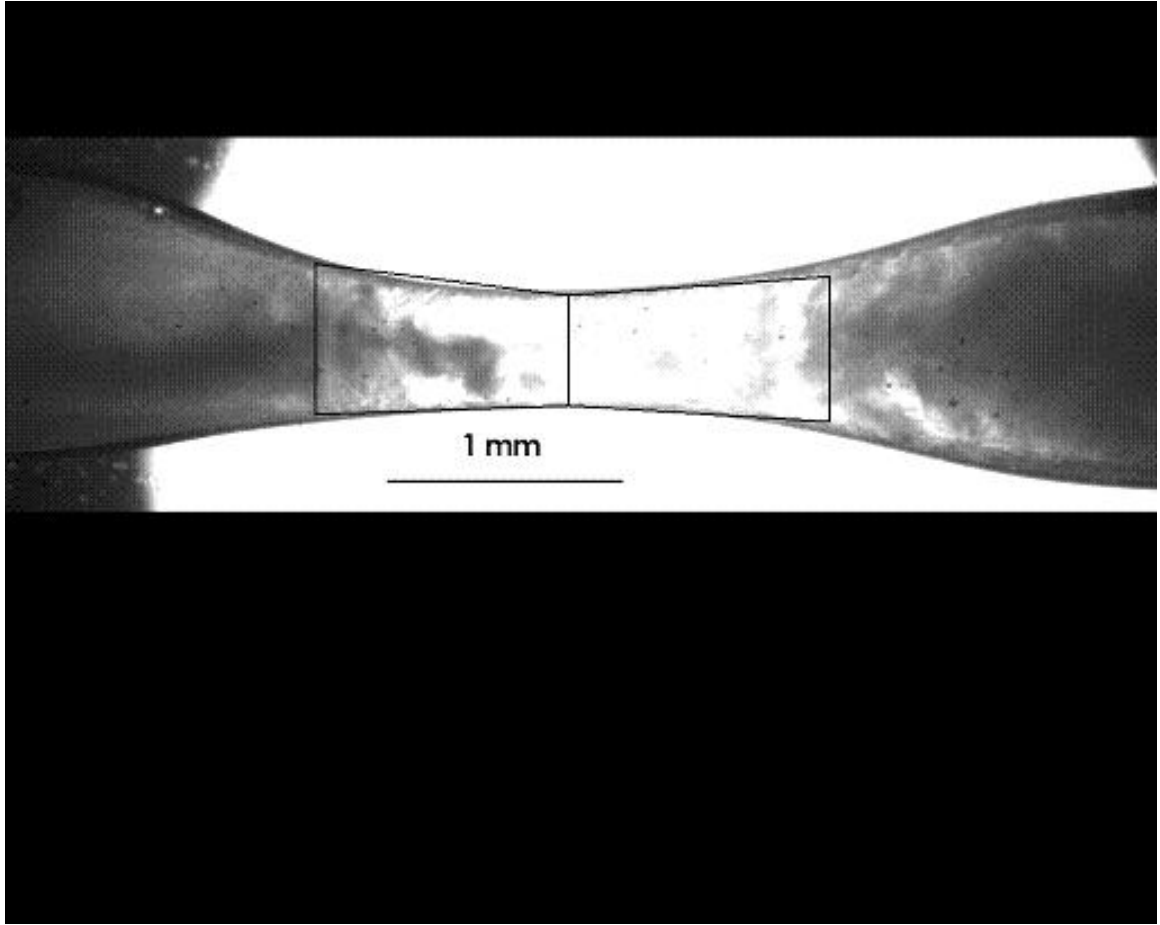


Figure 46. Outline of the visible area at the time of total occlusion (16.5 minutes). Length determined to be 2.5 mm. The throat diameter was 610 μm . The visible area in this example was 1.48 mm^2 . Same 85% stenosis as in previous steps.

The number of pixels in the visible area was similar to the total number of pixels that were counted at the time of flow cessation. The total number for this example is approximately 100,000 based on the value at 16.5 minutes in Figure 46 above. Platelet deposition (PD) was determined with Equation 12 and for this example was 1.13 billion platelets/ cm^2 based on 100,000 pixels over the threshold and 537 platelets per pixel conversion.

$$PD = \# \text{ pixels} \times \frac{\# \text{ platelets}}{1 \text{ pixel}} \times \frac{1}{SA} \quad \text{Equation 12}$$

where the number (#) of pixels is the value obtained from Step 6, SA is the surface area of the cylinder, calculated by $\pi \times D \times L$, and the number of platelets per pixel conversion is determined by Equation 13:

$$\# \text{ platelets} = f \times \frac{V_{thrombus}}{MPV} \quad \text{Equation 13}$$

where f is the proportion of platelets in a thrombus, $V_{thrombus}$ is the volume of the thrombus in the visible area, and MPV is the mean platelet volume for the particular blood sample, approximately 8.6 femtoliters. The thrombus volume is calculated by the equation of a cylinder: $\pi \times D^2 \times L/4$. The difference between Equation 10 and Equation 13 is that the volume of thrombus in Equation 13 is that which exists in the visible area only. The conversion of the number of platelets per pixel was used as a scaling constant for all the subsequent images during thrombus formation.

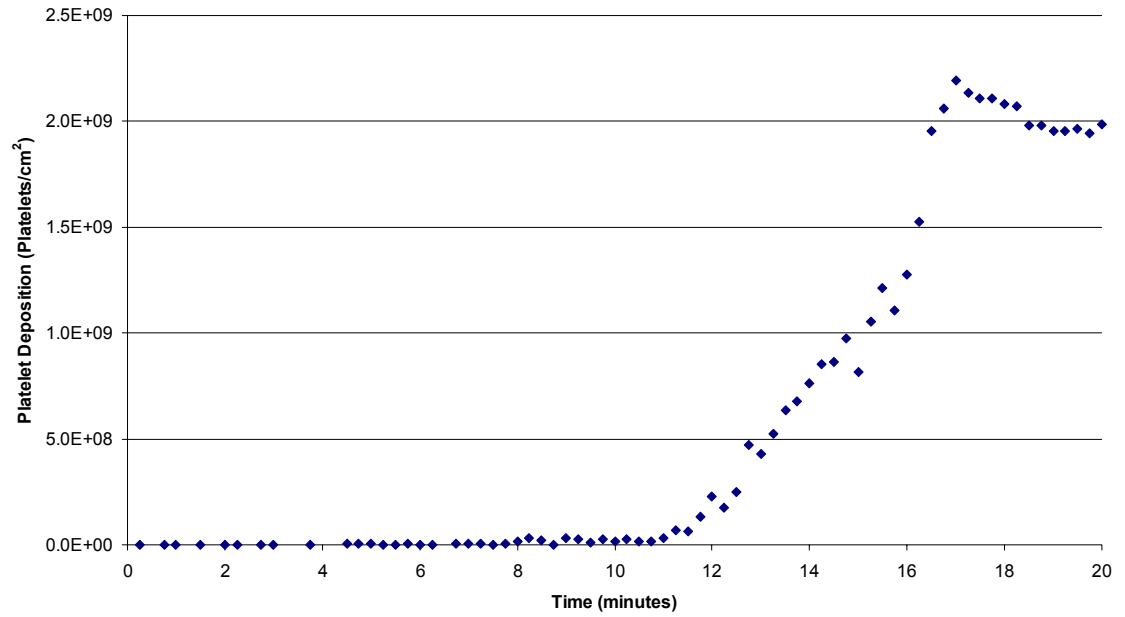


Figure 47. 85% stenosis. Platelet deposition based on analysis of the image sequence in Figure 36. Time of flow cessation was at 16.5 minutes. Experiment 12.15.9.

Platelet deposition in Figure 47 shows that platelet deposition is negligible before 10 minutes when it begins an acute deposition phase that does not terminate until after flow cessation. Platelet deposition after the time of flow cessation in this model, 16.5 minutes in Figure 36, should not be evaluated because separation in the glass tubes distal to the throat created white pixels which were not indicative of platelet deposition.

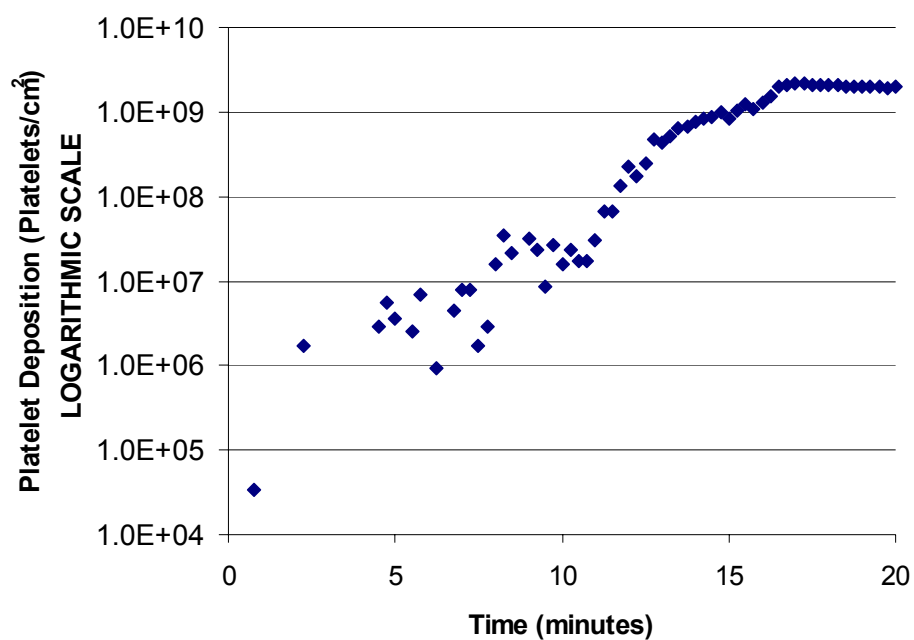


Figure 48. Reproduction of Figure 47 with a logarithmic scale for platelet deposition. Platelet deposition increased to the order of millions within the first five minutes and then slowly increased until the acute phase began around 12 minutes. Negative values were omitted.

An acute deposition rate constant was determined by fitting a line to the data between 12 and 16.5 minutes in Figure 47. The slope of this line is the acute deposition rate constant. In this case, the rate constant was 5×10^6 platelets/cm²/s.

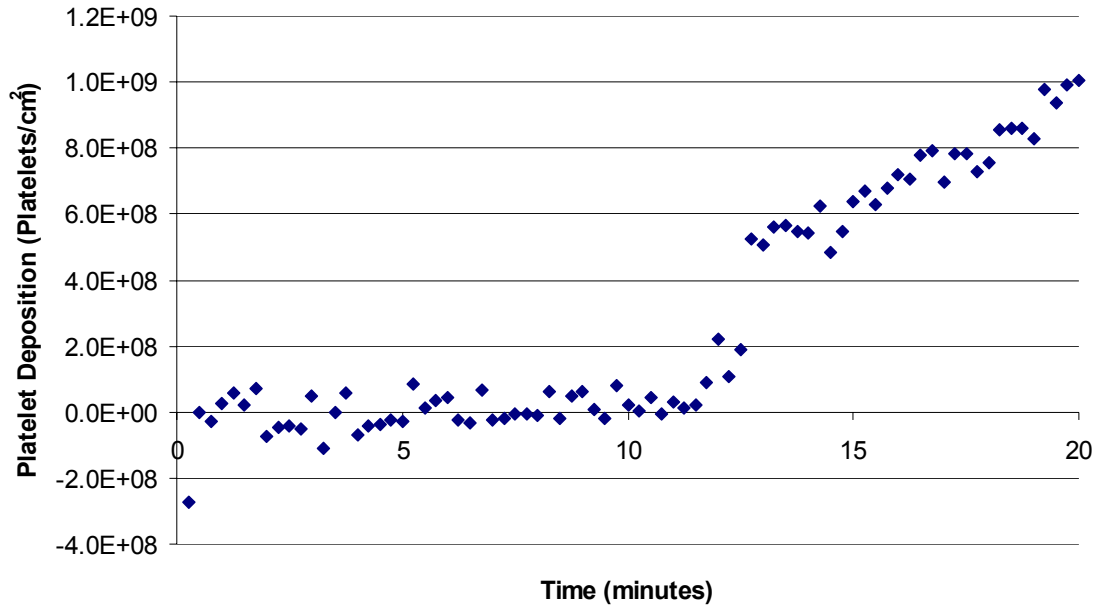


Figure 49. 96% stenosis. Platelet deposition based on analysis of the image sequence in Figure 38. Time of flow cessation was at 13.5 minutes. Experiment 12.15.33.

The errors for these values are on the order of $100 \text{ million platelets/cm}^2$, therefore the fluctuation and negative values before 10 minutes are understandable. The important value is the rate of acute deposition which was found for the time between 11 and 13.5 minutes to be $5 \times 10^6 \text{ platelets/cm}^2/\text{s}$.

In one experiment, shown in Figure 50 below, movement of the test section inhibited the continuous analysis of platelet deposition. Movement of the test sections was due to surface tension in the glycerin bath pulling the test section in one direction. Therefore, the mask was started after 8.25 minutes.

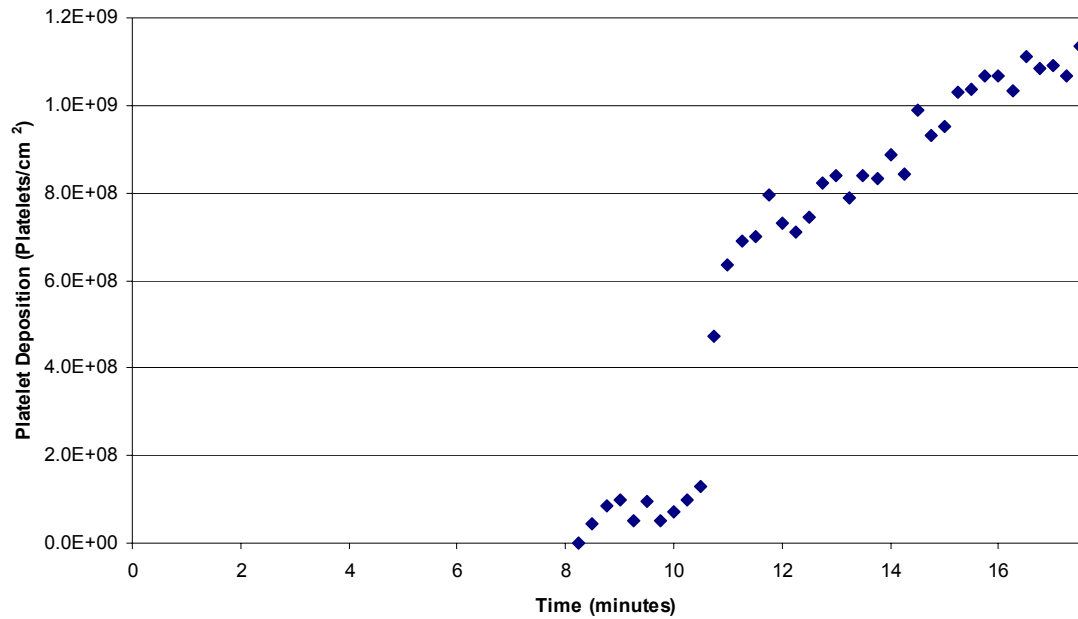


Figure 50. 85% stenosis. Platelet deposition based on analysis of the image sequence in Figure 37. Time of flow cessation was at 17.5 minutes. Experiment 12.8.9.

The acute rate of platelet deposition was calculated between 11 and 13.5 minutes to be 1.7×10^6 platelets/cm²/s.

Rate of Platelet Deposition under High Shear Rates

The rate of platelet deposition increased with shear rate using the acute rate as a comparable between experiments. Both platelet deposition models were used to compare the effect of high shear rates. There was good agreement between the models for 2 out of 3 experiments and all had the same order of magnitude.

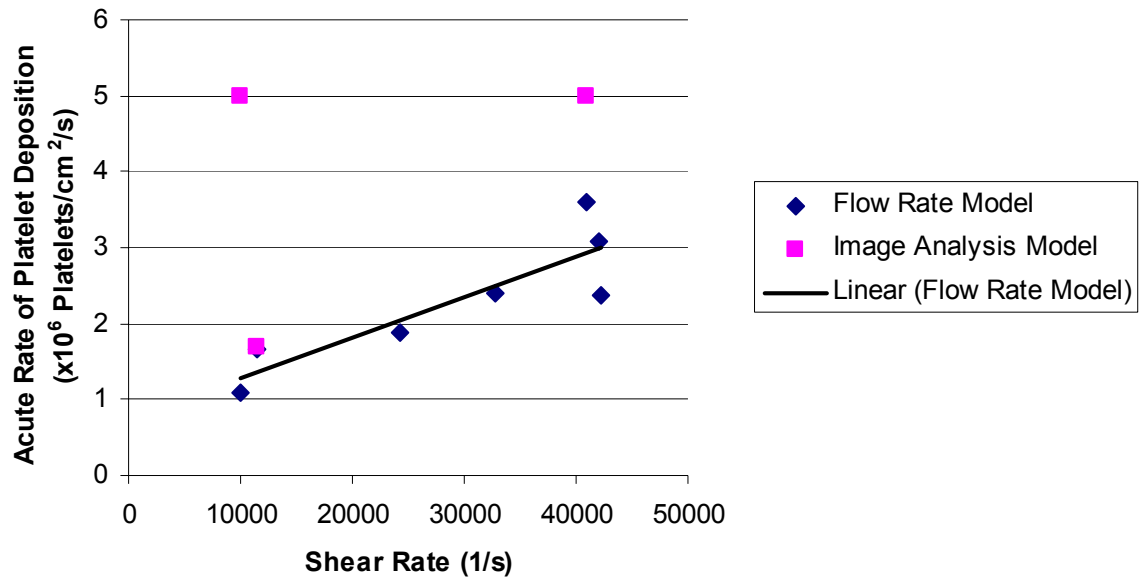


Figure 51. Both platelet deposition models showed that the acute rate of platelet deposition increased with shear rate. Plot included all 7 experiments that led to complete thrombotic occlusion, where 3 had analysis from both models. This data has also been presented in Table 4 below.

For the flow rate model, the rate of acute platelet deposition for each experiment increased with shear rate until $42,000 \text{ s}^{-1}$. The rate of platelet deposition was between 1.1 and 3.6 million platelets/cm²/s. Only three experiments had image analysis, so at these initial shear rates, the acute rate of platelet deposition was compared. They are on the same order of magnitude, but the image analysis model predicts a higher rate.

Table 4. The acute rates of platelet deposition for each platelet deposition model.

Percent Stenosis by Area	Experiment	Time of Flow Cessation (min)	Shear Rate (1/s)	Re # in Throat	Acute Rate of PD ($\times 10^6$ plts/cm ² /s)	Total Rate of PD ($\times 10^6$ plts/cm ² /s)	Acute Rate of PD ($\times 10^6$ plts/cm ² /s)
85	12.8.1.9	17.5	11,500	135	1.67	1.88	1.7
85	12.15.2.9	17.5	10,000	129	1.1	1.25	5
Avg \pm S.D.	85%	17.5 \pm 0.0	10,750 \pm 1,060	132 \pm 4	1.39 \pm 0.40	1.57 \pm 0.45	3.35 \pm 2.33
95	10.27.4.7	16.5	24,200	118	1.88	0.9	
96	11.3.3.33	10	32,700	96	2.4	1.95	
96	11.22.4.33	18	42,100	129	3.08	1.57	
96	12.1.2.33	13	42,200	138	2.37	2.03	
96	12.15.2.33	13.5	40,900	136	3.6	1.38	5
Avg \pm S.D.	$\geq 95\%$	14.2 \pm 3.1	36,420 \pm 7,890	123.4 \pm 17.2	2.67 \pm 0.67	1.57 \pm 0.46	

In summary, in the higher shear regime of $\geq 95\%$ stenosis by area, under an average initial shear rate of $36,420 \pm 7,890 \text{ s}^{-1}$ platelets deposited at an acute rate of 2.67 ± 0.67 million platelets/cm²/s as opposed to only 1.39 ± 0.40 million platelets/cm²/s under a lower average initial shear rate of $10,750 \pm 1,060 \text{ s}^{-1}$. The p-value for the comparison of acute rate was $p < 0.054$ using a two tailed t-Test. The average time of flow cessation was greater for the 85% stenosis at 17.5 ± 0.0 minutes in comparison to 14.2 ± 3.1 minutes for $\geq 95\%$ stenoses, $p < 0.078$ using a two tailed t-Test.

Histology and Composition Analysis

Five samples that caused blockage as a result of thrombotic occlusion were chosen for histological examination, as well as one embolus and some other various thrombi. A list of the samples and their status has been presented in Table 5 below.

Table 5. Status of Histological Samples.

TYPE	SAMPLE	DESCRIPTION	EMBEDDING	STAINED
<i>Occluding Thrombus</i>	11.8.1.33	Thrombus; 1-1.2 mm length originally	Longitudinal	NO
	11.22.4.33a	Thrombus and propagating tail;	Longitudinal	CARSTAIRS
	11.22.4.33b	red clot found on the propagating tail	Longitudinal	CARSTAIRS/vWF
	12.1.2.33	Thrombus; 1-1.2 mm length originally, sample tore in half before processing	X-SEC	CARSTAIRS/vWF
	12.8.1.9	Thrombus; downstream end of clot is the bottom end of section on the slide	Longitudinal	CARSTAIRS/vWF
	12.15.2.33	Thrombus connected to tail and red packet	Longitudinal	CARSTAIRS/vWF
<i>Emboli</i>	11.17.2.7	Embolus found	X-SEC	CARSTAIRS
<i>Other</i>	11.10.3.33	Thrombus on leading edge	X-SEC	NO
	11.17.2.33	Thrombus found on converging side	Longitudinal	CARSTAIRS
	12.8.1.39	Thrombus and possible embolus united	X-SEC	CARSTAIRS
<i>Control</i>	COAG	Coagulated Porcine Blood	X-SEC	

Other completely occlusive thrombi included 12.15.2.9 which was lost while removing it and 10.27.4.7 and 11.3.3.33 which were not saved for histological examination. 11.8.1.33 formed from thrombotic occlusion, although it had a non-steady

control and was exempt from analysis on this condition. 11.22.4.33 was split into two sections for embedding although they came from the same side of the occluding thrombus.

Table 6 lists the blood species and their respective characteristics after Carstairs staining.

Table 6. Appearance of Blood Species after Carstairs Staining.

Species	Appearance
Red Blood Cells (RBCs)	red or orange, large discoid cells (7-8 μm)
White Blood Cells	Purple, large spherical cells (~10 μm)
Platelets	Blue, small cell fragments (2-4 μm)
Fibrin	Purple or pink strands

In order to detect vWF, an anti-human vWF primary antibody was also used in an alkaline phosphatase detection system for immunohistochemistry. Secondary antibody was a biotintylated goat anti-rabbit. A red marker was matched to the secondary antibody and a background hematoxylin counter-stain was used to identify the remainder of the thrombus.

Dense packets of platelets were identified which may have been the dense areas described as striations during the experiment. The perimeter of the clots has a significant layer of fibrin. The following color images show the composition of the various clots.

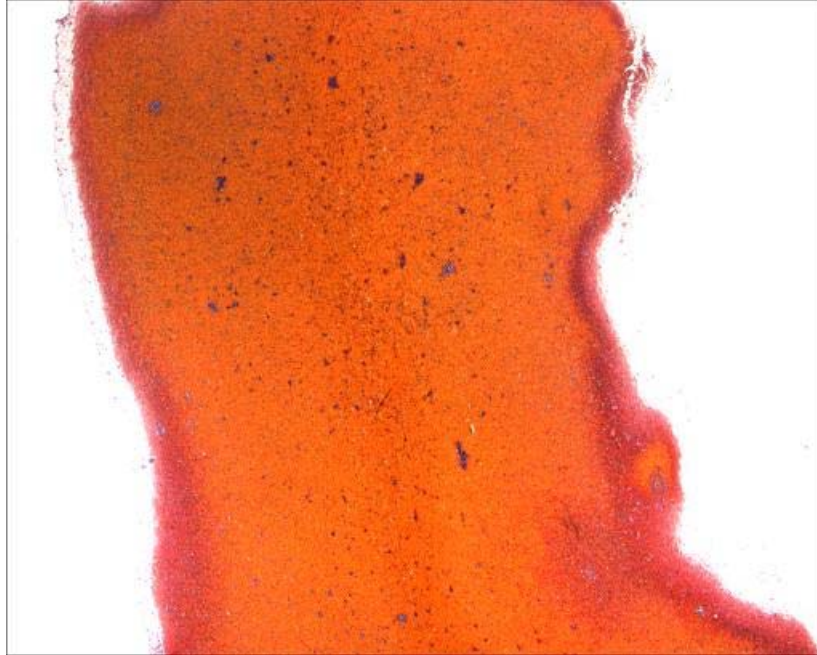


Figure 52. 4x magnification. Control. Porcine pig blood that had heparin anticoagulant but coagulated after 24 hours and was then fixed in formalin. Primarily RBCs with some platelet aggregates.

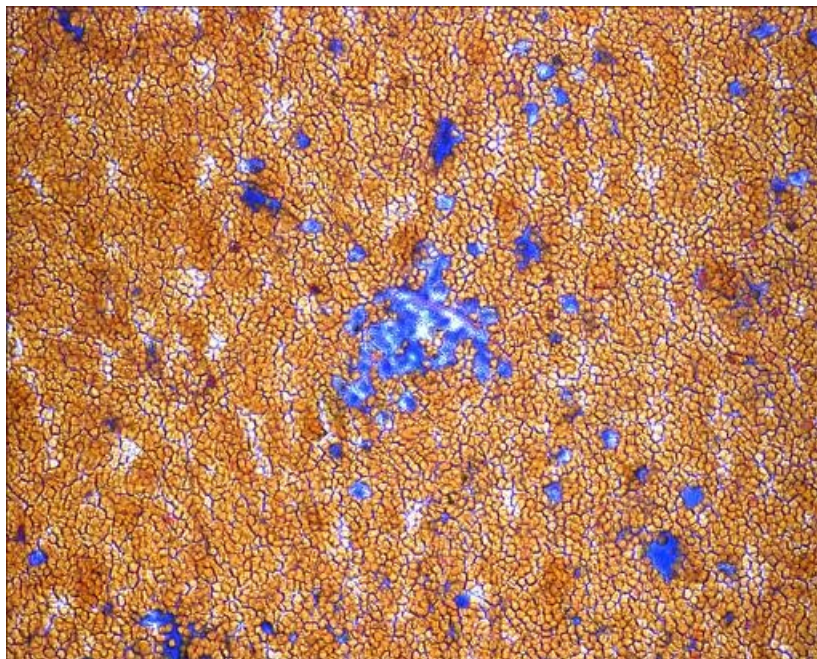


Figure 53. 40x magnification. Control. Primarily RBCs with some platelet aggregates.

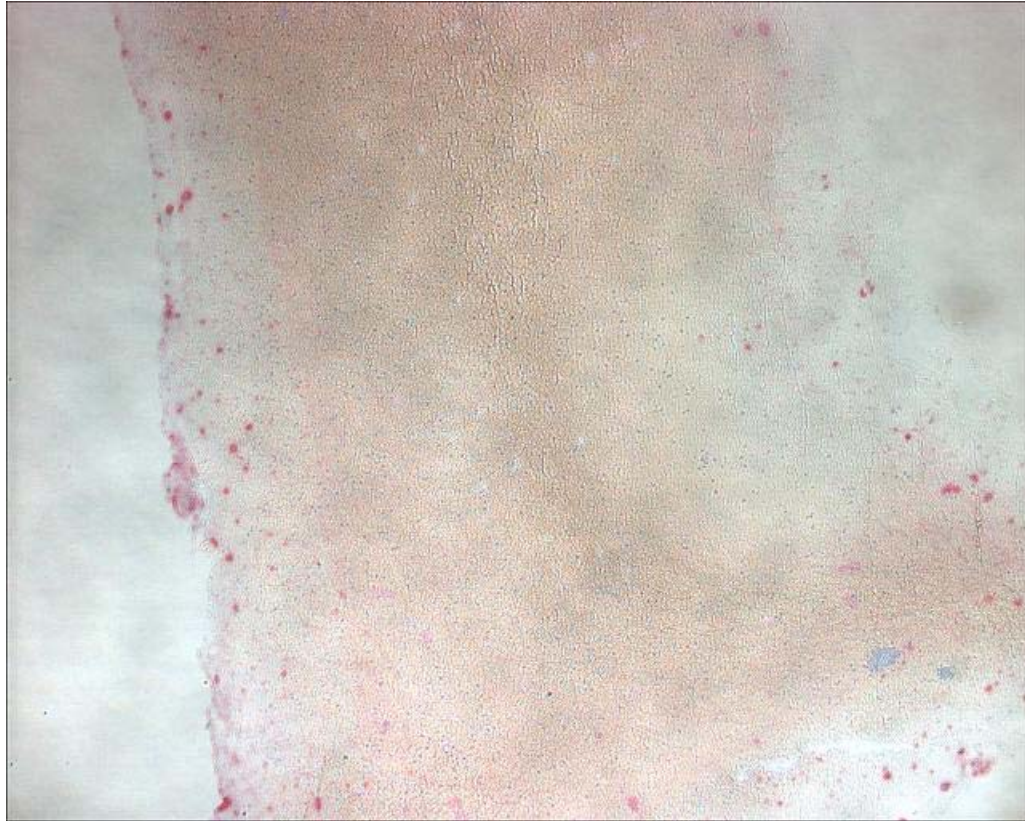


Figure 54. 4x magnification. Control. vWF antibody with a vector red stain and background with a hematoxylin counter-stain.

Von Willebrand Factor is present in the control coagulated porcine sample, especially on the periphery.

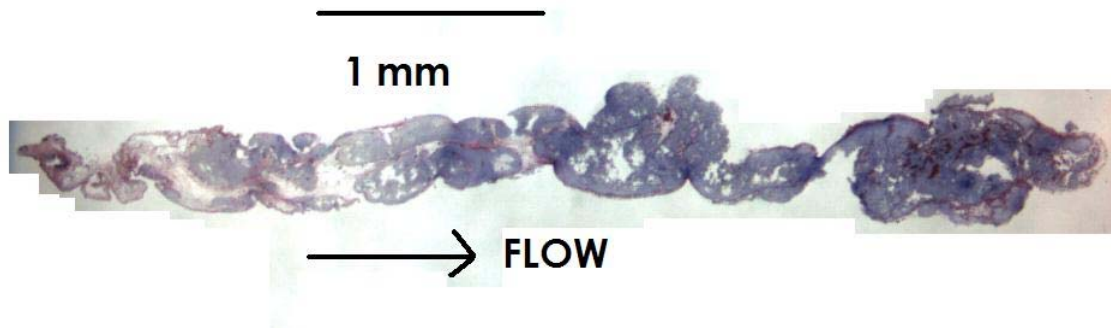


Figure 55. Sample 12.8.1.9. 85% stenosis. Occluding thrombus was composed primarily of platelets and fibrin. Original length was measured as 6 mm. After processing it shrunk to 4.8 mm as has been presented. Average width was about 0.4 mm. The inner diameter of the stenosis throat was 0.61 mm. Upstream end was fibrin rich and downstream end was bulky with RBCs trapped in rows. Multiple images were photographed at 10x and then photostitched together.

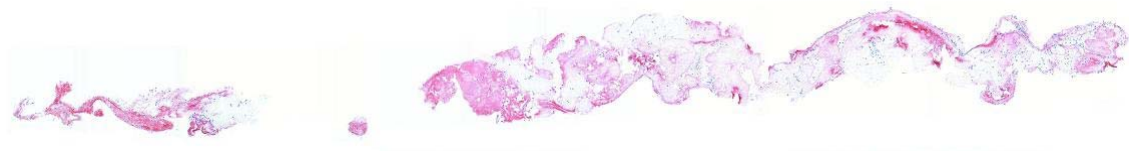


Figure 56. Sample 12.8.1.9. 85% stenosis. vWF antibody used with red stain indicates that vWF is present in the occluding thrombus. Cross section taken approximately 200 microns from Figure 55 above.

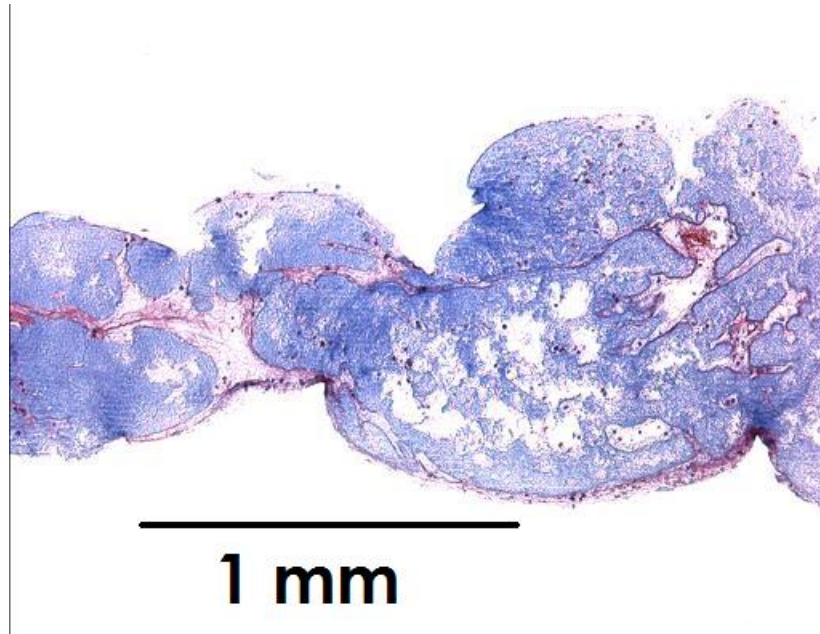


Figure 57. Sample 12.8.1.9. 10x magnification. Fibrin layer was evident not only on the perimeter but has also formed centrally in lines parallel with the axis. Scattered WBCs could be identified by their circular shape. The parallel lines on the lower end of image were artifacts of sectioning.

The relative percentage of platelets was determined from Figure 55 of sample 12.8.1.9. The percentage of platelets, WBCs, RBCs, and fibrin was 81%, 1%, 1%, and 17%. Images were taken on a Nikon E600 microscope at 10x magnification. The images were stitched together with Canon Photostitch 3.1.



Figure 58. Sample 12.8.1.9. 10x magnification. vWF was present in regions of platelets and has varying density.

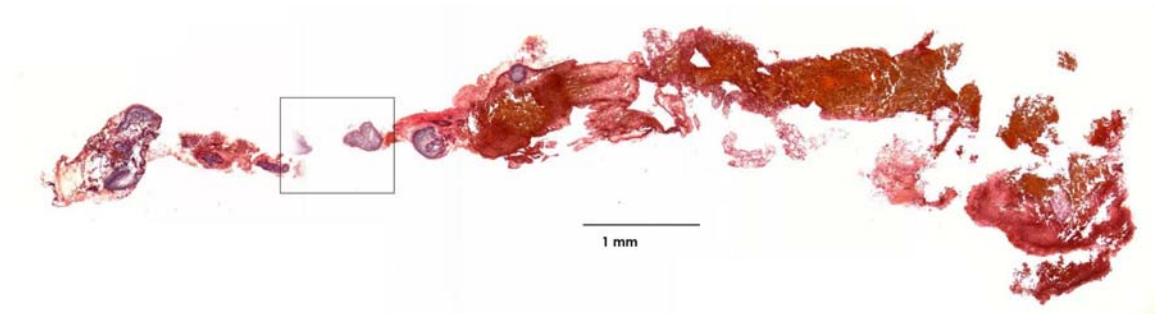


Figure 59. Sample 11.22.4.33. Occluding thrombus is on the left and a propagating tail of thrombus was identified as primarily RBCs and fibrin. Photostitched image at 4x magnification. The box shows the zone that has been magnified in Figure 60 below although it is from another cross section that represents the occluding thrombus better.

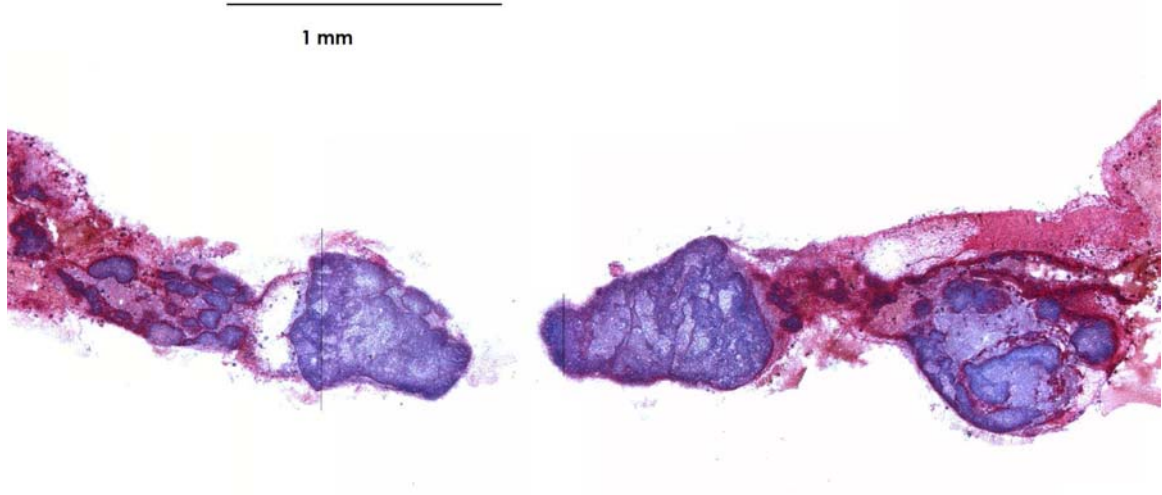


Figure 60. Sample 11.22.4.33. Occluding thrombus. 10x magnification. Thrombus was heavily composed of platelets and lines of fibrin. There were platelet dense regions and the most dense regions exist where blue was most intense. The clot was not connected because either (1) this longitudinal cross section was at the throat of the stenosis but it was not in the center of the lumen, or (2) it was cleaved during processing. The clot on the left is magnified in Figure 61 below.

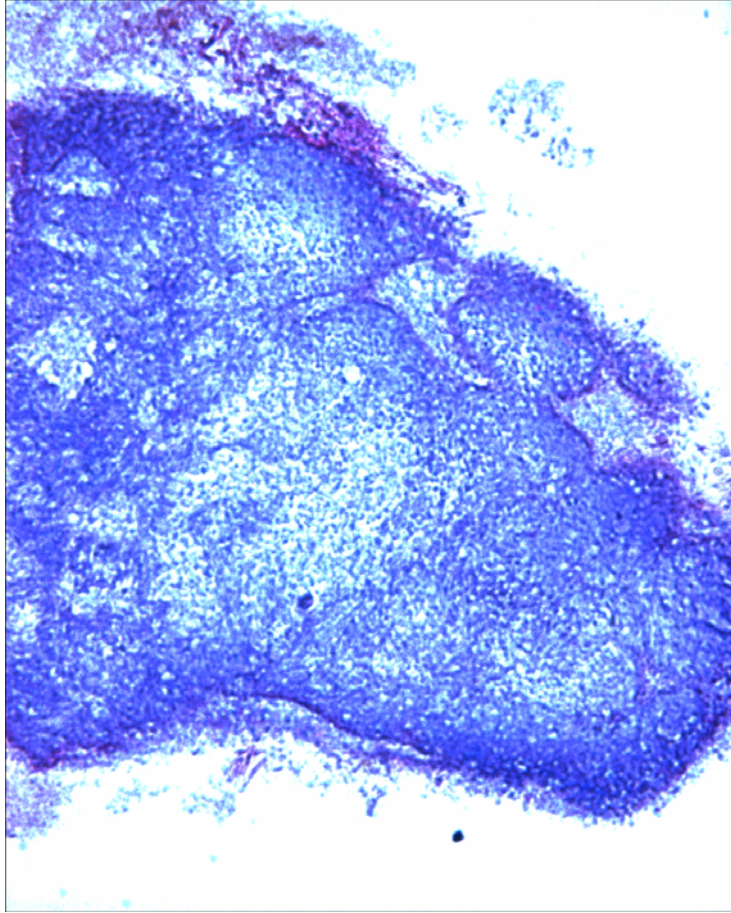


Figure 61. Sample 11.22.4.33. Occluding thrombus. 40x magnification. The clot has varying densities of platelets as was observed from the intensity of blue shade. Only a small amount of fibrin was visible on the top right and along the perimeter.



Figure 62. Sample 11.22.4.33. vWF present in thrombus. Four images photostitched as in Figure 59 above.

In this next sample, a fibrin tail formed distal to a 96% stenosis. The thrombus in this experiment migrated or rolled from the converging section into the throat of the stenosis, visible in the movie discussed earlier. The thrombus is visible at the back end of the occluding thrombus featured in Figure 63 below. It has a high platelet concentration but is not as long as the previous examples. The connections between each of the sections are highlighted because the species in that connection were under extreme stresses. The connection from the occluding thrombus to the RBC packet was probably under high stress during formation. The connection to the fibrin tail may have been under relatively less stress as a result of the low-shear expansion region. It was unknown whether the tail formed on the upstream or downstream side of the stenosis.

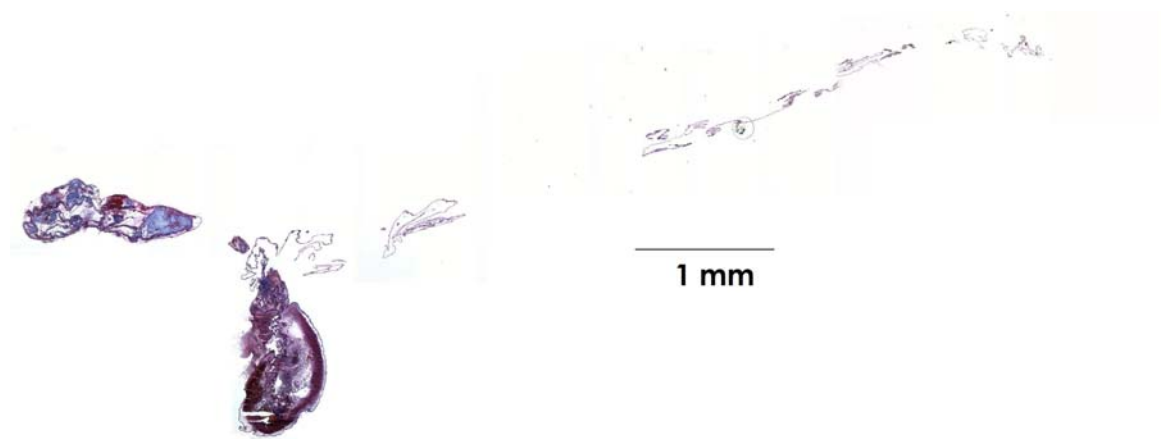


Figure 63. Sample 12.15.2.33. Images taken at 4x and photostitched together. Distal to the occluding thrombus is a large packet of fibrin and RBCs with some strings of platelets. Distal to the connection between the thrombus and the packet is a propagating tail of 9 mm length. After processing and histology it shrunk to approximately 5.7 mm. The tail can be seen in Figures 68 and 69 below.

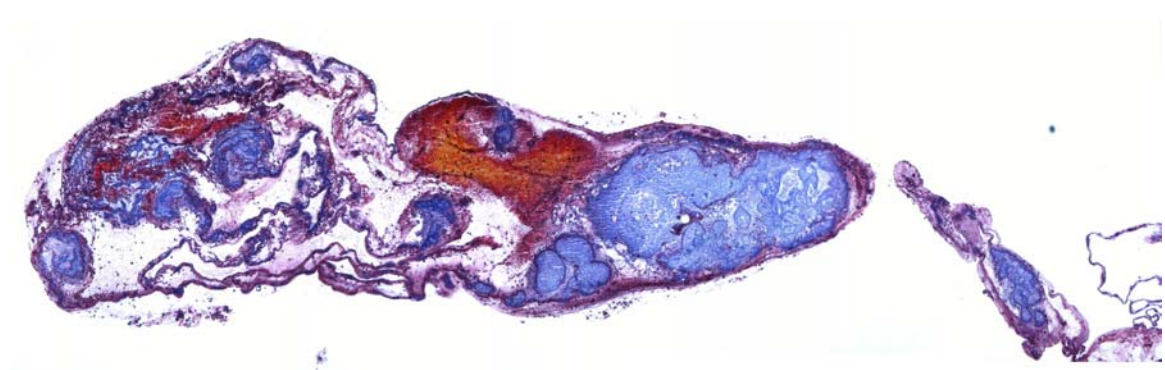


Figure 64. Sample 12.15.2.33. Occluding thrombus. Images taken at 10x and photostitched together. The composition is primarily platelets, although in the center there is a large deposit of RBCs which is surrounded by fibrin. The connection to the remainder of the clot is magnified in Figure 66 below.

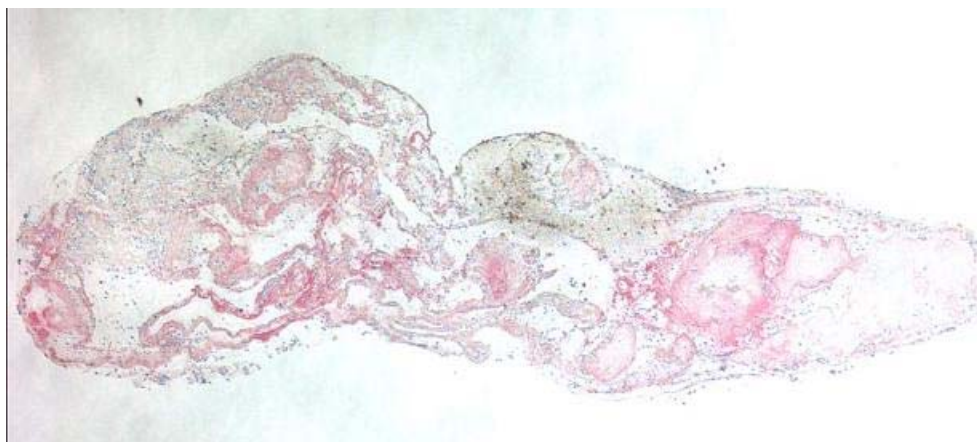


Figure 65. Sample 12.15.2.33. Occluding thrombus with vWF marker. Images taken at 4x and photostitched together.

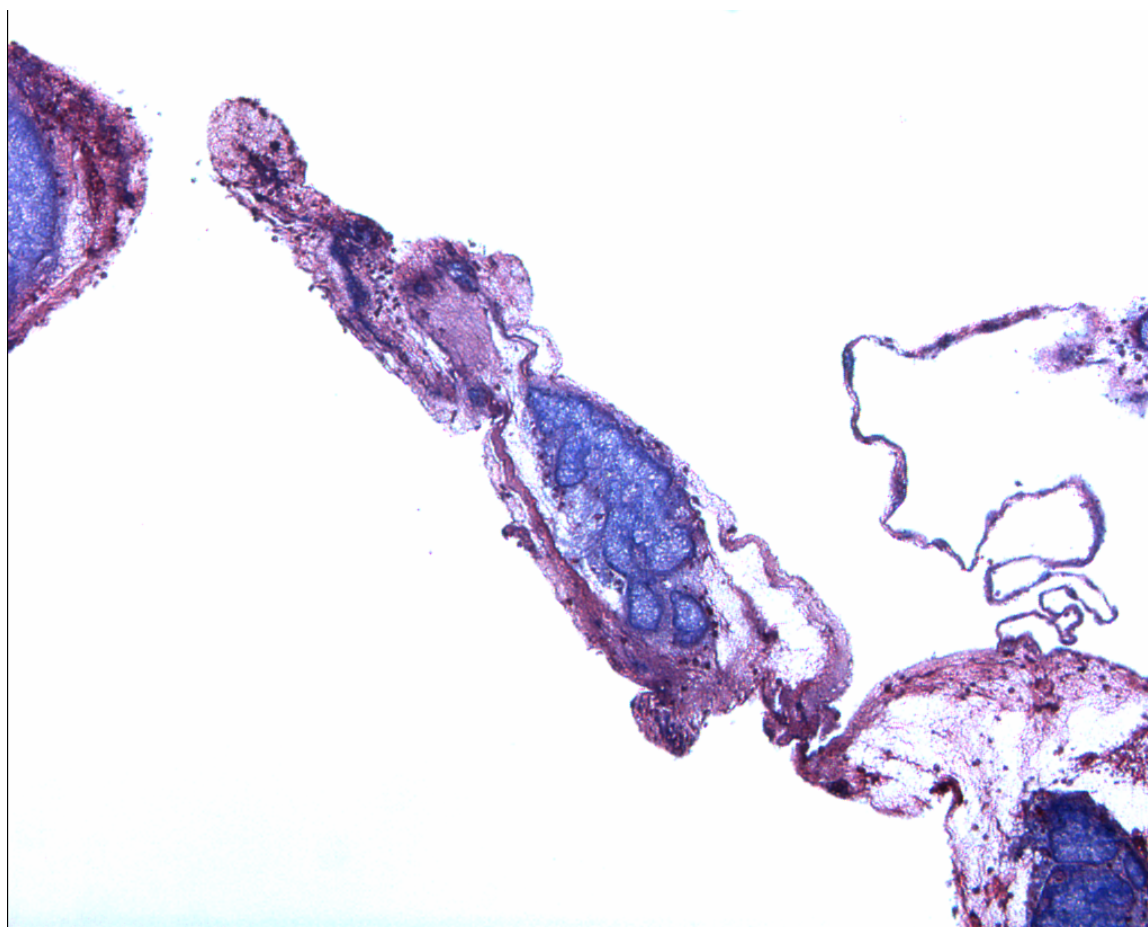


Figure 66. Sample 12.15.2.33. Connection between occluding thrombus and RBC packet. 10x magnification. Some large deposits of platelet rich thrombus and a few scattered RBCs attached. Connection was primarily fibrin with some lines of platelets.

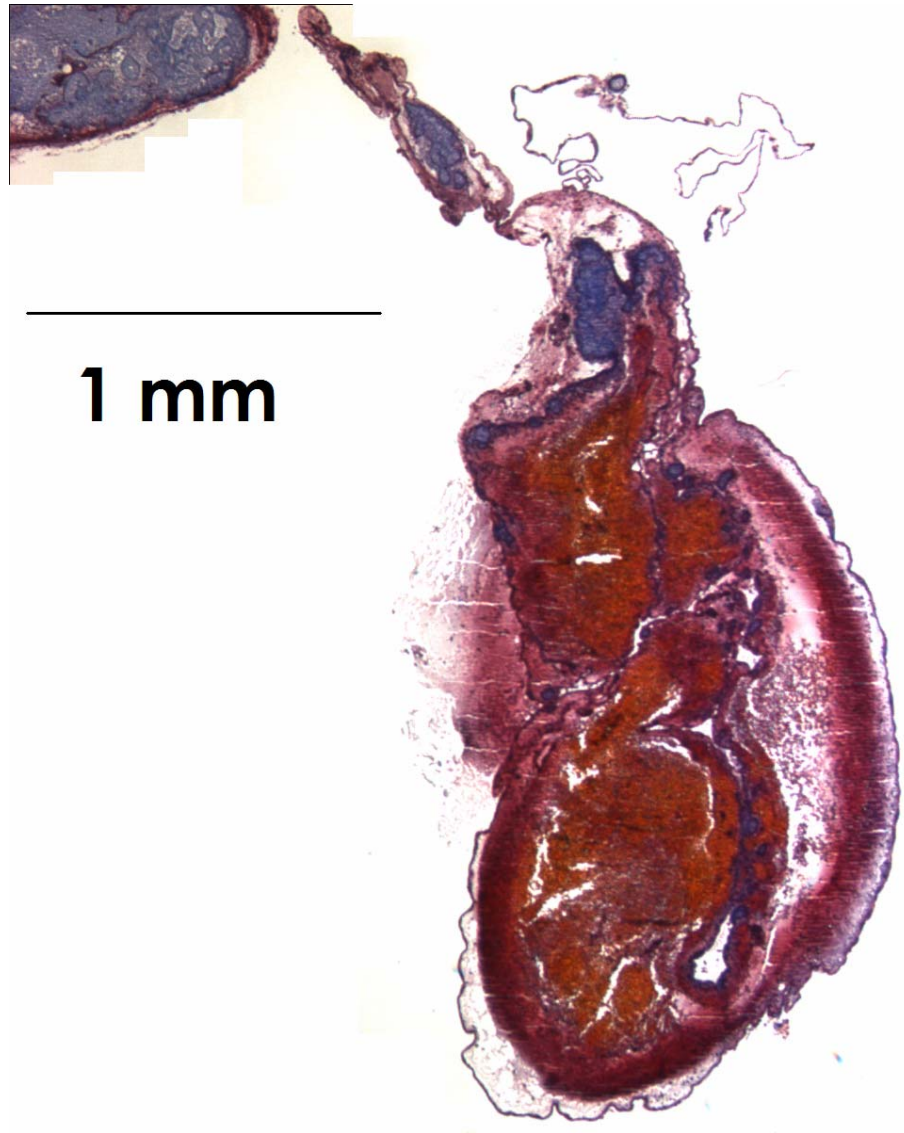


Figure 67. Sample 12.15.2.33. RBC packet. 4x magnification. Fibrin clearly on the perimeter and a one layer deeper is a dense RBC region. Platelets are mostly at the top closest to the connection as well as on the borders of a channel that goes through the packet.

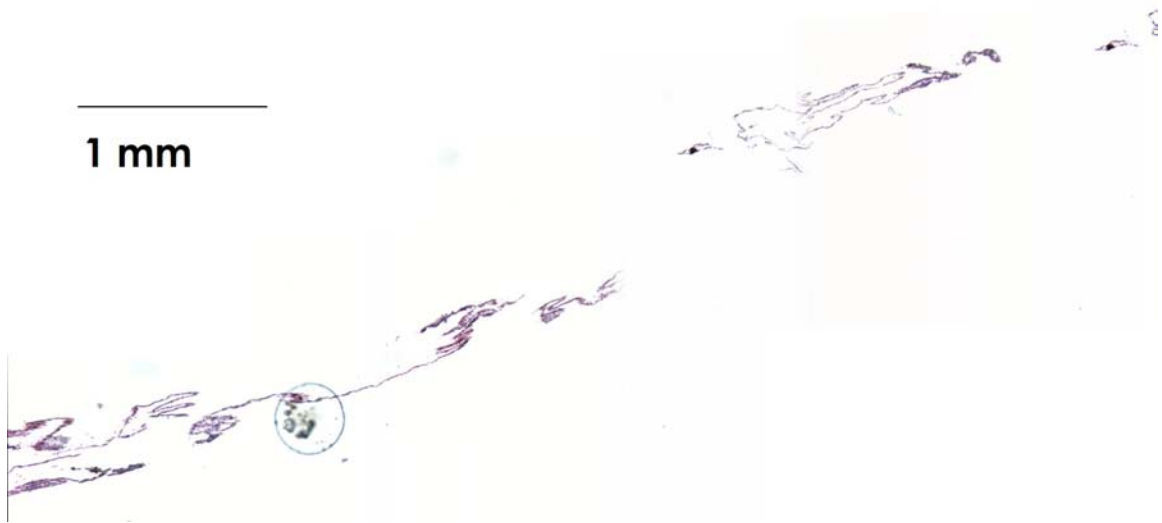


Figure 68. Sample 12.15.2.33. Fibrin tail. Primarily fibrin with some platelets. 4x magnification.

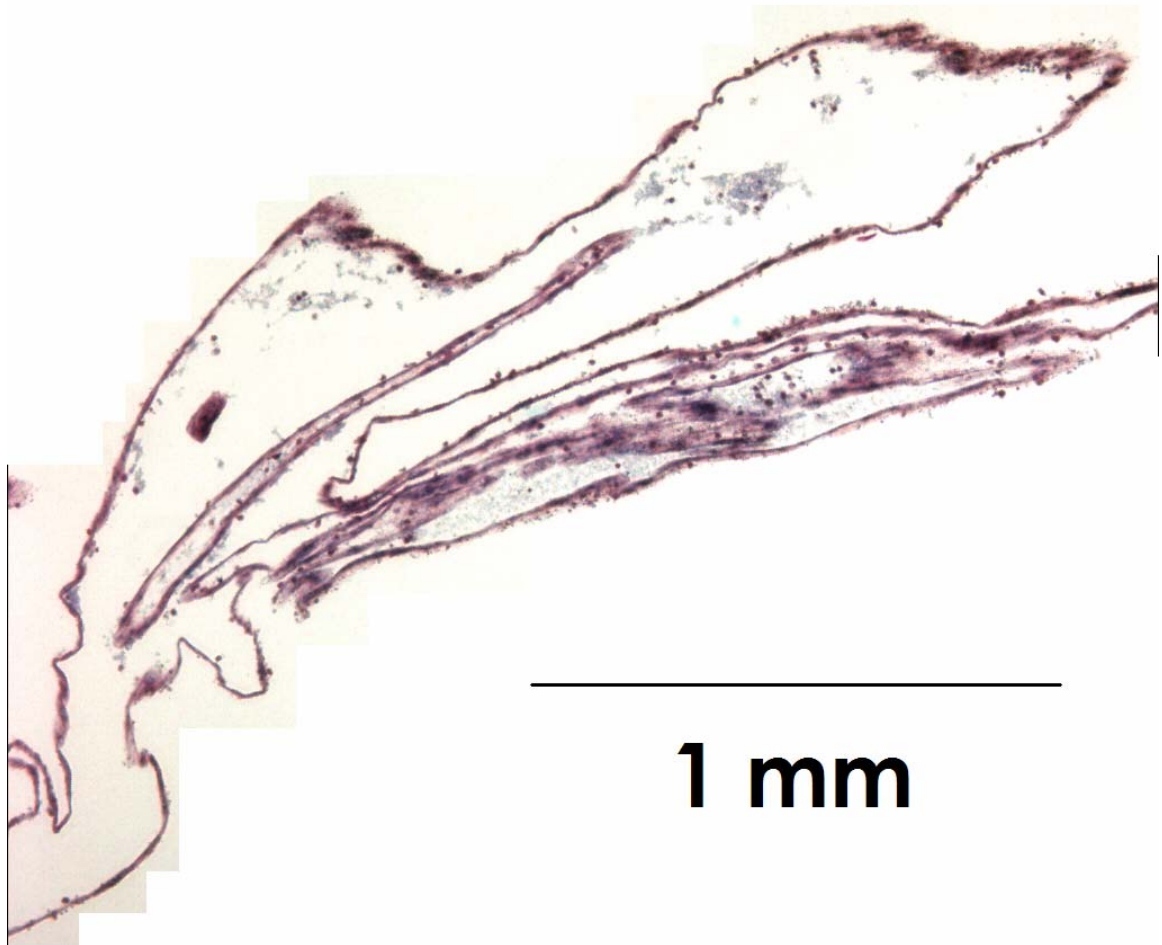


Figure 69. Sample 12.15.2.33. This is a segment of the fibrin tail which was primarily fibrin with some platelets and WBCs visible. The tail was one continuous sheet although when sectioned it only showing the folds which are the curves visible in the figure. 10x magnification.

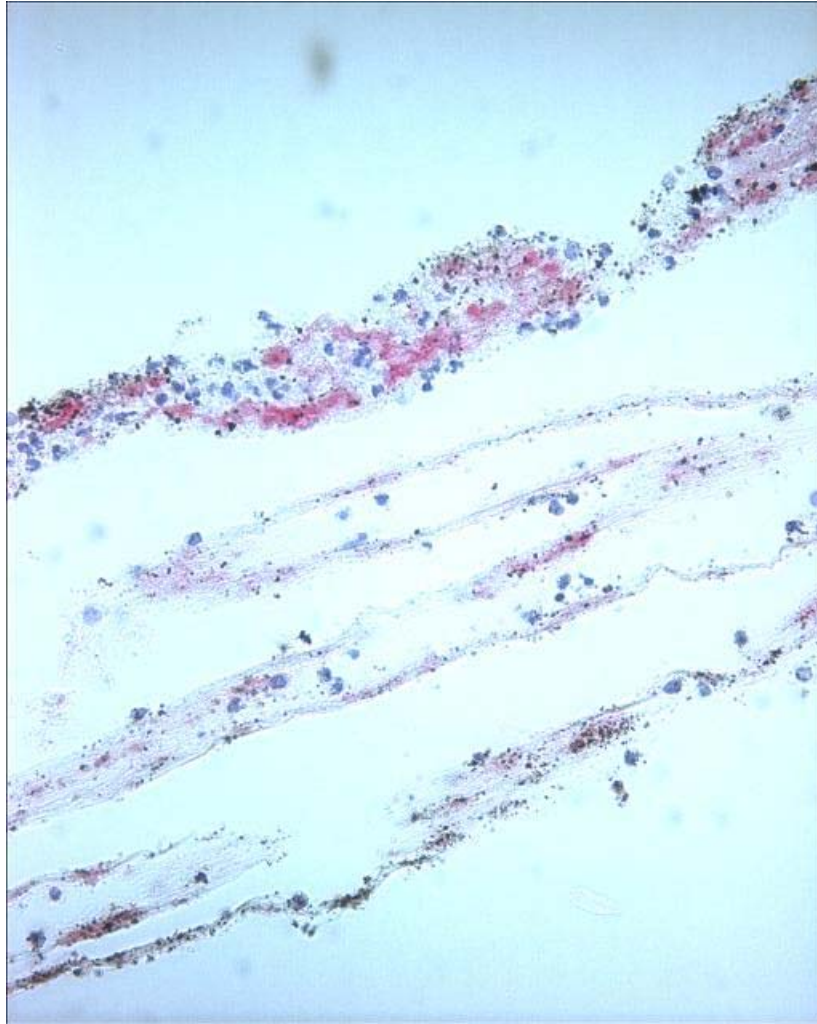


Figure 70. Sample 12.15.2.33. vWF is present in the propagating tail.

Thrombus formed in the stenosis was difficult to remove during cleaning whereas removal of embolus was very easy.

Fibrin Tail Propagation

Histological data demonstrate that the propagating tail in sample 12.15.2.33 was constituted primarily of fibrin with smaller amounts of platelets and WBCs. vWF has also been identified, and may be in conjunction with platelets or present as a plasma

protein. This was the single experiment where a fibrin tail was identified and therefore the occurrence was 1 out of 7 cases which led to complete occlusion. From thrombus formation images taken during the formation of the occluding thrombus, it is evident that only a small channel was patent on the side of the stenosis throat before total occlusion. Therefore the shear forces in the channel may have been enormous and the region distal had flow separation and regions of high residence time. The propagation of the tail was approximately 14.2 mm measured after fixation and 5.7 mm from histological analysis after processing.

CHAPTER V

RESULTS: DETACHMENT STRENGTH OF THROMBUS

The force required to detach the thrombus was estimated based on the maximum upstream pressure measured before removal. Thrombus removal was attempted in 4 out of the 7 cases of complete thrombotic occlusion. Based on results from 1 out of the 4 experiments that met the necessary criterion, the detachment force of the thrombus was approximately 9 milli-Newtons. Emboli were also removed in order to compare the maximum pressure required to remove an attached thrombus rather than a particle that occluded flow.

The thrombus was completely removed from the throat region in 3 out of 4 thrombus removal experiments. Thrombi covered primarily the converging, throat, and diverging sections of the stenosis and tended to stay united in one body, although some areas of the thrombus were denser than others. In the single removal experiment that did not detach in one body, a channel of blood flow formed in the thrombus and the thrombus did not detach from the wall.

The attachment of the thrombus was affected by stasis and the duration of time between the formation of the clot and the removal. Thrombus detached from the wall in two experiments where the removal experiment was completed 100 minutes or later from the occasion of thrombotic occlusion. Although in flow platelets aggregated and the thrombus firmly attached to the surface, in stasis thrombus detached from the wall. Table 7 below identifies the approximate duration of time between the time of flow cessation and the time of thrombus/embolus removal.

Table 7. Summary of all removal experiments including removal of emboli.

Number	Time between Occlusion and Removal (minutes)	Max Upstream Pressure (mmHg)	Experiment	TO/E	Did the Thrombus/Embolus Remove in One Piece?
1	40	438	12.1.2.33	TO	Yes
	30	-	12.1.2.7	E	Yes
2	90	66	12.8.1.9	TO	No
	75	-	12.8.1.39	E	Yes
3	100	182	12.15.2.9	TO	Yes
4	170	730	12.15.2.33	TO	Yes
	75	382	12.15.2.39	E	Yes

The four thrombus removal experiments are numbered 1 through 4 and designated Thrombotic Occlusion (TO) as opposed to Embolus (E). The maximum upstream pressures recorded at the time of thrombus removal has also been presented in Table 7 although only the 1st experiment was applicable for analysis of thrombus detachment strength because of the criterion listed below.

Detachment Strength of Thrombus

The force that acted on the thrombus at the time of detachment was calculated based on the maximum upstream pressure before removal. This analysis was done for removal experiments where the following conditions applied: (A) the thrombus remained adherent to the surface of the stenosis until removal, and (B) the thrombus dislodged completely from the throat. The only experiment in this work that met these conditions

was experiment 12.1.2.33, described below. Since only one data point was available, the calculation was an order of magnitude approximation.

The maximum upstream pressure at removal for this experiment was 438 mmHg. The maximum force at the time of removal was calculated using Equation 14.

$$F_{\max} = P_{\max} \times A \quad \text{Equation 14}$$

where the maximum force (F_{\max}) on the thrombus at the time of detachment was the product of the maximum pressure (P_{\max}) at that time and the cross-sectional area (A) at the widest part of the thrombus. The widest part of the thrombus was determined from dimensions measured from images taken after the removal. The maximum pressure acted on the area of $\pi \times D^2 / 4$, where D was the greatest width of the thrombus. For the thrombus in this experiment the max width of the thrombus, D , was 0.44 mm therefore the maximum pressure of 438 mmHg acted over 0.15 mm² which produced a force on the thrombus of 8.9 milli-Newtons (mN). The thrombus was assumed to be a rigid body and the cross section of the thrombus of the surface between the blood and the clot was assumed to be circular.

Thrombus Removal Experiments

Removal of thrombi was attempted on 4 completely occlusive thrombi and the maximum pressures reached were between 66 and 730 mmHg. Each of the removal experiments of the four thrombotic occlusions as well as one embolus removal experiment has been described below.

1. Experiment 12.1.2.33

In this experiment, the thrombus was attached to the surface of the stenosis and it was removed completely. Images taken before and after illustrate that the thrombus was attached throughout the throat of the stenosis, that it moved downstream after removal, and that only a minor layer of thrombus remained after removal.

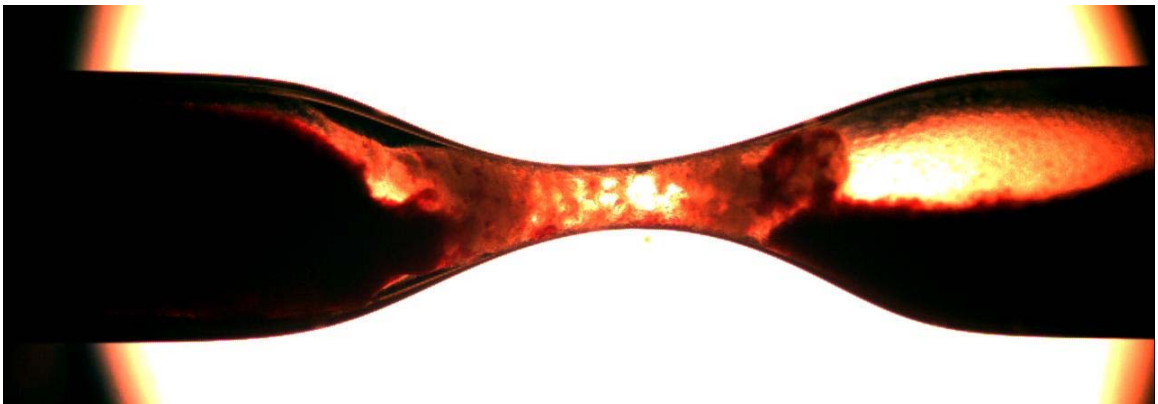


Figure 71. Image of occluding thrombus before removal. Blood separated on the downstream side due to stasis. Flow was from left to right. 2x magnification. Throat diameter is 310 μm in this 96% stenosis.

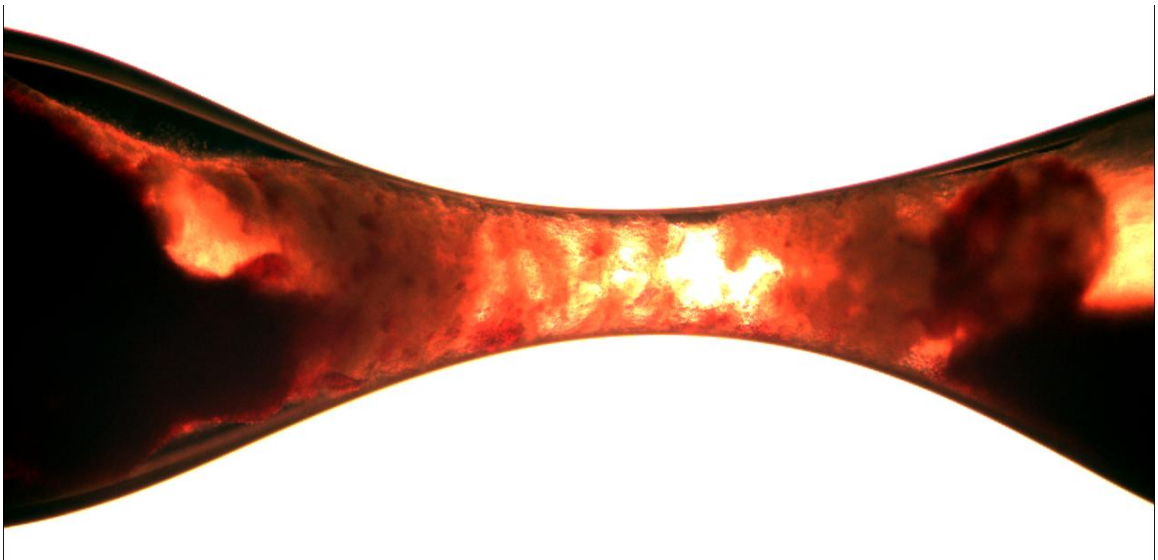


Figure 72. Higher magnification on apex of stenosis. Image of occluding thrombus before removal. Striations were visible and the clot was exposed due to the clear plasma

on the sides. Thrombus was attached to the walls. Flow was from left to right. 4x magnification. Throat diameter was 310 μm in this 96% stenosis.

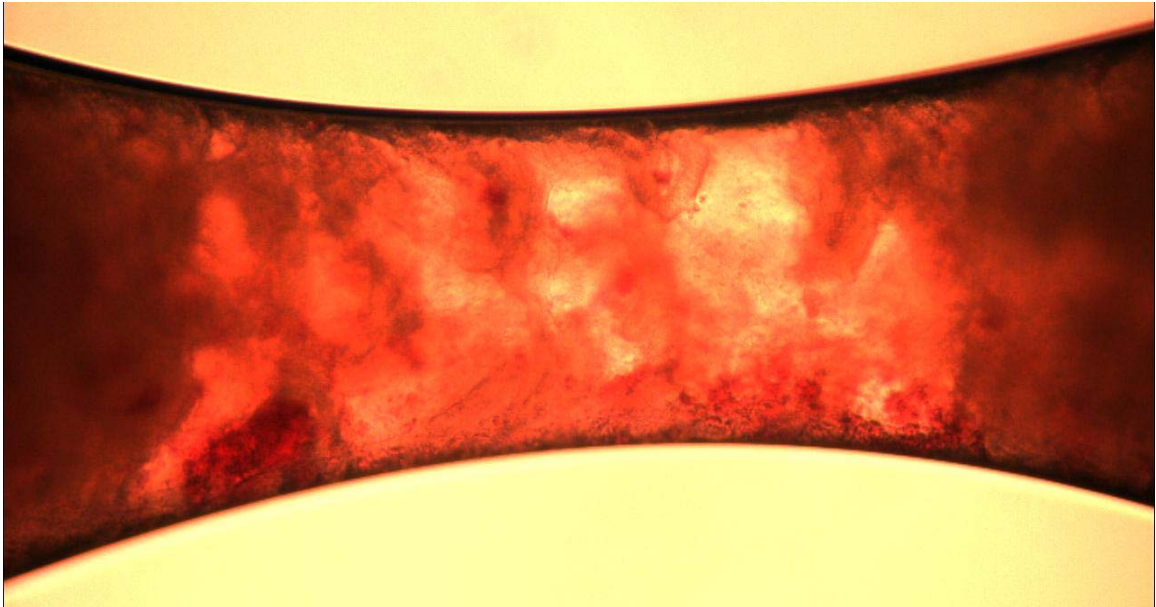


Figure 73. Thrombus was attached to the walls. Higher magnification on apex of stenosis before thrombus removal. 10x magnification.

For this experiment, blood was drawn at 8.30 am and the clot was formed by 12.07 pm. The images in Figures 71 to 73 were taken approximately 20 minutes later. Thrombus removal experiments began at 12.45 pm, within an hour of the thrombus formation. The images taken after removal in Figures 75 and 76 below were taken at 2 pm.

It was evident from visual observation during the experiment that the thrombus was almost one complete body when it detached. Figure 74 shows the rise of upstream pressure over time.

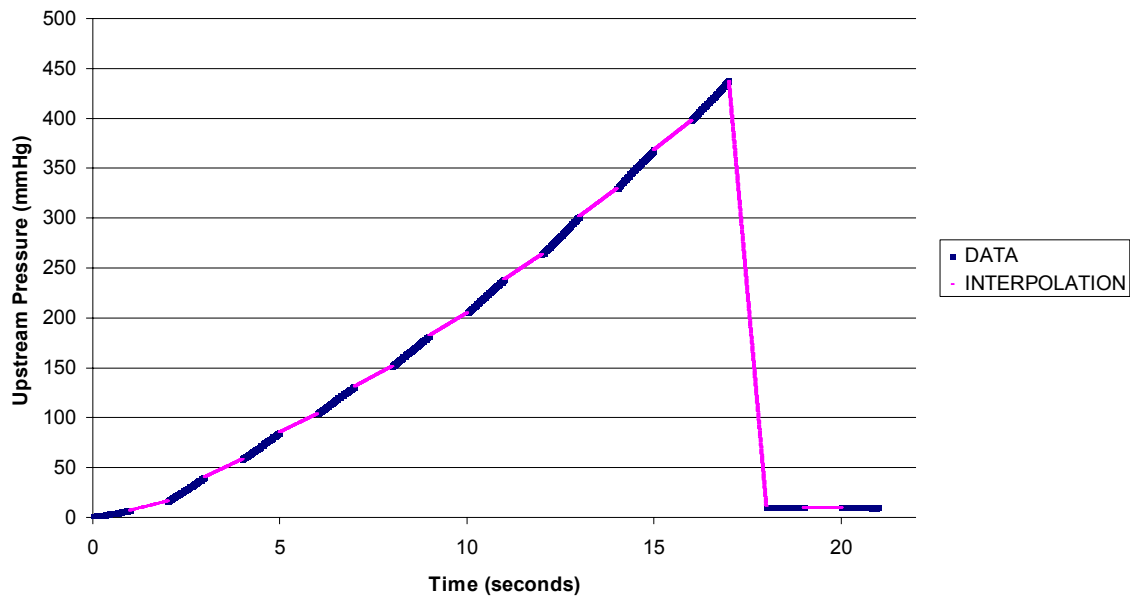


Figure 74. Upstream pressure reached a maximum around 450-500 mmHg. The data acquisition system recorded only one half of a cycle, therefore data measurement missed the peak. Gaps in data were filled in by interpolation. Experiment 12.1.33.

Based on the raw data alone, the upstream pressure reached a maximum at 438 mmHg. Interpolation of the last and first data points provided an estimate of a continuous pressure curve. This was a conservative underestimate within 10 mmHg (~ 2.5 %) of the pressure that the thrombus was removed because the interpolation was made from the greatest pressure recorded to the next measurement which was only 9 mmHg. Images taken after the removal showed that the thrombus was completely detached from the throat, but remained adhered distally, as seen in Figure 75.

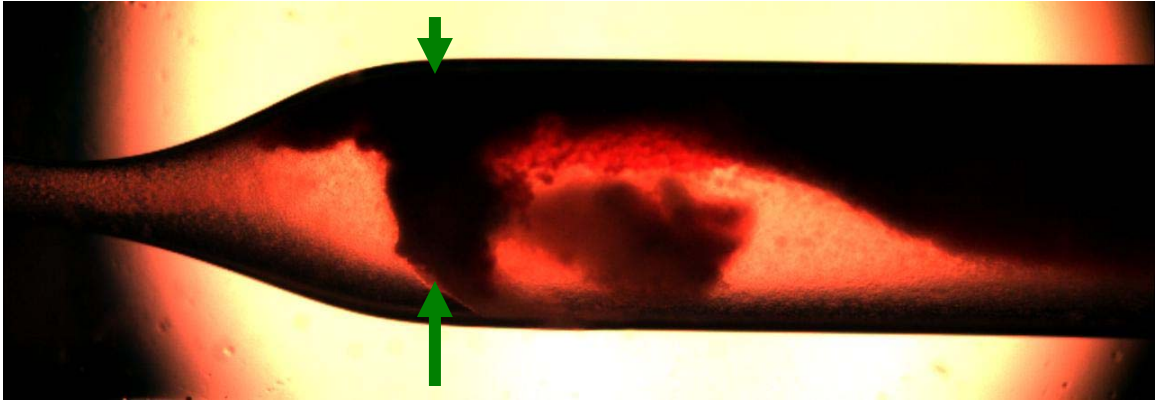


Figure 75. The downstream side of the stenosis. The thrombus was seen laying in the lumen and remained attached to the wall (indicated with green arrows) near the edge of the diverging segment. 2x magnification. The downstream inner diameter was approximately 1.62 mm.

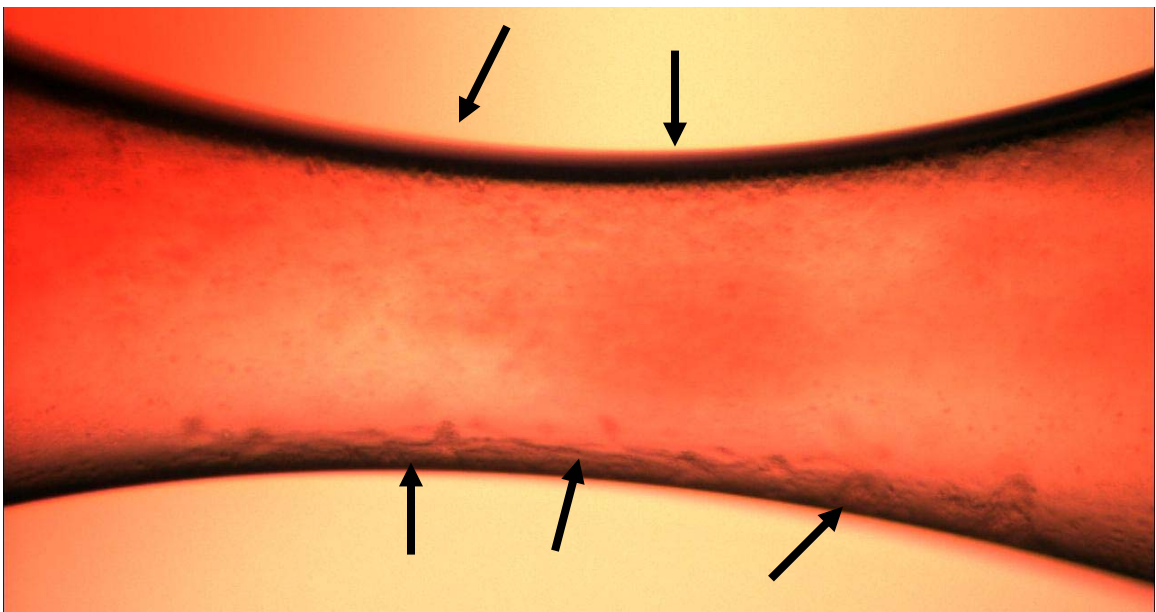


Figure 76. The apex of the stenosis showed a small amount of thrombus (indicated with arrows) still attached to the wall of the stenosis. Throat diameter was 310 μm . 10x magnification.

There was some remaining thrombus in the stenosis after removal as shown in Figure 76 above. The occluding thrombus was detached from this mural thrombus on the inner surface and left the lumen of the stenosis covered with a thin layer of visible

thrombus. Therefore the thrombus and collagen were not stripped off of the smooth glass surface together in this experiment. Collagen on the glass surface alone was not visible. This indicates that the weakest bond was platelet to platelet, not platelet to collagen or collagen to glass.

2. Experiment 12.8.1.9

In this experiment, the thrombus was attached throughout the stenosis throat but did not detach in one complete body. Pressure build up of around 60 mmHg was relieved by the formation of a channel of blood flow. The maximum pressure recorded was 66 mmHg as shown in Figure 78.

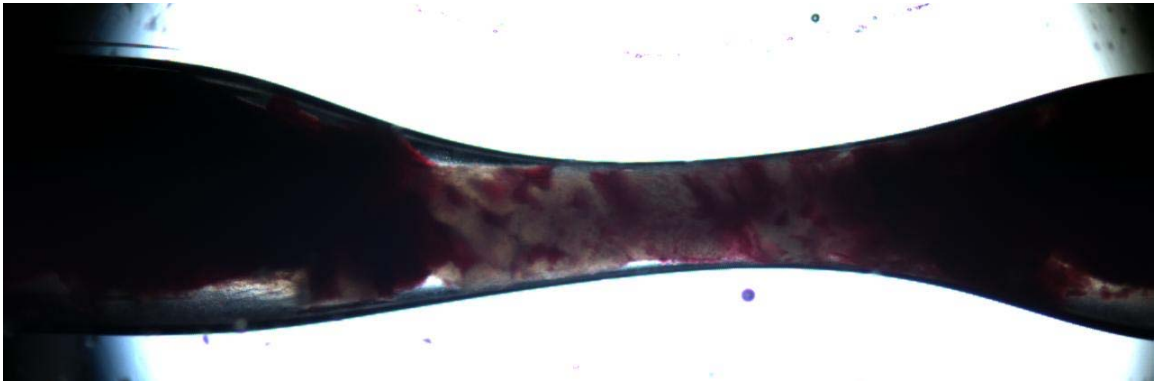


Figure 77. Image of the occluding thrombus before removal. The occluding thrombus was attached throughout the throat and was primarily white thrombus although it had pockets of RBCs intermittently. Throat diameter was 610 μm . 2x magnification.

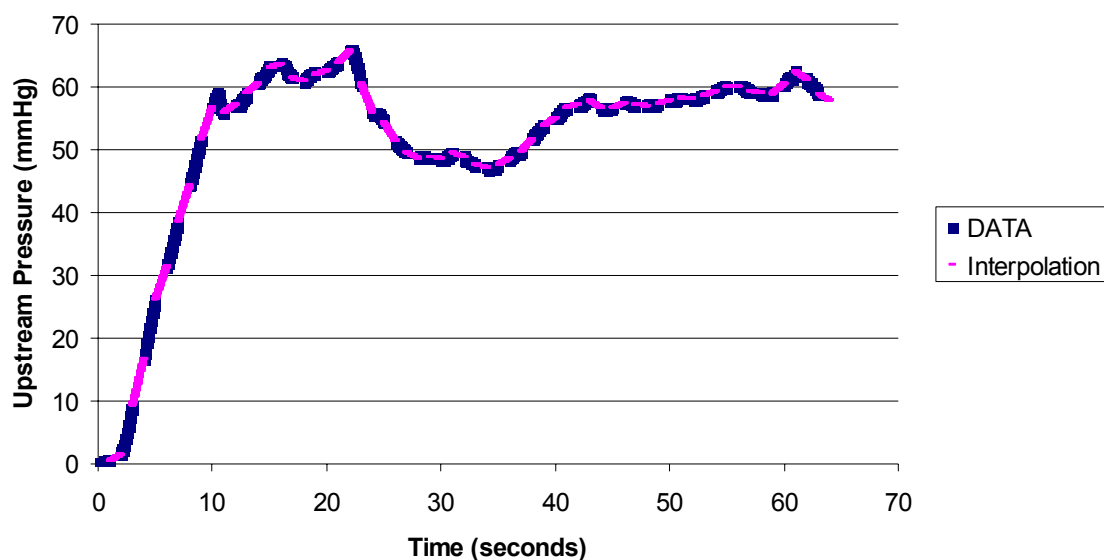


Figure 78. Upstream pressure reached a maximum around 66 mmHg. From visual observation, a channel opened through the center of the thrombus which relieved pressure but the thrombus did not detach from the walls. Interpolation of the last and first data points provided an estimate of a continuous pressure curve. Experiment 12.8.1.9.

After the removal experiment, the thrombus was still attached to the throat and was forced out with a pipette and formalin. The thrombus reversed directions as seen in Figure 79, but also remained attached to the glass tube at the region between the diverging and downstream sections. The thrombus was removed with some difficulty by suctioning and pumping formalin with the 2 mL plastic pipette.

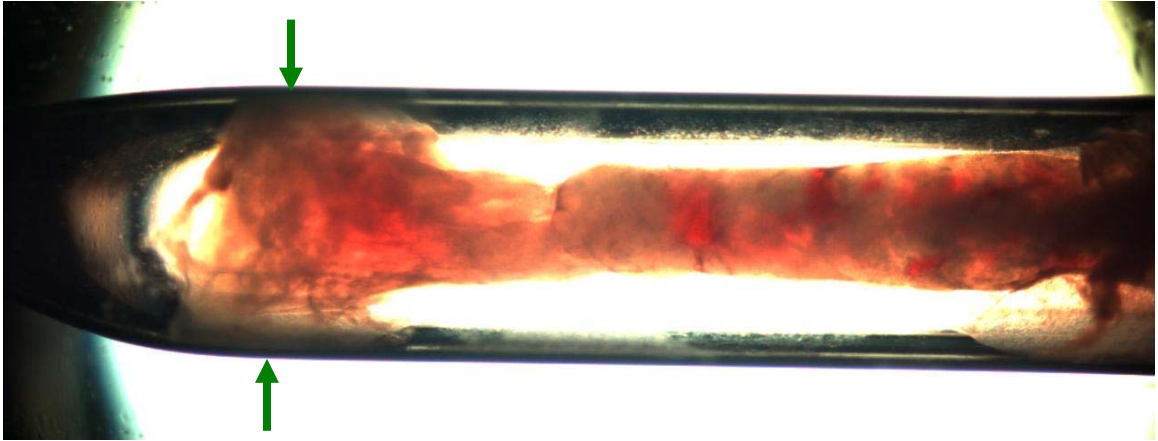


Figure 79. Image of the occluding thrombus after removal experiment and manual removal from throat. View of downstream side of stenosis. The occluding thrombus reversed direction and remained attached to a thrombus at the edge of the diverging and downstream regions (indicated with green arrows). Tube inner diameter was 1.54 mm. 2x magnification.

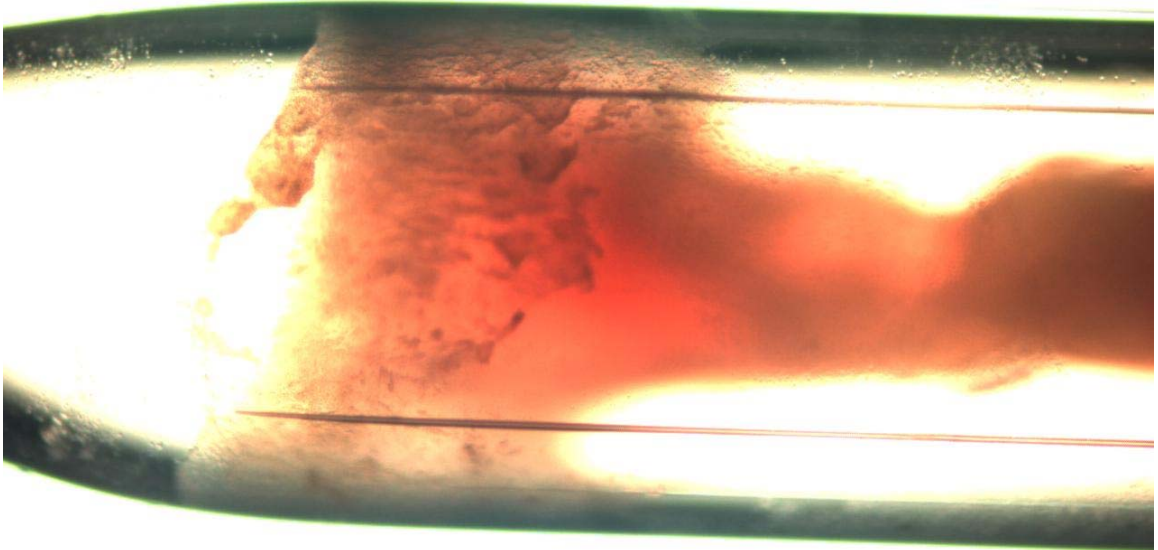


Figure 80. Magnification of the attached area in Figure 79. The occluding thrombus reversed direction and remained attached to a thrombus at the edge of the diverging and downstream regions. Tube inner diameter was 1.54 mm. 4x magnification.

3. Experiment 12.15.2.9

In this experiment, thrombus was not completely attached to the walls of the stenosis and it detached from the throat in one body upon application of 182 mmHg upstream.



Figure 81. Upstream end of stenosis showed occluding thrombus before removal. Throat diameter was 610 μm . 2x magnification.

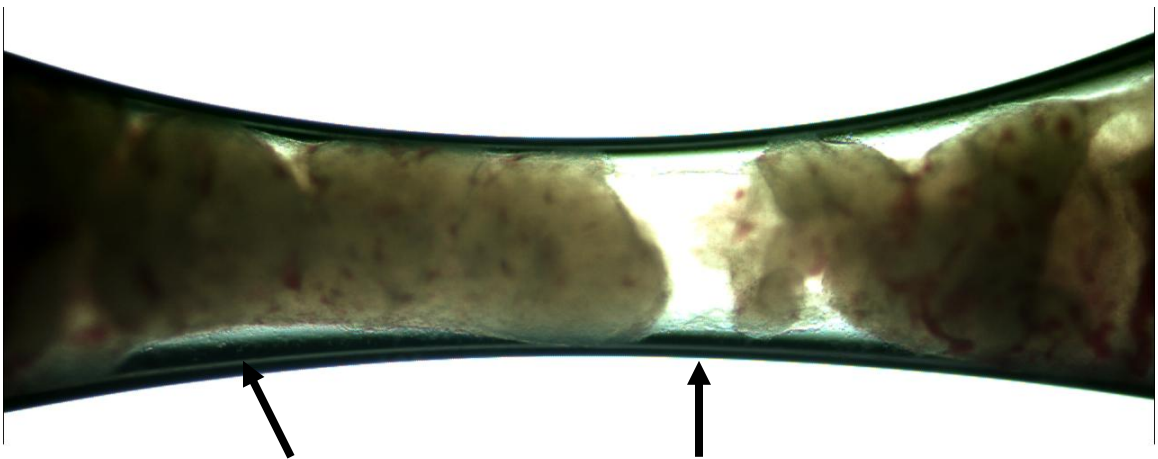


Figure 82. Throat of stenosis showed occluding thrombus before removal. The clot separated from the walls at the locations indicated with arrows. Throat diameter was 610 μm . 4x magnification.

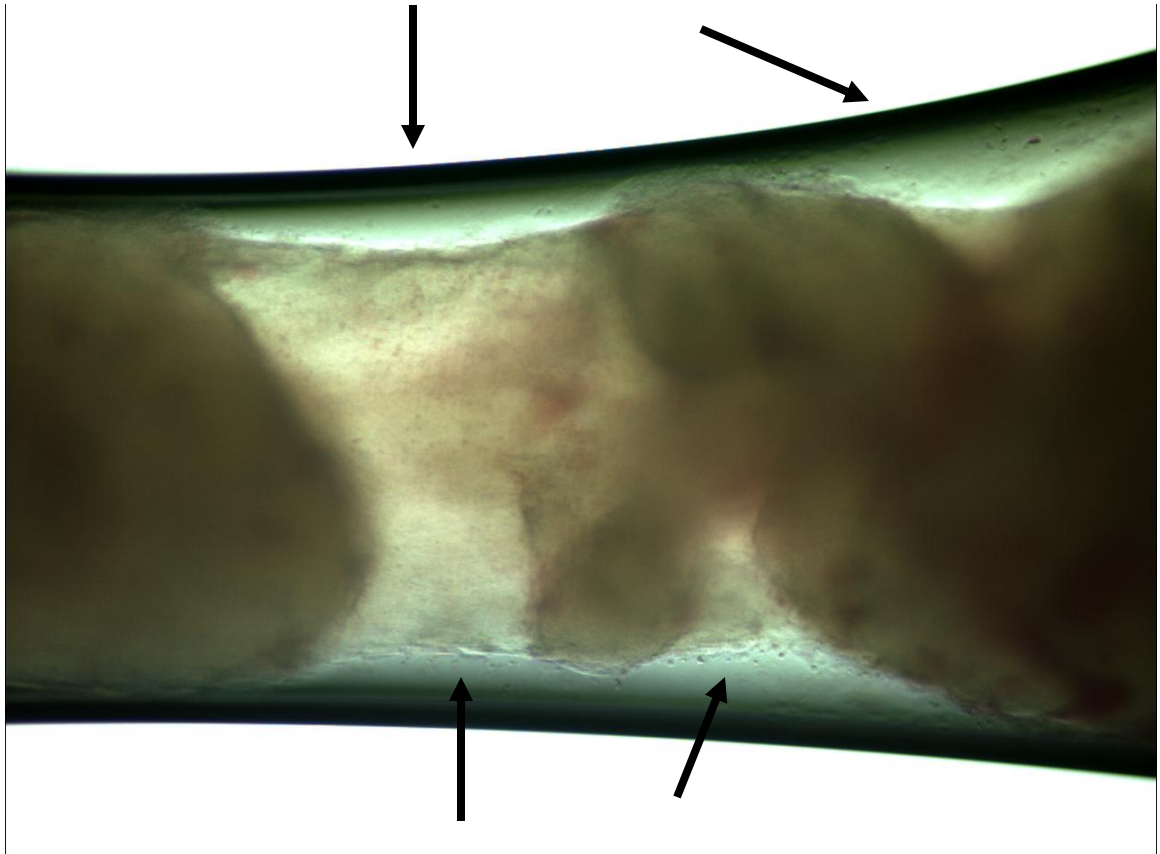


Figure 83. The clot separated from the walls at the locations indicated with arrows. The thrombus was non-homogeneous and had greater density in certain areas. Throat diameter was 610 μm . 10x magnification.

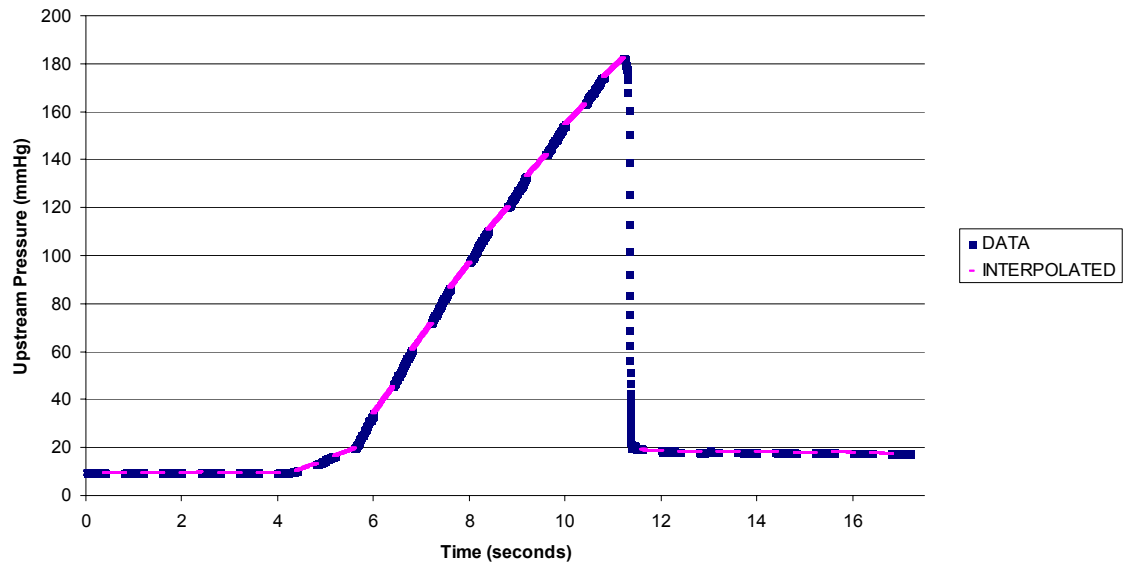


Figure 84. Upstream pressure reached a maximum around 182 mmHg. Interpolation of the last and first data points provided an estimate of a continuous pressure curve.
Experiment 12.15.2.9.

The maximum upstream pressure was recorded correctly at 182 mmHg. This relatively low pressure may have been a result of the decreased surface area of attachment shown in Figures 13 and 14 prior to the thrombus removal experiment. Photographs of the test sections after this experiment were not taken.

4. Experiment 12.15.2.33

In this experiment the thrombus was fully detached from the wall and when pressure was applied, it squeezed through the throat and moved downstream as one complete body. In this experiment the time between the formation of thrombotic occlusion and the removal experiment was 170 minutes, the longest interval of these experiments. This time interval may have been responsible for the adverse effect on attachment.

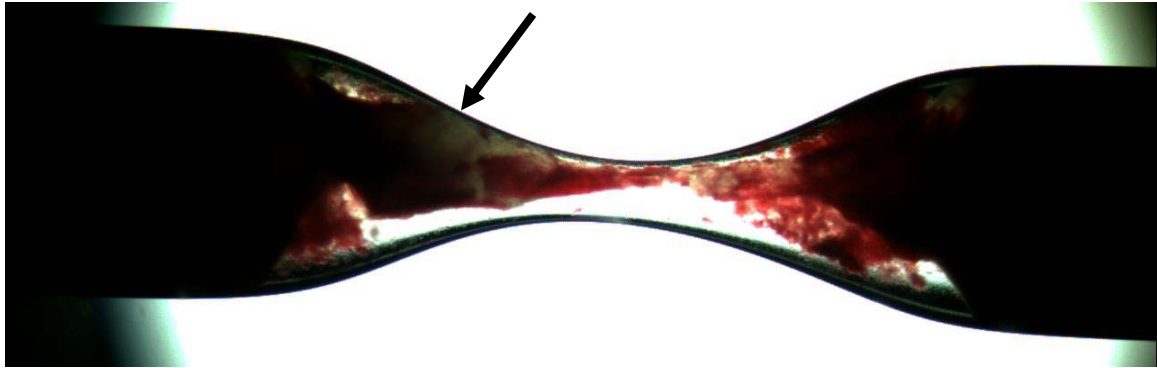


Figure 85. Image of the occluding thrombus before removal. The thrombus detached from the wall and the bulk of the occluding thrombus (identified with arrow) shifted into the converging section. Throat diameter was 310 μm . 2x magnification.

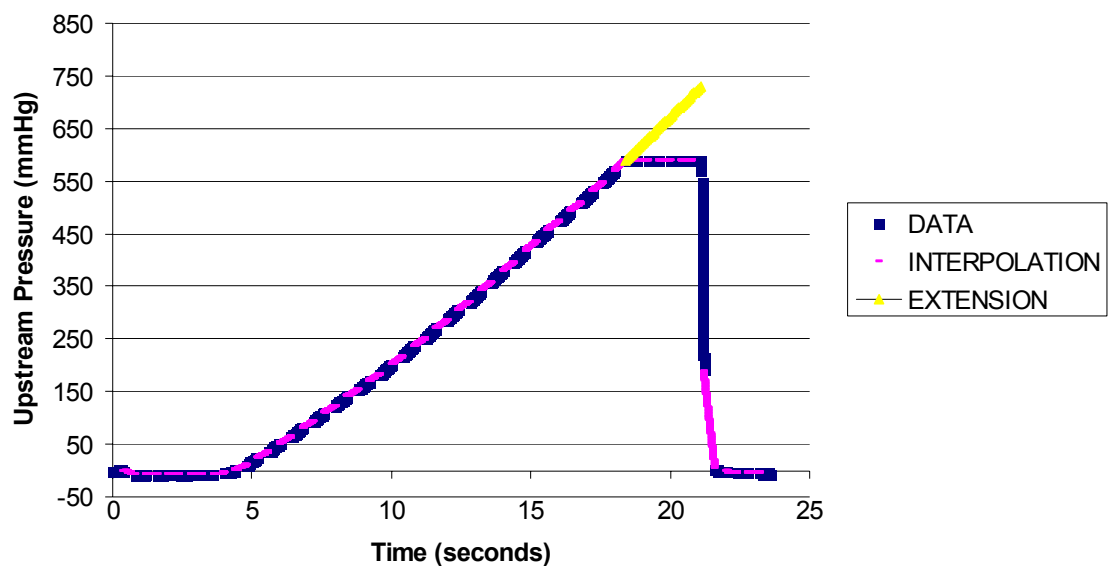


Figure 86. Upstream pressure could not be measured at the maximum pressure for removal because of a voltage threshold (590 mmHg) although it may have reached a maximum around 730 mmHg. Interpolation of the last and first data points provided an estimate of a continuous pressure curve and an extension based on the last pieces of data estimated the maximum pressure. Experiment 12.15.2.33.

The bulk of the occluding thrombus rested in the converging section, as seen in Figure 85 above, until pressure was applied and the thrombus moved into the throat and

was squeezed through the throat. From visual observation during the removal experiment, this occurred within the first moments of the experiment.

The data acquisition system had a voltage threshold at 5 Volts. To compensate for this, the pressure transducer was zeroed at -163 mmHg to provide more range. In this experiment, the maximum pressure to remove the thrombus was greater than the threshold and therefore the data had a plateau at 590 mmHg. The maximum pressure was estimated as 730 mmHg by generation of an extension line ($y = 51.908x - 365.41$) based on the last segment of data and assignment of a cutoff at 21.1 seconds which was the last recorded data point of the plateau. Photographs of the test sections after this experiment were not taken.

Embolus

Three emboli were also forced through the throat at the site of blockage using the thrombus removal protocol. The dimensions of the emboli were unknown. In the following embolus experiment, the embolus was not attached to the walls and was forced downstream at 382 mmHg.

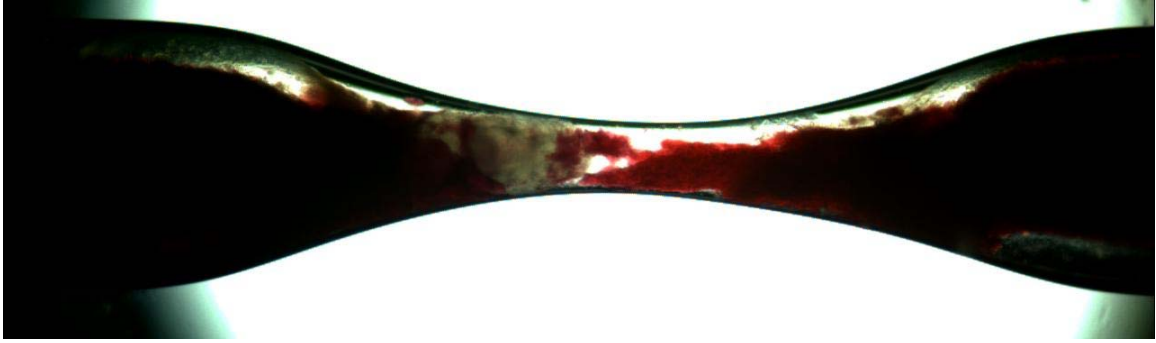


Figure 87. Image of the embolus stuck in converging section of throat before removal. The appearance was not unlike that of the thrombus, but the immediate pressure rise of 4 mmHg at flow cessation and the sudden appearance in the thrombus formation video indicated that it was a thrombus. Throat diameter was 430 μm in this 93% stenosis. 2x magnification. Experiment 12.15.2.39.

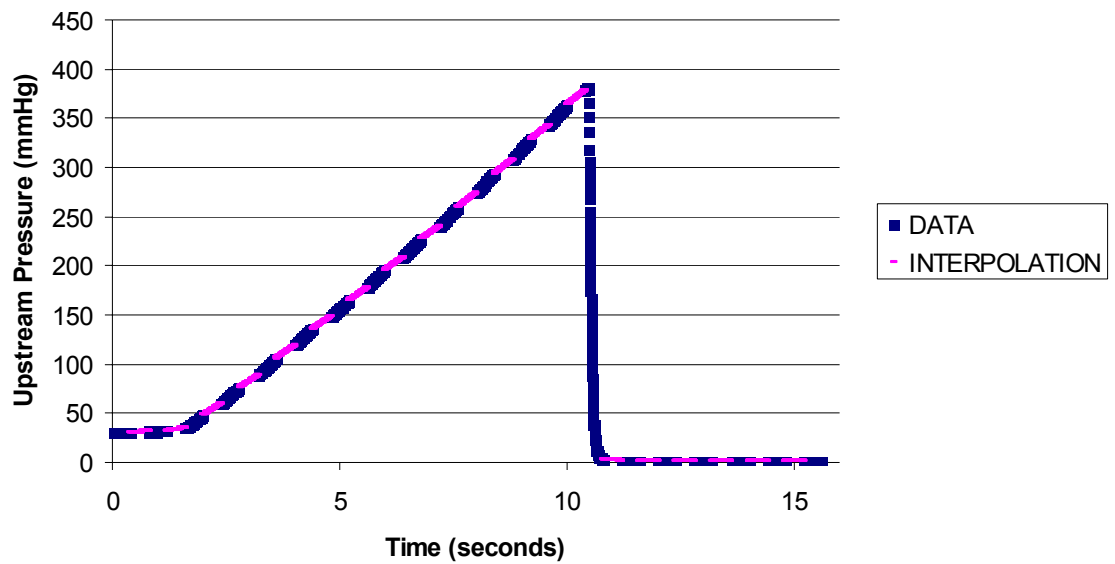


Figure 88. Upstream pressure reached a maximum around 382 mmHg. Interpolation of the last and first data points provided an estimate of a continuous pressure curve. Experiment 12.15.2.39.

The pressure curve for the embolus was very similar to the other experiments and the data acquisition system recorded the maximum upstream pressure at 382 mmHg.

CHAPTER VI

DISCUSSION

A method to optically record thrombosis and occlusion of whole blood flowing through high grade hour-glass-shaped stenoses has been presented. Thrombus formed on collagen-coated walls of the stenosis region in this *in vitro* model has been visualized by light scattering from whole porcine blood flow under high shear. Total occlusion at the throat of the stenosis has been achieved with reproducible conditions and video, flow, and histological recordings.

This work has shown that the rate of platelet deposition on collagen increases until $40,000\text{ s}^{-1}$ and that platelets sustain accumulation even at these very high shear rates. In comparison to similar thrombosis studies on collagen, this follows the trend and predicts that the growth of thrombus increases even at these high shear rates.

The 85% stenosis by area (~61% stenosis by diameter) is mildly stenotic, yet in this work it led to thrombotic occlusion in a time similar to the 96% stenosis. Stenosis below 75% by diameter is considered to be moderate yet it is associated with sudden cardiac death. Therefore this model may be useful in learning more about the mechanisms in acute thrombosis and may be used in future studies that quantify the adhesion strength per platelet in this high shear regime.

The thrombus in this work was detached at a maximum upstream pressure of ~450 mmHg, which is six-tenths of an atmosphere, or roughly 4 times mean arterial blood pressure. The total thrombus detachment strength was calculated to be approximately 8.9 mN. In this chapter, the adhesion strength of a platelet on the

periphery of the thrombus has been estimated to be on the order of 30 nN based on the thrombus removal data. This is consistent with the *in vitro* measurements of glycoprotein surface density and adhesion strength found in literature review. This number can be used to estimate the bond strength of single glycoproteins.

In Vitro Model of Occlusive Thrombosis

In the flow system presented in this work, stenosis equal to or greater than 65% by area reduced flow. Autoregulation which occurs *in vivo*, when the downstream vessels dilate in order to provide greater flow distal to the stenosis, would be expected to maintain an unreduced flow until the percent stenosis may be greater than 65%.

Experiments in this model were conducted at room temperature which is lower than body temperature. The viscosity of the blood as well as the kinetics of blood constituents may be affected by the lower temperature. Experiments could be more like body temperature, 37°C, by submerging the platelet transfer bag in an isothermal bath.

Formation of Completely Occlusive Thrombus

In *ex vivo* and *in vitro* models that do not achieve complete occlusion, the possible causes may include short exposure duration or depressed platelet deposition from anticoagulant. This model achieved total occlusion in 7 experiments, roughly 25% of the total number of severely stenotic test sections tested. This model shows that maximum platelet deposition occurs at the throat as described by the Badimon et. al.[41] and Markou et. al. [42] experiments.

The observations of completely occlusive thrombus in these experiments were the platelet dense regions in the thrombus, the concentric striations of thrombus in the throat region, flow cessation by visual and flow measurement, and the ability to form a propagating fibrin string under high shear stress.

In the thrombus formation video of the 96% stenosis a thrombus may have migrated into the throat of the stenosis. The white pixels in these images identify thrombus development on the walls and at first a significant thrombus forms in the converging region, which corresponds to the location of peak shear rate. This thrombus may have migrated into the throat because the white pixels in the initial location return to gray and a group of white pixels slowly shift towards the throat in each time lapse. Once in the throat, the number of white pixels increased until total occlusion.

After formation of totally occlusive thrombus, thrombus was observed to become compact and detach from the walls of the stenosis. The strength of bonds within the thrombus may be stronger than those between collagen and thrombus because with time the thrombus pulled away from the wall and became more compact.

Angiographic data in patients suffering from acute myocardial infarction demonstrated total occlusion and demonstrated that much intracoronary thrombus may form distal to the occlusion [68]. The incidence of certain angiographic features in this study such as cutoff pattern of occlusion, accumulated thrombus (>5 mm) proximal to the occlusion, and floating thrombus all indicated “high-burden thrombus formation” and were used as predictors of slow-flow and no-reflow phenomenon.

The model of platelet deposition using images correlated well with the model platelet deposition based on flow rate measurements. The image calculations basically

used a threshold around 0.5 or 128 grayscale in order to define thrombus and was sensitive enough to detect thrombus growth continuously. The flow rate model can be argued to be the more accurate representation of platelet deposition because thrombus formation was based on the increased resistance and the hydraulic diameter. In comparison, the image analysis model was based on the light scattering of thrombus which may be high on the surface in view but not throughout the throat cross-section. The image analysis may have predicted a higher platelet deposition because of other contributions to light scattering such as blood separation. If blood separated in the vicinity of the stenosis, then the translucent plasma would also be represented by the white pixels.

Rate of Platelet Deposition versus Shear Rate

Thrombosis is clearly a function of shear rate and the rate of platelet deposition increases until beyond 40,000/s. The acute phase of platelet deposition can be identified from continuous data and exists in thrombosis models by Markou et al.[42] and Badimon et. al.[41] and the experiments in this work. The rate of acute phase platelet deposition is a good comparable across thrombosis models because it does not take into account the accelerating phase which may vary in length based on parameters of the model such as anticoagulation and blood source. Figure 88 below identifies the upward trend of the rate of acute phase platelet deposition as a function of shear rate for the three models that have continuous platelet deposition measurements. The flow rate model had a lower rate of acute platelet deposition than Badimon et al. and Markou et al., who used non-

anticoagulated blood, potentially as a result of anticoagulation. The blood sources of Badimon et al. and Markou et al. were porcine and primate, respectively.

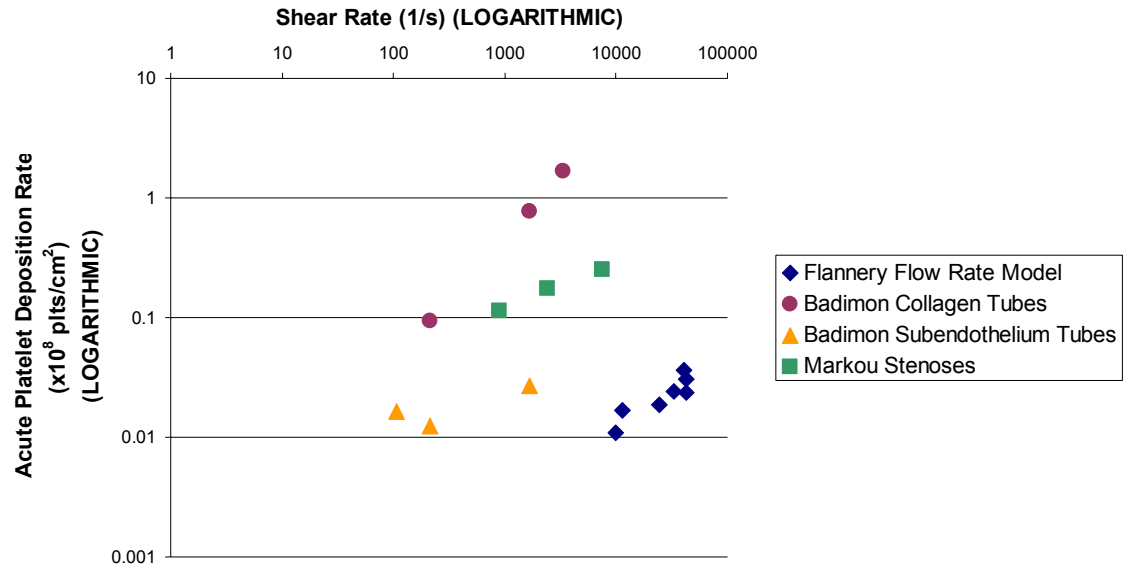


Figure 89. Acute rate of platelet deposition constants determined for each experiment that had continuous platelet deposition measurements. Variation exists between the thrombosis models but the trend of increasing deposition rate as a result of higher shear rate is apparent. [41, 42, 44, 45]

Although the rate of platelet deposition decreased in the highest shear experiments for Barstad et al. [44], the experiments in this work demonstrate that platelet accumulation onto collagen still increases at an increasing rate until 40,000/s. The Barstad et. al. experiments utilized an eccentric stenosis in a parallel plate chamber at Reynolds number 20. This is not as physiologically relevant as the tube flow experiments by Markou et. al. and Badimon et al. or the experiments in this work.

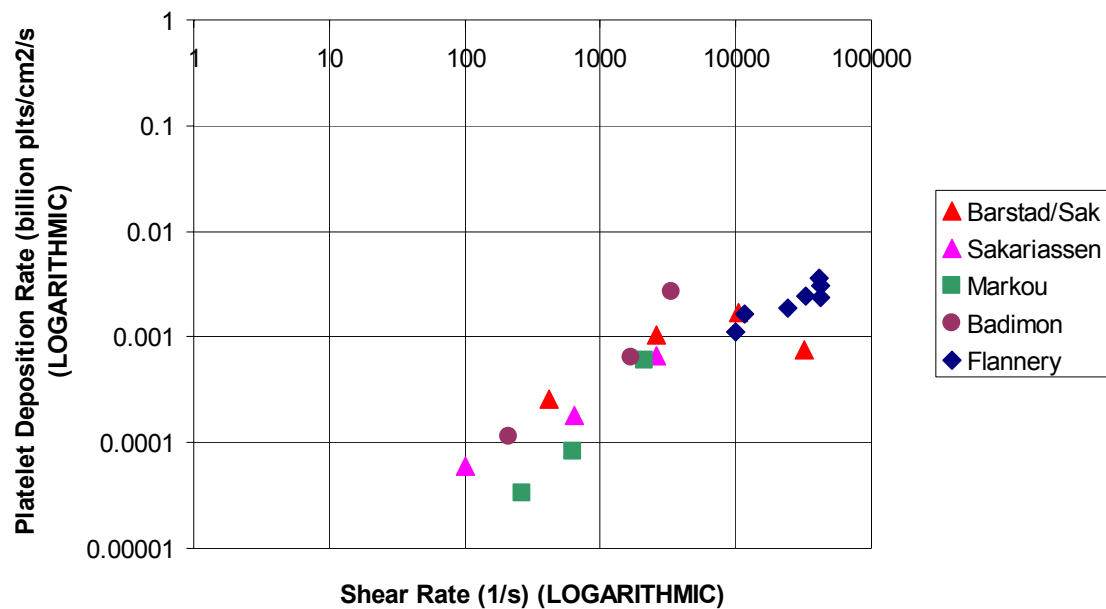


Figure 90. Platelet deposition onto collagen as a function of shear rate at 5 minutes of exposure time in comparison to Flannery acute rate platelet deposition based on flow rate. Platelet deposition rate at 5 minutes was calculated from platelet deposition data using a straight line method or differentiation from regression curves. [41, 42, 44, 45]

The rate of platelet deposition may vary remaining in the acute deposition phase until flow cessation or by decelerating and even decreasing to form a stable mural thrombus. Both of these conditions occur *in vivo* and the thrombosis models discussed here may be used to determine if flow conditions affect this variation. Thrombus formation onto collagen progressively increases and consistently led to complete occlusion at shear rates greater than 2,000/s by Markou et. al. and in some observed experiments by Badimon et al. and Barstad et. al.

Thrombus Removal Experiments

Thrombi detached from the throat region in complete units in 3 out of 4 experiments. Often, an edge was seen in the throat region where thrombus had torn away from the layer that covered the tube.

After removal from the confines of throat, thrombus in these experiments proceeded to aggregate further and change dimension, therefore the thrombus must be fixed quickly. Only the interactions with the wall were studied here because knowledge of the boundary conditions was known *a priori*. Therefore experiments that did not detach from the wall but formed a channel at a location in the thrombus could not be analyzed. Data indicated that thrombus removal experiments need to occur as soon as is possible from the time of total occlusion. The time in between thrombotic occlusion and thrombus removal was important because as the blood next to the clot separated as a result of stasis, it may also have been possible that the integrity of the clot was susceptible to changes with time.

Adhesive forces may be strong between platelets because they aggregate and this may be the reason that the thrombus detached from the wall. The concentric striations of platelet aggregates are very significant and demonstrated rapid growth until flow cessation. Based on histological examination, the density of platelets is high in certain areas and it is this structure scaffolded by fibrin that caused flow cessation. Dense aggregates pulled together after flow was terminated and it is possible that strong platelet bonds are also the reason for the thrombus detaching from the wall of the collagen coated stenosis. The two thrombus removal experiments that detached from the surface before removal had a long duration between thrombotic occlusion and thrombus removal,

although since they both occurred on the same day, it is possible that the blood sample may have played a part.

Collagen as a substrate is useful to estimate the higher end of glycoprotein bond strength because it has been shown to yield irreversible platelet aggregation and the detachment strength is greater than for even vWF and fibrinogen substrates [52].

Thrombi are typically removed *in vivo* through thrombolytic agents such as tPA described earlier or through mechanical removal of the thrombus or distal embolization protection devices or even laser ablation techniques [69]. The knowledge of platelet adhesion strength and platelet aggregation may be used to create anti-platelet therapies by weakening the bonds.

Estimation of the Adhesive Strength of Platelets

Platelets attached and aggregated onto collagen Type I at initial shear rates between $10,000 \text{ s}^{-1}$ and $40,000 \text{ s}^{-1}$ in this *in vitro* model. The adhesion strength of platelets was estimated in two ways by (1) a force balance using the measurement of maximum upstream pressure before thrombus removal, and (2) a force analysis based on the initial shear rate in the stenosis. Table 8 below has listed the results for these estimations.

Table 8. Adhesion force estimates based on detachment and attachment strengths.

	Detachment Method, P_{\max}	Attachment Method, τ
Force on Thrombus	8.9 mN	0.25 mN
Force on Platelet	32 nN	0.89 nN

The detachment strength for the thrombus and the platelet was a factor of 36 times greater than the attachment strength. Platelet adhesion strength was estimated for experiments where the occluding thrombus was (1) attached throughout the surface before removal, and (2) detached completely from the region of stenosis. Only 1 out of 4 experiments met these criteria, therefore these estimates of platelet adhesion strength are merely an approximation of the order of magnitude required for detachment/attachment of platelets.

1. Platelet Detachment Strength based on Removal of Thrombus

The maximum upstream pressure at removal for the experiment described in Chapter V was 438 mmHg which produced a maximum force on the thrombus of 8.9 milli-Newtons (mN). The maximum force was equal to the sum of all the receptor-ligand bonds on the surface between the thrombus and the collagen, as in Equation 15.

$$F_{\max} = \sum_{n=1}^N F_{R-L} \quad \text{Equation 15}$$

where the maximum force F_{\max} was equal to the sum of the adhesive forces for all the receptor-ligand ($R-L$) bonds for N adhesive molecules at the time of thrombus removal.

The thrombus was assumed to be attached to the collagen surface by platelets alone therefore Equation 15 applied to receptor-ligand bonds between platelets and collagen or platelets and platelets. This assumption was based on the high relative proportion of platelets in the occluding thrombus although it neglected potentially strong bonds from other species. It may have been possible to use a composite analysis in order to evaluate the adhesive strength of multiple species such as platelets, fibrin, and vWF given knowledge of the density of those bonds and the relative contribution.

The surface that the platelets detached from was estimated based on the representation in Figure 91 below.

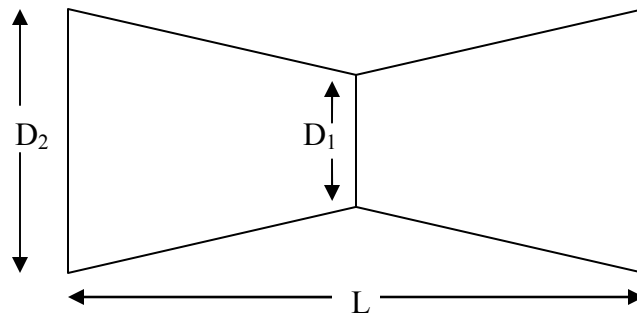


Figure 91. Two-dimensional representation of thrombus in throat of stenosis. The axis of the stenosis was left to right across the page.

In Figure 91, L was the length of the thrombus and D_1 was the inner diameter at the stenosis throat. The dimensions of the thrombus were approximated geometrically as two truncated cones joined together by the base with the smallest diameter. The two-dimensional side view has been shown in Figure 91. For the thrombus in this experiment the max width of the thrombus, D_2 , was 0.44 mm. The surface area between the thrombus and the collagen surface was calculated from Equation 16.

$$SA = \frac{\pi}{2} \left(D_2 \sqrt{D_2^2 + \left(L + \frac{D_1 L}{D_2 - D_1} \right)^2} - D_1 \sqrt{D_1^2 + \left(\frac{D_1 L}{D_2 - D_1} \right)^2} \right) \quad \text{Equation 16}$$

where the surface area (SA) of the model in Figure 91, not including the bases, was calculated from the reference dimensions in Figure 91. Given the throat diameter of 0.310 mm, the max width of the thrombus of 0.44 mm and the length of 1.3 mm, the surface area was calculated to be 1.54 mm² between the thrombus and the collagen-coated surface.

The number of platelets on the throat surface was estimated by Equation 17.

$$\# \text{ Platelets} = f_p \times \frac{SA}{MPA} \quad \text{Equation 17}$$

where the number of platelets was evaluated from the surface area (SA), the mean platelet area (MPA), and the proportion of platelets (f_p) in the thrombus from histological analysis. MPA was calculated from the mean platelet volume, MPV , for the specific blood sample provided the assumption that platelets were spherical. For this sample, the MPA was 5.31×10^{-6} mm² per platelet with a platelet diameter of 2.6 μm which was typical. The distribution of platelets was assumed to be homogeneous and uniform throughout the thrombus.

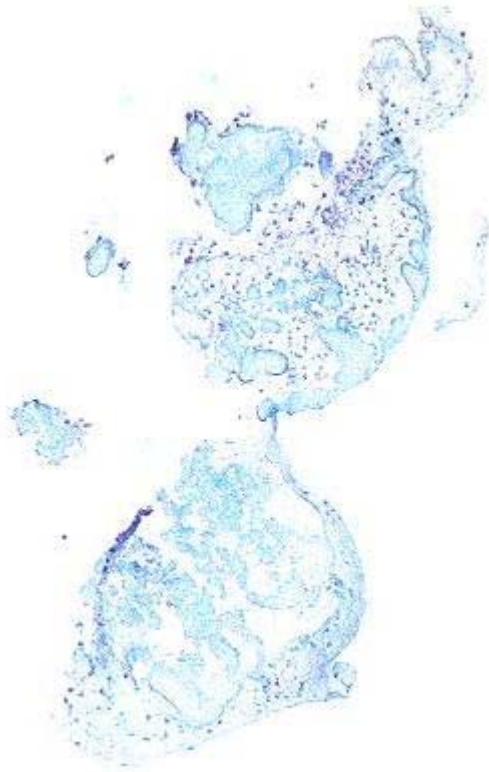


Figure 92A

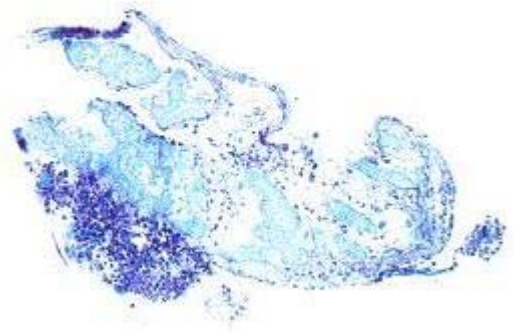


Figure 92B

Figure 92. The thrombus in this experiment tore in half during processing. Each half has been shown in Figure 92A and 92B stained with Carstairs which highlighted platelets in blue, fibrin in pink, WBCs in purple, and RBCs in red. The orientation of the thrombus was unknown.

The relative proportion of platelets, fibrin, WBCs, and RBCs was acquired from histological composition analysis of Figure 92A and was 96%, 2%, 2%, and 0%, respectively. Of course, fibrin overlapped on platelets and WBCs. Hence, the proportion of platelets, f_p , in the thrombus was 0.96. Using Equation 17, the number of platelets in contact with the collagen surface was estimated as 280,000 platelets.

Assuming that the force was distributed only by the platelets the adhesive strength per platelet was approximately 32 nN, or 30 nN to one significant figure. There may have been many platelet glycoproteins that were responsible for this adhesion strength.

One important collagen receptor on platelets is GPIa/IIa which has approximately 1000-2000 copies per platelet [26-28, 70]. If this was the only receptor-ligand pair responsible and half of the copies were in contact with collagen, the adhesive strength of each GPIa/IIa bond would be 30-60 pN. This was on the right order of adhesion strength in comparison to the adhesion strength between platelet GPIb α and vWF which was determined with optical tweezers to be approximately 11 pN and in flow to be in the range of 36-217 pN [56-58].

2. Platelet Attachment Strength based on Shear Rate

The force necessary for attachment was estimated as the viscous force on the surface area between the occlusive thrombus and the stenosis throat. The attachment force, F , was estimated by Equation 18.

$$F = \tau \times SA \quad \text{Equation 18}$$

where the attachment force was the product of the shear stress in the throat, τ , and the surface area, SA , calculated as in the first method. The surface area was calculated as in the first method to be 1.54 mm². Shear stress was calculated to be 161 Pa (1610 dyn/cm²) using Equation 6 in Chapter III assuming Poiseuille flow. The initial shear rate in experiment 12.1.2.33 was 42,200/s based on the average flow rate of 7.4 \pm 0.9 mL/min and throat diameter of 0.310 mm. The average flow rate was calculated for the first 4 minutes and 15 seconds while the upstream pressure was constant at 20 mmHg. The force on the surface was then estimated to be 2.5 mN by Equation 16 above.

Distributed among 280,000 platelets, the force per platelet for attachment was estimated as 0.89 nN. This was approximately a thirty-sixth of the estimated detachment strength calculated above.

The number of variables in the average value of adhesive strength per platelet is many and accounting for them would require detailed knowledge of the surface interactions at the periphery of the thrombus. Some of the factors in adhesion strength of platelets include the initial shear stress at adhesion, conformational changes and density of platelet glycoproteins, kinetic rates, surface chemistry, the time between adhesion and detachment, and platelet density and morphology among others. The work presented has provided an estimate of the adhesive strength of platelets in the range between the attachment and detachment strength and this may be used as an order of magnitude approximation.

In many studies, platelet adhesion strength has been interpreted as the percent surface coverage under varied shear rate which has demonstrated that platelets detach under high shear flow [50, 51, 54, 55]. Kuwahara et. al. determined that adhesive strength of spread platelets ($>2.5\ \mu\text{m}$) was much greater than non-spread platelets which had a reversible binding. Kumar found that $\sim 50\%$ of platelets detached when increasing shear stress from 0.5 to 32 dynes/cm² [55]. In this work, the platelet adhesion strength has been interpreted as the strength necessary to form and detach a thrombus which completely occluded the vessel.

At what depth in the thrombus did thrombus removal occur? This is an important question in deciphering the weakest receptor-ligand interaction that would be responsible for the detachment. Based on images of the throat surface taken after the removal

experiment, it is evident that a 1-10 μm layer of thrombus existed on the walls of the throat. Therefore it may be that the cleavage occurred between both platelet-platelet bonds and between platelet-collagen bonds. Also there is the contribution of vWF and fibrin as mediators in adhesion which are present throughout the thrombus especially in locations with platelets. The study of these interactions involves many variables and is outside the scope of this work. The order of magnitude approximations of adhesion strength per platelet and per glycoprotein have been estimated and have been shown to be consistent with studies on that scale.

The force required for detachment of the thrombus is clinically significant because it may be used to modulate thrombolectomy forces and in cases where catheters are guided to the thrombus and the operator needs to know how much force to apply.

Fibrin Tail Propagation

In non-anticoagulated ex vivo studies, fibrin tails have also been observed in arterial stenotic flow, but under different shear forces. In Markou's study, fibrin tails were observed at lower shear 265/s and 630/s (in the 4mm and 3mm straight tubes) and not in higher shear experiments or stenotic experiments [42]. The Reynolds number in those experiments was 130 which is the same as this work presented and is physiologically relevant. In Cadroy expansion chamber, fibrin tails embolized more rapidly under increased shear rate and therefore were identified as a low shear phenomena [71]. In contrast, the Barstad et. al. study observed fibrin tail downstream to the collagen-attached platelet thrombus that was regularly observed for high-shear stenoses (10,500/s and 32,000/s) [44]. The Reynolds number in those experiments was

20 and therefore the tail may have formed because of the low flow conditions. The models and the existence of propagating fibrin tails have been compared in Table 9 below.

Table 9. Comparison of Fibrin Tail Observation. Literature sources: Dichek et al. [72], Cadroy et al. [71, 73], Markou et al. [42], and Barstad et al. [44].

Study	Shear Rate (1/s)	Existence of Tail	Reynolds #
Dichek et al.	106	Yes	60
Cadroy et al.	0-100	Yes	40
Markou et al.	265	Yes	160
Markou et al.	630	Yes	240
Cadroy et al.	0-780	Yes	190-280
Markou et al.	2120	Not Measured	320
Barstad et al.	100-2600	Not Measured	20
Markou et al.	0-5000	Not Measured	160
Barstad et al.	17-10,500	Yes	20
Markou et al.	0-20,000	Not Measured	160
Barstad et al.	12-32,000	Yes	20
Flannery	40,900	Yes	136

In the experiments in this work, thrombus propagation at high shear was found in at least two experiments and in one of them a long thin fibrin tail was identified. The conditions that led to the formation of this tail may be conjectured from the images taken during thrombus formation. The single experiment that had a propagating fibrin tail

distal to an occluding thrombus and a RBC packet was at very high shear rates of 40,900/s initially and a Reynolds number of 136 in the throat. The occluding thrombus slowly migrated into the throat and left a narrow channel on the order of 10-50 μm patent on one side of the thrombus. This narrow channel persisted for a minute or so and may have produced the fibrin tail in the distal area of high residence. Given the length and width of 14.2 mm and 0.8 mm, respectively, and an initial shear rate of 42,200/s, the force on the tail was approximately 1.8 mN.

The role of fibrinogen in platelet aggregation has been recognized for over 35 years. Propagation of fibrin has been identified in 'flow niches' at the separation region and the fiber orientation was associated with diverging streamlines at this site [74]. In this flow system, flow likely separated in all of the stenoses because they had Reynolds number greater than 10 and many had an angle of divergence from the throat of the stenosis to the diverging section that was greater than 7° , which is accepted to be the critical angle. The separation of flow may limit the flow although this is common in most coronary arteries simply because of the low Reynolds number threshold.

The propagation of thrombus distal to the lesion is dysfunctional hemostasis. It is an event typically associated with thrombosis that applies to venous thrombi, pulmonary embolism, and arterial atherothrombosis. This last application has been elucidated in this research although further sampling is necessary to make a more firm conclusion. In this experiment the vessel occluded at the throat and not at a point on the propagating thrombus. The tail itself was extremely flimsy and folded in on itself easily.

CHAPTER VII

CONCLUSIONS

The following have been demonstrated by this work:

- The *in vitro* experiments of flowing whole porcine blood demonstrated total occlusion in the presence of platelets, collagen, fibrin, vWF and high shear stress
- Complete occlusions occurred in about 25% of the cases with severe stenoses
- The rate of platelet deposition was between 1.1 and 3.6 million platelets/cm²/s and it increased with shear rates between 10,000 s⁻¹ and 40,000 s⁻¹
- Propagating fibrin tails formed occasionally under high shear stress when thrombosis led to total occlusion
- Thrombus adhesion strength was between 0.25 and 9 mN
- Thrombus removal from the throat of the stenosis was measured with a force of detachment being at the high end of about 9 mN

Future Work

This model can visualize thrombus formation in stenotic flow with high resolution in whole blood. The morphological change of platelet aggregates after adhesion is not well understood and the study of aggregate development and changes in platelet packing may be possible with this gain of resolution. A direct marker such as fluorescently labeled platelets may be used to quantify the number of platelets in the throat region and to extract the density of the aggregate from the light intensity measured.

This model has shown that platelet adhesion strength can be determined from thrombus removal. It could be used to determine the effect of different initial shear rates on platelet adhesion strength. In order to use this model to detect platelet strength it is important to directly measure thrombus development with a direct marker such as fluorescently labeled platelets which may be possible in a scaled down version of this model. When this model is scaled down, the occurrence of embolus will likely be frustrating, therefore a new blood source or modification of the anticoagulant dosage is recommended. This model could easily be adapted into an ex vivo shunt and would be most clinically relevant with human non-anticoagulated blood. At a smaller scale on the order of $\sim 100\text{ }\mu\text{m}$, less blood volume would be required.

Although only evident in one thrombus formation video, the thrombus location appeared to migrate in the 96% stenosis video. This may be of interest because the thrombus formed initially in the approximate location of peak shear rate. And over 6 minutes, the thrombus appeared to migrate into the throat of the stenosis leading ultimately to complete occlusion. The movement and tethering of thrombus may be studied further using this model by collecting a greater number of images during thrombus formation.

A number of variations of this model may be made to be more physiologically relevant. The effects of pulsatile flow on the formation of platelet dense regions may be studied by adding a pulsatile pump. An addition of an emboli detector from light scattering may be used to study the rate of embolization from the thrombogenic surface. Blood flow patterns that are affected by thrombus development may also be studied. This glass model in combination with fluorescence microscopy may be used to study the

affect of focal thrombus which has occurred in concentric striations in this model and the possible vortices and changes in the recirculation region that may arise.

One of the most clinically relevant questions in SCD is how total thrombotic occlusion occurs in moderate (55% by diameter) or non-stenotic arteries. This model may be used to address thrombus formation in non-stenotic flows with a high volume of blood over longer exposure times. From each porcine sample, a harvesting of 5 liters of blood may be possible.

The event of occlusive thrombus formation may be altered by applying therapies such as pharmacological agents or by using a blood source deficient in key mediators such as fibrinogen or vWF.

APPENDIX

APPENDIX A-1

Matlab Code to Count the Number of White Pixels in Thrombus Formation Images

METHOD 1

```
clear all;  
close all;
```

```
% Thrombus Formation Images used for Platelet Deposition Analysis  
% Method 2  
% Both codes in Method 1 and Method 2 yield the same number of pixels over the threshold  
% Experiment 12.15.9  
% Conor Flannery, March 7, 2005
```

```
N=79;  
x=0;
```

```
% Images to be analyzed includes the mask and appropriate succeeding images  
filename={'0015.tif','0030.tif','0045.tif','0100.tif','0115.tif','0130.tif','0145.tif','0200.tif','0215.tif',  
'0230.tif','0245.tif','0300.tif','0315.tif','0330.tif','0345.tif','0400.tif','0415.tif','0430.tif','0445.tif',  
'0500.tif','0515.tif','0530.tif','0545.tif','0600.tif','0615.tif','0630.tif','0645.tif','0700.tif','0715.tif',  
'0730.tif','0745.tif','0800.tif','0815.tif','0830.tif','0845.tif','0900.tif','0915.tif','0930.tif','0945.tif',  
'1000.tif','1015.tif','1030.tif','1045.tif','1100.tif','1115.tif','1130.tif','1145.tif','1200.tif','1215.tif',  
'1230.tif','1245.tif','1300.tif','1315.tif','1330.tif','1345.tif','1400.tif','1415.tif','1430.tif','1445.tif',  
'1500.tif','1515.tif','1530.tif','1545.tif','1600.tif','1615.tif','1630.tif','1645.tif','1700.tif','1715.tif',  
'1730.tif','1745.tif','1800.tif','1815.tif','1830.tif','1845.tif','1900.tif','1915.tif','1930.tif','1945.tif',  
'2000.tif'};
```

```
% Create mask 'c' from first image, designated '0015.tif'  
a = imread('0015.tif');  
b = im2bw( a , 254/255);  
c = b*(-1)+1;  
d = double(a).*double(c);
```

```
for i=1:N+1
```

```
name=char(filename(i));
```

```
%j=imread(name);
```

```
% apply mask  
a = imread(name);  
d = double(a).*double(c);
```

```
% convert to black and white  
% white pixels are defined by Otsu's method using GRAYTHRESH  
LEVEL = GRAYTHRESH(a);  
BW = im2bw(a,LEVEL);
```

```
counter=0;
```

```
[m,n]=size(BW);
```

```

for p=1:m
    for q=1:n
        if BW(p,q)==1
            counter=counter+1;
        end
    end
end

x=x+1;
pixels(x,1)=counter;

end
% -----

```

METHOD 2

```

clear all;
close all;

% Thrombus Formation Images used for Platelet Deposition Analysis
% Method 1
% Both codes in Method 1 and Method 2 yield the same number of pixels over the threshold
% Experiment 12.15.9
% Conor Flannery, March 7, 2005

N=79;
x=0;

% Create a list of the images in an array
filename={'0015.tif','0030.tif','0045.tif','0100.tif','0115.tif','0130.tif','0145.tif','0200.tif','0215.tif',
'0230.tif','0245.tif','0300.tif','0315.tif','0330.tif','0345.tif','0400.tif','0415.tif','0430.tif','0445.tif',
'0500.tif','0515.tif','0530.tif','0545.tif','0600.tif','0615.tif','0630.tif','0645.tif','0700.tif','0715.tif',
'0730.tif','0745.tif','0800.tif','0815.tif','0830.tif','0845.tif','0900.tif','0915.tif','0930.tif','0945.tif',
'1000.tif','1015.tif','1030.tif','1045.tif','1100.tif','1115.tif','1130.tif','1145.tif','1200.tif','1215.tif',
'1230.tif','1245.tif','1300.tif','1315.tif','1330.tif','1345.tif','1400.tif','1415.tif','1430.tif','1445.tif',
'1500.tif','1515.tif','1530.tif','1545.tif','1600.tif','1615.tif','1630.tif','1645.tif','1700.tif','1715.tif',
'1730.tif','1745.tif','1800.tif','1815.tif','1830.tif','1845.tif','1900.tif','1915.tif','1930.tif','1945.tif',
'2000.tif'};

for i=1:N+1

    name=char(filename(i));

    % apply mask
    j=imread(name);

    % convert to black and white
    % white pixels are defined by Otsu's method using GRAYTHRESH
    LEVEL=GRAYTHRESH(j);
    BW = im2bw(j,LEVEL);

    counter=0;

    [m,n]=size(BW);
    for p=1:m

```

```
    for q=1:n
        if BW(p,q)==1
            counter=counter+1;
        end
    end
end
```

```
x=x+1;
pixels(x,1)=counter;
```

```
end
```

```
% -----
```

APPENDIX A-2

Matlab code used for Histological Composition Code

% Image Analysis of Histological Sections

```
clear all;  
close all;
```

```
% Area Proportion of Each Species  
% For each species, simply replace the title 'platelets' with the name of  
% the image  
% Conor Flannery, March 8, 2005
```

```
filename=[ 'platelets' ];  
j=imread([filename '.tif']);  
% G = rgb2gray(j);
```

```
% The image is already BW and binary, but go ahead and rename it anyway  
% Images were converted to BW by ImagePro software which  
% could convert the shade of interest to white and change the background to black
```

```
BW = im2bw(j,0.5);  
%imshow(BW)
```

```
counter=0;
```

```
[m,n]=size(BW)  
for a=1:m  
    for b=1:n  
        if BW(a,b)==1  
            counter=counter+1;  
        end  
    end  
end  
end
```

```
pixels=counter;
```


REFERENCES

1. K.D. Kochanek, S.L. Murphy, R.N. Anderson, and C. Scott., *Deaths: final data for 2002*. National Vital Statistics Reports, 2004. **53**(5): p. 1-116.
2. H.V. Huikuri, A. Castellanos, R.J. Myerburg, *Sudden death due to cardiac arrhythmias*. N Engl J of Med, 2001. **345**(20): p. 1473-1482.
3. R.J. Myerburg, R. Mitrani, A. Interian, A. Castellanos, *Interpretation of Outcomes of Antiarrhythmic Clinical Trials: Design Features and Population Impact*. Circulation, 1998. **97**: p. 1514-1521.
4. M.J. Davies, J.M. Bland, J.R.W. Hangartner, A.A. Thomas, A.C. Thomas., *Factors influencing the presence or absence of acute coronary artery thrombi in sudden ischaemic death*. European Heart Journal, 1989. **10**: p. 203-208.
5. J.F. Viles-Gonzalez, V. Fuster, and J.J. Badimon, *Atherothrombosis: A widespread disease with unpredictable and life-threatening consequences*. European Heart Journal, 2004. **25**: p. 1197-1207.
6. Z.M. Ruggeri, *Platelets in atherothrombosis*. Nature Medicine, 2002. **8**(11): p. 1227-1234.
7. D.N. Ku, *Blood flow in arteries*. Ann. Rev. Fluid Mech., 1997. **29**: p. 399-434.
8. S.A. Berger, L-D. Jou, *Flows in Stenotic Vessels*. Annu. Rev. Biomed. Eng., 2000. **32**: p. 347-382.
9. D.M. Wootton, D.N. Ku, *Fluid mechanics of vascular systems, diseases, and thrombosis*. Annu. Rev. Biomed. Eng., 1999. **01**: p. 299-329.
10. J. McKinsey, B.N. McCord, T. Aoki, D.N. Ku., *Can mechanical stress cause fatigue of the atherosclerotic plaque?* Surgical Forum, 1991. **42**: p. 319.
11. D.N. Ku, B.N. McCord, *Cyclic stress causes rupture of the atherosclerotic plaque cap*. Suppl. to Circulation, 1993. **88**(No. 4 part 12): p. 1362.

12. M.J. Davies, A.C. Thomas, P.A. Knapman, J.R.W. Hangartner, *Intramyocardial platelet aggregation in patients with unstable angina suffering sudden ischemic cardiac death*. Circulation, 1986. **73**(3): p. 418-427.
13. M. Shepard, M.J. Davies, *Practical Cardiovascular Pathology*. 1998: Oxford University Press.
14. M. Madjid, A. Zarrabi, S. Litovsky, J.T. Willerson, and Ward Casscells., *Finding vulnerable atherosclerotic plaques. Is it worth the effort?* Arterioscler Thromb Vasc Biol, 2004. **24**: p. 1775-1782.
15. E. Falk, *Unstable angina with fatal outcome: dynamic coronary thrombosis leading to infarction and/or sudden death. Autopsy evidence of recurrent mural thrombosis with peripheral embolization culminating in total vascular occlusion*. Circulation, 1985. **71**(4): p. 699-708.
16. A.G. Zaman, G. Helft, S.G. Worthley, J.J. Badimon, *The role of plaque rupture and thrombosis in coronary artery disease*. Atherosclerosis, 2000. **149**: p. 251-266.
17. E. Falk, *Coronary thrombosis: pathogenesis and clinical manifestations*. Am. J. Cardiol., 1991. **68**: p. 28B-35B.
18. J.A. Ambrose, C.E. Hjerdahl-Monsen, *Arteriographic anatomy and mechanisms of myocardial ischemia in unstable angina*. J. Am Coll Cardiol, 1987. **9**(6): p. 1397-402.
19. M.J. Davies, A.C. Thomas., *Thrombosis and acute coronary-artery lesions in sudden cardiac ischemic death*. N Engl J of Med, 1984. **310**(18): p. 1137-40.
20. AHA, *Sudden Cardiac Death*.
21. R.S. Cotran, V. Kumar, T. Collins, S.L. Robbins, *Robbins Pathologic Basis of Disease*. 1999: p. 662-663.
22. F. Li, J.L. Moake, and L.V. McIntire, *Characterization of von Willebrand factor interaction with collagens in real time using surface plasmon resonance*. Ann. Biomed. Eng., 2002. **30**: p. 1107-1116.

23. B. Savage, E. Sadivar, Z.M. Ruggeri, *Initiation of platelet adhesion by arrest onto fibrinogen by translocation on von Willebrand Factor*. Cell, 1996. **84**: p. 289-297.
24. Y.P. Wu, J.J. Sixma, P.G. de Groot, *Cultured endothelial cells regulate platelet adhesion to their extracellular matrix by regulating its von Willebrand Factor*. Thrombosis and Haemostasis, 1995. **73**(4): p. 713-718.
25. B. Savage, F. Almus-Jacobs, Z.M. Ruggeri, *Specific synergy of multiple substrate-receptor interactions in platelet thrombus formation under flow*. Cell, 1998. **94**: p. 657-666.
26. L. Alberio, and G.L. Dale, *Flow cytometric analysis of platelet activation by different collagen types present in the vessel wall*. British Journal of Haematology, 1998. **102**: p. 1212-1218.
27. T.J. Kunicki, R. Orzechowski, D. Annis, Y. Honda., *Variability of integrin $\alpha 2\beta 1$ activity on human platelets*. Blood, 1993. **82**: p. 2693-2703.
28. E.U.M. Saelman, H.K. Nieuwenhuis, K.M. Hese, P.G. DeGroot, H.F.G. Heijnen, E.H. Sage, S. Williams, L. McKeown, H.R. Gralnick, and J.J. Sixma, *Platelet adhesion to collagen types I through VIII under conditions of stasis and flow is mediated by GPIa/IIa ($\alpha 2\beta 1$ integrin)*. Blood, 1994. **83**: p. 1244-1250.
29. J.D. Hellums, *1993 Whitaker lecture: biorheology in thrombosis research*. Ann. Biomed. Eng., 1994. **22**: p. 445-455.
30. J-F Dong, M.C. Berndt, A. Schade, L.V. McIntire, R.K. Andrews, and J.A. Lopez, *Ristocetin-dependent, but not botrocetin-dependent, binding of von Willebrand factor to the platelet glycoprotein Ib-IX-V complex correlates with shear-dependent interactions*. Blood, 2001. **97**: p. 162-168.
31. J.A. Lopez, *The platelet glycoprotein Ib-IX complex*. Blood Coagul Fibrinolysis, 1994. **5**: p. 97-119.
32. M. Arya, J.A. Lopez, G.M. Romo, J-F Dong, L.V. McIntire, J.L. Moake, and B. Anvari, *Measurement of the binding forces between von Willebrand factor and variants of platelet glycoprotein GPIba using optical tweezers*. Lasers in Surgery and Medicine, 2002. **30**(30): p. 306-312.

33. B.R. Alevriadou, J.L. Moake, N.A. Turner, Z.M. Ruggeri, B.J. Folie, M.D. Phillips, A.B. Schreiber, M.E. Hrinda, L.V. McIntire, *Real-time analysis of shear-dependent thrombus formation and its blockade by inhibitors of von Willebrand Factor binding to platelets*. Blood, 1993. **81**(5): p. 1263-1276.
34. H. Ni, C.V. Denis, S. Subbarao, J.L. Degen, T.N. Sato, R.O. Hynes, and D.D. Wagner, *Persistence of platelet thrombus formation in arterioles of mice lacking both von Willebrand factor and fibrinogen*. J. Clin. Invest., 2000. **106**: p. 385-392.
35. J.M. Reese, D.S. Thompson, *Shear stress in arterial stenoses: a momentum integral model*. J. Biomech., 1998. **31**(11): p. 1051-57.
36. J.M. Siegel, C.P. Markou, D.N. Ku, S.R. Hanson, *A Scaling Law for Wall Shear Rate Through an Arterial Stenosis*. J. of Biomech. Eng., 1994. **116**: p. 446-451.
37. Young D.F., *Fluid Mechanics of Arterial Stenoses*. J. of Biomech. Eng., 1979. **101**: p. 157-175.
38. J. Strony, A. Beaudoin, D. Brands, and B. Adelman, *Analysis of shear stress and hemodynamic factors in a model of coronary artery stenosis and thrombosis*. Am. J. Physiol., 1993. **265**: p. 1787-1796.
39. J. Folts, *An in vivo model of experimental arterial stenosis, intimal damage, and periodic thrombosis*. Circulation, 1991. **83**[suppl. IV]: p. IV3-IV14.
40. A. Merino, M. Cohen, J.J. Badimon, V. Fuster, L. Badimon, *Synergistic action of severe wall injury and shear forces on thrombus formation in arterial stenosis: definition of a thrombotic shear rate threshold*. JACC, 1994. **24**(4): p. 1091-1097.
41. L. Badimon, J.J. Badimon, A. Galvez, J.H. Chesebro, and V. Fuster., *Influence of arterial damage and wall shear rate on platelet deposition. Ex vivo study in a swine model*. Arteriosclerosis, 1986. **6**: p. 312-320.
42. C.P. Markou, S.R. Hanson, J.M. Siegel, D.N. Ku., *The role of high wall shear rate on thrombus formation in stenoses*. Advances in Bioengineering ASME, 1993. **26**: p. 555-558.
43. D.M. Wootton, *Mechanistic Modeling of Occlusive Arterial Thrombosis*. 1998, Georgia Institute of Technology. p. 421.

44. R.M. Barstad, P. Kierulf, K.S. Sakariassen., *Collagen induced thrombus formation at the apex of eccentric stenoses - a time course study with non-anticoagulated human blood*. Thrombosis and Haemostasis, 1996. **75**(4): p. 685-692.
45. K.S. Sakariassen, R. Joss, R. Muggli, H. Kuhn, T.B. Tschopp, H. Sage, and H.R. Baumgartner., *Collagen Type III induced thrombogenesis in humans: role of platelets and leuokcytes in deposition of fibrin*. Arteriosclerosis, 1990. **10**: p. 276-284.
46. K.S. Sakariassen, H. Kuhn, R. Muggli, and H.R. Baumgartner., *Growth and stabilit of thrombi in flowing citrated blood: assessment of platelet surface interactions with computer-assisted morphometry*. Thrombosis and Haemostasis, 1988. **60**(3): p. 392-398.
47. S. Sukavaneshvar, K.A. Solen, *Effects of hemodynamics on thromboembolism in coronary stents and prototype flow cells in vitro*. ASAIO Journal, 1998. **44**: p. M388-M392.
48. S. Sukavaneshvar, G. Rosa, and K.A. Solen, *Enhancement of stent-induced thromboembolism by residual stenoses: contribution of hemodynamics*. Ann. Biomed. Eng., 2000. **28**: p. 182-193.
49. S. Falati, P. Gross, G. Merrill-Skoloff, B.C. Furie, B. Furie, *Real-time in vivo imaging of platelets, tissue factor, and fibrin during arterial thrombus formation in the mouse*. Nature Medicine, 2002. **8**(10): p. 1175-1180.
50. H. Matsui, M. Sugimoto, T. Mizuno, S. Tsuji, S. Mijata, M. Matsuda, and A. Yoshioka, *Distinct and concerted funcitons of von Willebrand factor and fibrinogen in mural thrombus growth under high shear flow*. Blood, 2002. **100**: p. 3604-3610.
51. M. Kuwahara, M. Sugimoto, S. Tsuji, H. Matsui, T. Mizuno, S. Miyata, and A. Yoshioka, *Platelet shape changes and adhesion under high shear flow*. Arterioscler Thromb Vasc Biol, 2002. **22**: p. 329-334.
52. Y-P Wu, P.G. de Groot, J.J. Sixma, *Shear stress-induced detachment of blood platelets from various surfaces*. Arterioscler Thromb Vasc Biol, 1997. **17**: p. 3202-3207.

53. B.G. Keselowsky, D.M. Collard, A.J. Garcia, *Surface chemistry modulates focal adhesion composition and signaling through changes in integrin binding*. Biomaterials, 2004. **25**: p. 5947-5954.
54. P.R.M. Siljander, I.C.A. Munnix, P.A. Smethurst, H. Deckmyn, T. Lindhout, W.H. Ouwehand, R.W. Farndale, J.W.M Heemskerk, *Platelet receptor interplay regulates collagen-induced thrombus formation in flowing human blood*. Blood, 2004. **103**: p. 1333-1341.
55. R.A. Kumar, J-F Dong, J.A. Thaggard, M.A. Cruz, J.A. Lopez, L.V. McIntire, *Kinetics of GPIb α -vWF-A1 tether bond under flow: effect of GPIb α mutations on the association and dissociation rates*. Biophysical Journal, 2003. **85**: p. 4099-4109.
56. T.A. Doggett, G. Girdhar, A.Lawshe, D.W. Schmidtke, I.J. Laurenzi, S.L. Diamond, T.G. Diacovo, *Selectin-like kinetics and biomechanics promote rapid platelet adhesion in flow: the GPIb α -vWF tether bond*. Biophysical Journal, 2002. **83**: p. 194-205.
57. A.J. Schade, M. Arya, S. Gao, R. Diz-Kucukkaya, B. Anvari, L.V. McIntire, J.A. Lopez, J-F Dong, *Cytoplasmic truncation of glycoprotein Iba weakens its interaction with von Willebrand factor and impairs cell adhesion*. Biochemistry, 2003. **42**: p. 2245-2251.
58. M. Arya, B. Anvari, G.M. Romo, M.A. Cruz, J-F Dong, L.V. McIntire, J.L. Moake, and J.A. Lopez, *Ultralarge multimers of von Willebrand factor form spontaneous high-strength bonds with platelet glycoprotein Ib-IX complex: studies using optical tweezers*. Blood, 2002. **99**: p. 3971-3977.
59. B.G. Brown, C.A. Gallery, R.S. Badger, J.W. Kennedy, D. Mathey, E.L. Bolson, H.T. Dodge., *Incomplete lysis of thrombus in the moderate underlying atherosclerotic lesion during intracoronary infusion of streptokinase for acute myocardial infarction: quantitative angiographic observations*. Circulation, 1986. **73**(4): p. 653-661.
60. L. Badimon, and J.J. Badimon., *Mechanisms of arterial thrombosis in nonparallel streamlines: platelet thrombi grow on the apex of stenotic severely injured vessel wall: experimental study in the pig model*. J. Clin. Invest., 1989. **84**: p. 1134-1144.

61. B.J. Folie, L.V. McIntire, A. Lasslo., *Effects of a novel antiplatelet agent in mural thrombogenesis on collagen-coated glass*. Blood, 1988. **72**(4): p. 1393-1400.
62. J.M. Ross, L.V. McIntire, J.L. Moake, and J.H. Rand., *Platelet Adhesion and Aggregation on Human Type VI Collagen Surfaces Under Physiological Flow Conditions*. Blood, 1995. **85**(7): p. 1826-1835.
63. A. Einstein, *Neue Bestimmung der Molekuldimensionen*. Annalen der Physik, 1911. **34**: p. 309-316.
64. A.V. Cardoso, A.O. Camargos, *Geometrical Aspects During Formation of Compact Aggregates of Red Blood Cells*. Materials Research, 2002. **5**(3): p. 263-268.
65. Fung Y.C., *The flow properties of blood*, in *Biomechanics: mechanical properties of living tissues*. 1993, Springer Verlag: New York, NY.
66. MJ Barnes, *Collagen in atherosclerosis*. Collagen Rel. Res., 1985. **5**: p. 65.
67. Y.C. Fung, *Biomechanics: Circulation*. 1996: Springer-Verlag.
68. H-K Yip, M-C Chen, H-W Chang, C-L Hang, Y-K Hsieh, C-Y Fang, and C-J Wu, *Angiographic morphological features of infarct-related arteries and timely reperfusion in acute myocardial infarction: Predictors of slow-flow and no-reflow phenomenon*. CHEST, 2002. **122**: p. 1322-1332.
69. J.B. Dahm, D. Ebersole, T. Das, H. Madyhoon, K. Vora, J. Baker, D. Hilton, and O. Topaz, *Prevention of distal embolization and no-reflow in patients with acute myocardial infarction and total occlusion in the infarct-related vessel: a subgroup analysis of the cohort of acute revascularization in myocardial infarction with excimer laser-CARMEL multicenter study*. Catheterization and Cardiovascular Interventions, 2005. **64**: p. 67-74.
70. N. Kieffer, D.R. Phillips, *Platelet membrane glycoproteins: functions in cellular interactions*. Ann. Rev. Cell Biol., 1990. **6**: p. 329-57.
71. Y. Cadroy, T.A. Horbett, S.R. Hanson, *Discrimination between platelet-mediated and coagulation-mediated mechanisms in a model of complex thrombus formation in vivo*. J. Lab Clin Med, 1989. **113**: p. 436-448.

72. D.A. Dichek, J. Anderson, A.B. Kelly, S.R. Hanson, L.A. Harker, *Enhanced in vivo antithrombotic effects of endothelial cells expressing recombinant plasminogen activators transduced with retroviral vectors*. *Circulation*, 1996. **93**: p. 301-309.
73. Y. Cadroy, S.R. Hanson, *Effects of Red Blood Cell Concentration on Hemostasis and Thrombus Formation in a Primate Model*. *Blood*, 1990. **75**(11): p. 2185-2193.
74. A.J. Reininger, U. Heinzmann, C.B. Reininger, P. Friedrich, L.J. Wurzinger, *Flow mediated fibrin thrombus formation in an endothelium-lined model of arterial branching*. *Thrombosis Research*, 1994. **74**(6): p. 629-641.